A Multi-Scale Reservoir Characterization of the Main Buntsandstein Subgroup in the Tilburg Area for Geothermal Operations

By

Ewoud Winand Morobe Hartemink

In partial fulfilment of the requirements for the degree of

Master of Science
In Applied Earth Sciences
Track Geo-Energy Engineering

At the Delft University of Technology,
To be defended on Tuesday October 12, 2021 at 15:45

Ewoud Hartemink, 5168880

Supervisor:	Dr.	H.A. Abels	TU Delft Applied Geology
Thesis committee:	Prof.	A.W. Martinius	TU Delft Applied Geology
	Dr.	J.E.A. Storms	TU Delft Applied Geology
	Dr.	D. Voskov	TU Delft Reservoir Engineering
	MSc.	E. Cecchetti	TU Delft Applied Geology

Preface

This research concludes my Master studies in Applied Earth Sciences with specialization towards the Geo-Energy Engineering track, which has been a great inspiring time over the last two years and a bit. During this period, I had the grateful opportunity and pleasure to work with many other pleasant students and academics. Before moving on to the actual content of the report, I would like to show my gratitude towards everyone that has supported me during the process of my thesis.

First, I want to thank my daily supervisor Emilio Cecchetti for the numerous supportive meetings, excellent advice, and enjoyable discussions on the thesis topic. Thanks for always taking the time to discuss problems, conceptualize the theory, and bring up new ideas. I have much enjoyed our daily exchange on the geological concepts as well as the latest trends within the cryptocurrency markets. You have proven to be an excellent supervisor and I am sure you will continue doing a great job towards your Ph.D. degree. I would like to express my gratitude towards my supervisors Dr. H.A. Abels and Prof. A.W. Martinius for their valuable comments and scientific input in the project. Your constructive feedback and experience were reflected in our meetings, which strongly helped me to focus on the bigger picture and the overall structure of the report. I want to thank Dr. D. Voskov for his participation in the thesis committee and his input during the final green-light meeting. Lastly, I want to thank Dr. J.E.A. Storms for his last-minute participation in my thesis committee.

I would also like to thank the NAM and TNO for the possibility to visit their core storages in the middle of the pandemic. Moreover, I want to express my appreciation towards A. Slupnik of TNO for giving me the enjoyable opportunity to work part-time at the TNO core storage from June onwards. This gave me a great balance to spend time between my research and my work.

Furthermore, I want to thank my family and friends for their unconditional encouragement on the way through.

Ewoud Hartemink
Amsterdam, October 2021

Abstract

The rising demand for clean energy has drawn the attention for more geological research to low enthalpy geothermal applications in the Netherlands. A multi-scale reservoir characterization is carried out with the aim to understand the geothermal reservoir potential of the Triassic Main Buntsandstein (RBM) in the Tilburg area. Seismic data, well logs and petrophysical data are used to evaluate the reservoir architecture, stratigraphy, and quality of the potential Main Buntsandstein geothermal aquifer. It was found that the study area is located within a horst- and graben system bounded by normal faults where the top boundary of the RBM is located at depths of 1900 – 2100 m for the horsts and 3300 – 3500 m for the grabens. The horsts and grabens range from circa 3000 to 4000 meters in width. Well log correlations and thickness maps at RBM scale suggest thicknesses of the Subgroup from ca. 160 to 220 meter. The thickness of the Main Buntsandstein generally decreases on the horsts and increases towards the grabens, suggesting higher temperatures of up to 100° C and thicker sand units in the grabens. Thickness generally decreases on the horsts and increases towards the graben suggesting faults were active at time of deposition and better geothermal potential in the grabens due to greater depths and thicker RBM unit. The core analysis of the study showed that the potential Main Buntsandstein reservoir is composed of a variation of sand- and mudstones interlayers, which were deposited on a large fluvial-fan system terminating in a playa-lake environment towards the basin center. Four different facies associations were distinguished within the cores of wells AND-06, KWK-01, SPC-01 and WWN-01-S2. Optimal reservoir connectivity is, according to the facies architecture model, expected in the Lower Volpriehausen and Detfurth Sandstone Members due to the presence of stacked amalgamated fluvial fan sandstone facies. It appeared that aquifer quality does not correlate with increasing depth or stratigraphic position, although the Volpriehausen- and Detfurth Claystone Members display significant poorer reservoir properties. These members, which can be correlated at well distance due to its widespread deposition as playa-lake sediments, are likely to act as a baffle to flow in the subsurface. Best reservoir potential, considering petrophysical measurements on porosity and permeability, is within the fluvial fan sandstones of all facies associations whereas the fine grained cross bedded sandstones show best reservoir quality of all encountered lithofacies. The data showed highly variable measurements where highest mean values for the porosity (11 %) and permeability (105 mD) are encountered in the Lower Detfurth Sandstone Member of well HVB-01. It turned out that northern located wells of Tilburg (AND-06, KWK-01, WWN-01-S2 and SPC-01) showed considerable poor reservoir potential with mean values of below 10% and 10 mD for the porosity and permeability. The southern wells, however, appear to have generally higher reservoir properties compared to the northern wells suggesting better geothermal potential in the area south of Tilburg.

Table of Contents

1. Background Information

1.1 Introduction

The demand for low carbon energy resources has caused the rise of geothermal applications in the Netherlands where it is mainly used for the heating of greenhouses and residential areas (Mijnlieff, 2020). In the Netherlands, sedimentary aquifers are commonly exploited by a doublet system, consisting of a hot-water production and cold-water injection well. Downhole well distance ranges from 1000 to 2000 m and both wells need to target the same aquifer to avoid loss of reservoir pressure. From a geological point of view, a geothermal project requires a porous and permeable reservoir with connectivity between the wells that has the capacity to heat the geothermal fluid from the injection to production well. One of the greatest geological challenges for a geothermal project is the prediction of fluid flow through the target reservoir, thus predicting the productivity of the production well and final breakthrough time of the geothermal doublet (Mijnlieff, 2020). Hence, understanding of the subsurface and, more specifically, the reservoir geology is fundamental for the success of a geothermal project. In addition, an earlier Triassic exploration target of the Naalwdijk-GT-1 well showed extremely low transmissivity values indicating that Triassic siliciclastic reservoirs pose a high risk and should therefore be thoroughly investigated (Mijnlieff, 2020).

In the Netherlands, geothermal reservoirs that are of potential interest are found in Permian, Lower Triassic and Lower Cretaceous sandstones, as well as two Tertiary sand units (Lokhorst and Wong, 2007). This proposed research is focused on the Lower Triassic sandstones of the Main Buntsandstein Subgroup (RBM), which is already a proven geothermal aquifer in Zuid-Holland (Mijnlieff, 2020). In the Brabant area, specifically around Tilburg, no geothermal projects targeting the Main Buntsandstein have been carried out due to the many uncertainties related to a lack of integration of the different available data types.

Sandstones from the Main Buntsandstein Subgroup are generally located at depths greater than 1500 – 2000m, which makes them excellent for low enthalpy geothermal operations due to high in-situ temperature at these depths (Mijnlieff, 2020). However, RBM reservoir behavior is heterogeneous due to the interaction between complex tectonic history and local sedimentary heterogeneities controlled by its depositional environment which range from fluvial sandstones and floodplain mudstones in the south that grade northward into predominantly aeolian deposits. In terms of stratigraphy, the Main Buntsandstein is composed of the Volpriehausen, Detfurth and Hardegsen Formations, representing tectono-stratigraphic units (Geluk, 2005). Geluk and Rohling (1997) concluded that within each formation smaller-scale parasequences exist that can be correlated at regional-scale and are deposited as a result of Milankovitch climatic cycles. The main sediment input derived from the London-Brabant-Massif in the southwest As the geology and sedimentary heterogeneities of the Lower Triassic have been fairly well described by Geluk (2005) at a regional scale, the geology and its associated sedimentary heterogeneities at a local geothermal well-spacing scale are missing in the Tilburg area. This is an essential ingredient to understand before starting with geothermal operations since local scale heterogeneities potentially could harm

subsurface fluid flow from the injection to production well. Therefore, this study aims to bridge this knowledge gap by characterizing the structure of the potential Main Buntsandstein reservoir and capturing the different vertical and horizontal sedimentary heterogeneities around Tilburg at different scales for possible geothermal applications.

Besides characterizing the reservoir geology and its structure, the reservoir quality is a key parameter to assess the potential and exploitability of geothermal reservoir and aquifers (Slatt, 2013). Nowadays, as a benchmark, transmissivity values of 10 Dm and higher is the minimum for a successful producing geothermal doublet (Mijnlieff, 2020). In order to evaluate the reservoir quality of the RBM, porosity and permeability data are incorporated into the reservoir characterization process. Earlier work conducted by Panterra Geoconsultants B.V. showed base average porosity and permeability of 15.6 % and 93 mD for the Main Buntsandstein and its overlying Sölling Formation in four wells around the Tilburg area. However, the linkage between reservoir geology and quality is not yet discussed so far. Therefore, this remains to be one of the main challenges of this study to address as it will directly improve predictions of subsurface fluid flow in the Tilburg study area.

Considering the above-mentioned challenges for deep geothermal operations in the Tilburg area, a comprehensive multi-scale reservoir characterization workflow is required. A comprehensive multi-scale reservoir characterization approach describes a multidisciplinary process that attempts to describe the nature and heterogeneities of a geological reservoir at multiple scales. The results of a reservoir characterization process are used to design reservoir models in order to simulate flow and predict production, which are again the ingredients to optimize field development planning (Ringrose et al., 2008). During this process, the following research questions will be addressed:

- What is the size, thickness, and internal stratigraphy of geothermal reservoirs in the Main Buntsandstein? And how do these affect the connectivity of the reservoirs?
- What are the sedimentary heterogeneities and reservoir properties of the Main Buntsandstein? And how do these relate to each other?
- What is the potential of low enthalpy geothermal systems in the Main Buntsandstein with respect to the reservoir architecture, connectivity, and quality?

By using a multi-scale reservoir characterization approach, in which different steps and disciplines/data will be integrated, a more thorough understanding of the sedimentological, petrophysical and structural aspects of the subsurface will be obtained at different heterogeneity scales. This consequently increases future potential associated with Triassic Main Buntsandstein geothermal operations in the Tilburg area.

1.2 Regional Geology of the Study Area

The study area is located on the southern fringe of the Roer Valley Graben (RVG), around the town of Tilburg. The RVG is a NW-SE striking asymmetric graben and makes up the northwestern part of the Rhine Graben rift system that extends from Euskirchen in Germany to ‘s Hertogenbosch in the Netherlands (Geluk et al., 1994). In the Netherlands, the RVG gradually fades into the West Netherlands Basin in the northwest and is bounded by a series

of antithetic faults in the southwestern margin while the Peel boundary fault forms the boundary at the northeast side of the basin (Geluk et al., 1994). The northwestern part, in which the study area is located, shows structural wrench-faulting, which caused a period of strong subsidence during the Middle Jurassic to Early Cretaceous. Subsequently, complex inversion tectonics happened during the Late Cretaceous. The boundary between the two parts is gradual and located around the east west Veldhoven Fault (Geluk et al., 1994). See Figure 1 for a structural map of the Mesozoic and location of the Veldhoven fault and the town of Tilburg.

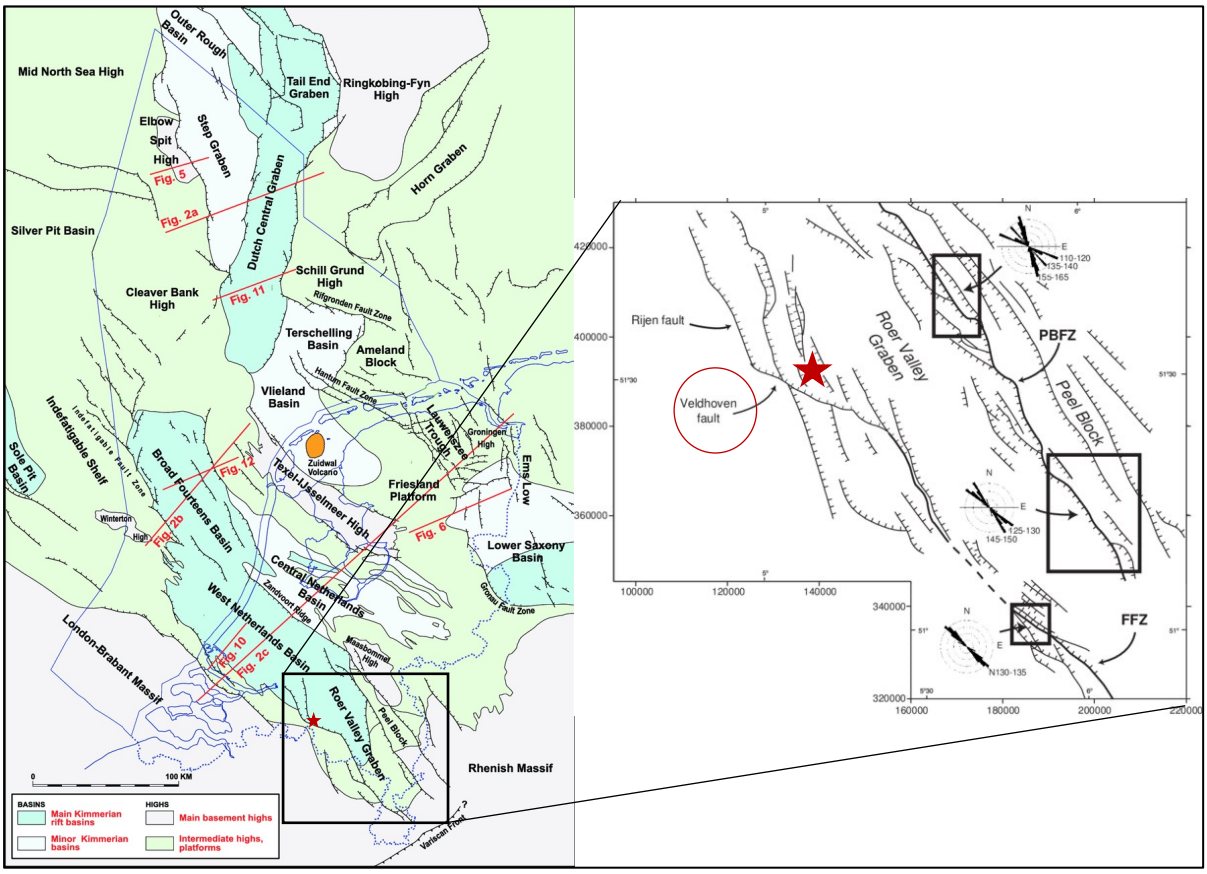

Figure 1: Structural elements map of the Netherlands showing Jurassic and Early Cretaceous basins, highs and platforms. The West Veldhoven Fault is located near the northwest edge of the RVG, close to the WNB (see red circle). The red star refers to the approximate location of Tilburg. Modified from Jager (2007) & Michon and Van Balen (2005).

The Roer Valley Graben was formed during the Mesozoic as a result of reactivation of deep NW-SE trending faults during the late stage of the Variscan orogeny (Geluk et al., 1994). The onset of the Triassic marked a distinct change from a period of tectonic inactivity and gradual thermal subsidence to NW-SE extension regime (Ziegler, 1990). Triassic sediments record the breaking up of supercontinent Pangea due to Mesozoic extensional tectonics. In the Netherlands, the thickness of the Triassic differs strongly as a result of highly differentiated subsidence during the Triassic and significant post-Triassic uplift and erosion (Geluk, 2007).

The Roer Valley Graben became the main area sediment feeder during the Early to Middle Triassic. The study area was at this time located within the alluvial fan regime where large fluvial systems transported clastics from the south to the southeast far into the basin. However, over time, the deposition of coarse sediments was confined to the basin margin and the supply of sediments from the SE eventually ceased during the Middle Triassic (Geluk

et al., 1996). Sediments derived mainly from the London-Brabant-Massif in the south and Rhenish Massif in the southeast, which together formed the northern rim of the Variscan orogeny (Geluk et al., 1996). A paleogeographic map of the Southern Permian Basin including the RVG during the Early Triassic is shown in Figure 2.

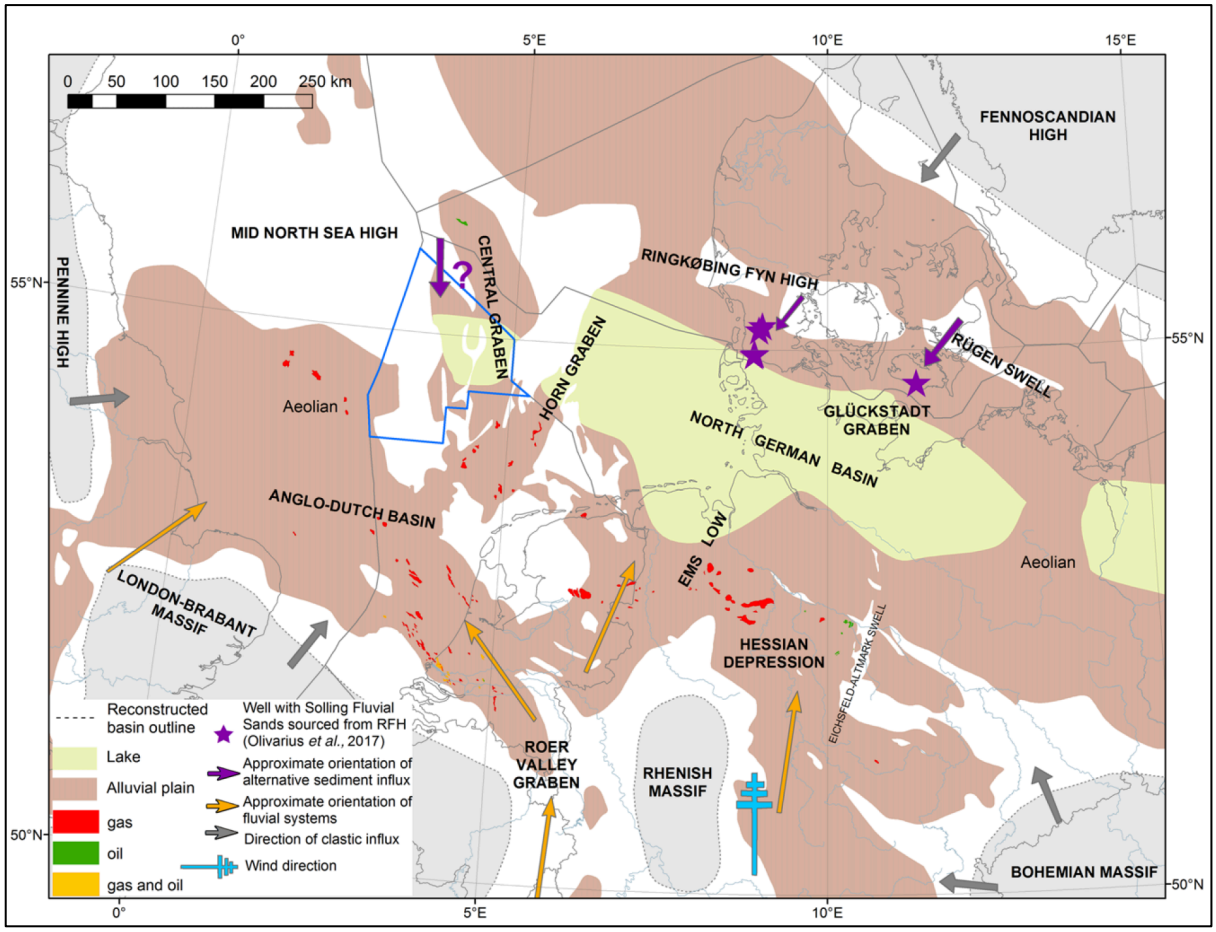

Figure 2: Palaeogeographical map of the Southern Permian Basin during the Early Triassic. The study area, located within the sub-basin Roer Valley Graben is highlighted by the black star. The red arrow indicates the main direction of sediment transport. Sediments were predominantly delivered from the south to the Roer Valley Graben. The source of these sediments was the London Brabant Massif and Rhenish Massif. After (Kortekaas et al., 2018).

1.3 Stratigraphy and Sedimentology of the Main Buntsandstein Subgroup

In the Netherlands, the Triassic stratigraphy is divided into two major lithostratigraphic groups: the Lower Germanic Trias Group, which consists of fluvial sandstones alternated with lacustrine claystones, and the Upper Germanic Trias Group that is composed of silty claystones, evaporites, carbonates and sandstones which were deposited in alternating shallow, restricted-marine, inland-playa lake and floodplain settings (Geluk et al., 1996; TNO-GSN, 2021c). The Triassic deposits display a layer-cake character in the Roer Valley Graben, which is visible on a regional scale as well as reservoir scale (Geluk and Rohling, 1997). See Figure 3 for stratigraphic column of the Triassic in the RVG.

The Main Buntsandstein Subgroup, which is the target stratigraphical layer for this research, belongs to the Lower Germanic Triassic Group. Its deposition marks the onset of regional differential subsidence due to extensional tectonics in Western Europe, which strongly affected the thickness and facies distribution (Geluk et al., 1996). The subgroup displays large-scale fining upwards sequences, where fluvial to aeolian sandstones gradually move upwards into lacustrine silt- to claystones. An important characteristic of the Main Buntsandstein are the tectonically driven unconformities at the bases of the Volpriehausen and Detfurth Formations, as well as on top of the Hardegsen Formation/base of the Sölling Formation. The strongest of these rift pulses caused the formation of the Hardegsen unconformity and is therefore known as the Hardegsen phase (Geluk, 2005; Geluk et al., 1996; Geluk and Rohling, 1997; Kortekaas et al., 2018).

The three present formations in the Main Buntsandstein Subgroup are thus tectono-stratigraphic units according to Geluk (2007). Each unit consists of a first order fining upward sequence. Within these sequences, a hierarchical system of small-scale cycles, i.e., parasequences exists. The cyclicity pattern within these formations is most likely formed as a results of Milankovitch climate variations (Geluk and Rohling, 1997). These sequences can be laterally correlatable over large distances and have a strong expression on well-logs according to the same authors.

1.3.1 Volpriehausen Formation (RBMV)

The Volpriehausen Formation consists of the Lower Volpriehausen Sandstone and Volpriehausen Clay-Siltstone Member in the Roer Valley Graben (Geluk, 2005). An unconformity exists at the base of the formation and locally cuts up to tens of meters in the Lower Buntsandstein (Geluk, 2007). The first member is composed of mainly sandstones whereas the latter contains several alternations of clay-siltstone and thin sandstones. The succession shows an overall coarsening upward sequence (Geluk, 2005).

The Lower Volpriehausen Sandstone Member was deposited during the first two phases of rifting, which created a significant difference in accommodation space. This caused a diversion of the main fluvial channels through the RVG and West Netherlands Basin into the Broad Fourteens Basin (Geluk, 2005). The sandstones of the Lower Member have a quartz content of slightly below 50% with an high amount of calcite and dolomite cement in the lowermost section (Geluk, 2005). The Volpriehausen Clay-Siltstone Member is composed of a succession of predominantly lacustrine siltstones and marls, and minor sandstones.

1.3.2 Detfurth Formation (RBMD)

The Detfurth Formation comprises of a Lower and an Upper Detfurth Sandstone Member. However, towards the North of the Netherlands, the Upper Detfurth gradually turns into the Detfurth Claystone Member (Geluk et al., 1996). Similar to the Volpriehausen Formation, the Detfurth Formation is composed of a basal sandstone, with a succession dominated by clay- and siltstones on top. Its occurrence is limited to the Early Triassic lows due to uplift and erosion prior to deposition of the Sölling Formation. Hence, the thickness of the formation shows considerable variations with a thickness of 20-40 m in the RVG. Here, the Detfurth

Formation consists predominantly of sandstones (Geluk, 2005). Detfurth Claystone has a clear expression on well logs and can be used as a regional correlation marker (Geluk, 2005).

1.3.3 Hardegsen Formation (RBMH)

The Hardegsen Formation is the uppermost formation of the Main Buntsandstein Subgroup and is characterized by alternations of siltstones and thin sandstone beds. Its thickness is strongly affected by the Hardegsen unconformity which caused a significant amount of erosion. During deposition of the Hardegsen formation, differential subsidence ceased in the RVG (Geluk, 2005). The member reaches a thickness of up to 70 m inside the Roer Valley Graben (Geluk, 2005). Geluk and Rohling (1997) considered the Hardegsen and Detfurth together as a whole sequence as there lacks a tectonic event between the two formations.

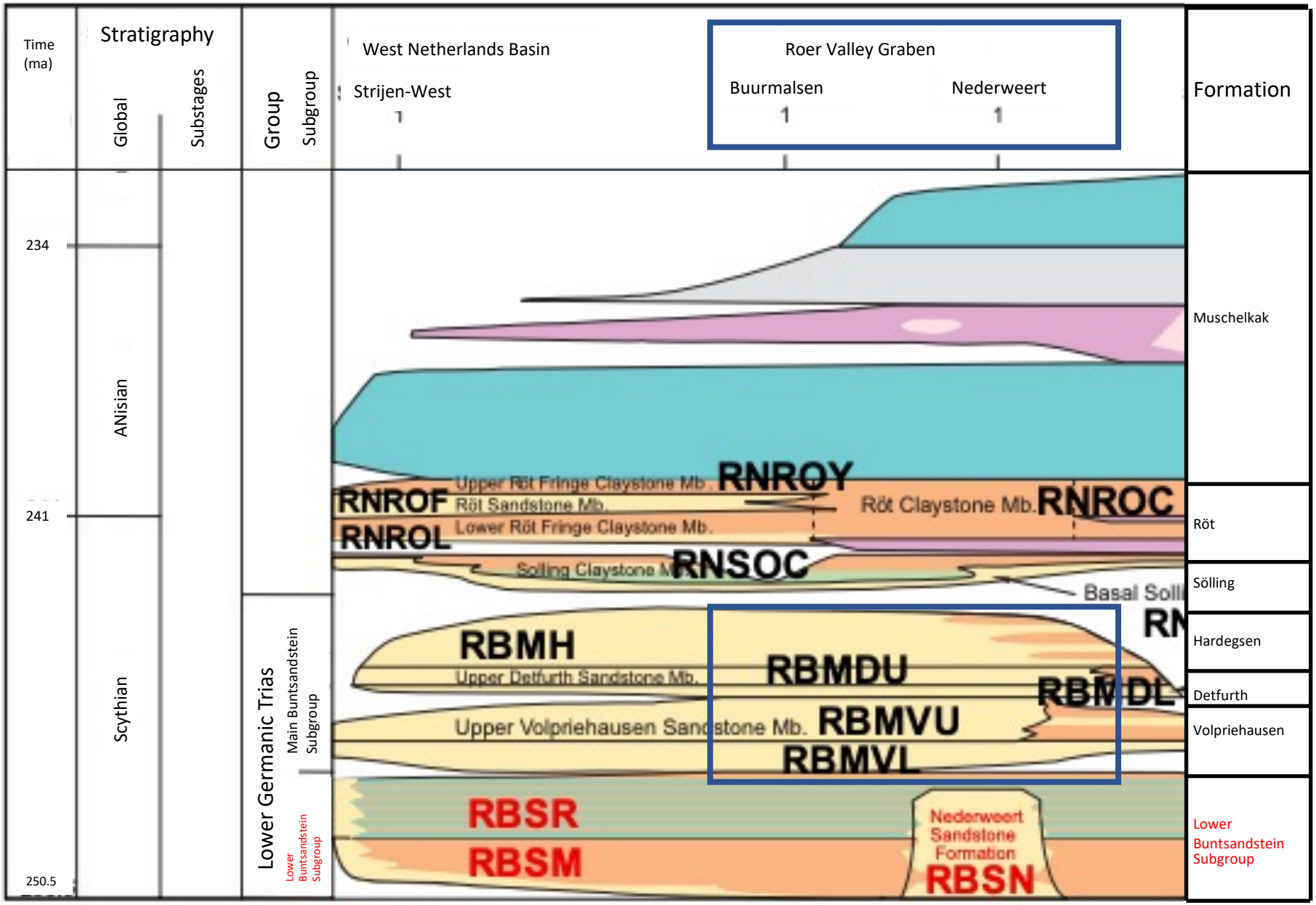

Figure 3: Stratigraphical column of the Triassic in the Netherlands. The stratigraphy of the Roer Valley Graben is highlighted by the blue box. RBML = Lower Volpriehausen Sandstone Member, RBMVU = Upper Volpriehausen Sandstone Member, RBMDL = Lower Detfurth Sandstone Member, RBMDU = Upper Detfurth Sandstone Member and RBMH = Hardegsen Formation. Modified from Adrichem-Boogaert and Kouwe (1993).

2. Data & Methods

For this thesis research, seismic, well log, core, and core plug data have been used. Together they represent a part of the subsurface from the largest to smallest scale, necessary to carry out a multi-scale reservoir characterization study. Figure 4 below displays the general workflow including the available data and the research aim to obtain for each step used during the reservoir characterization approach.

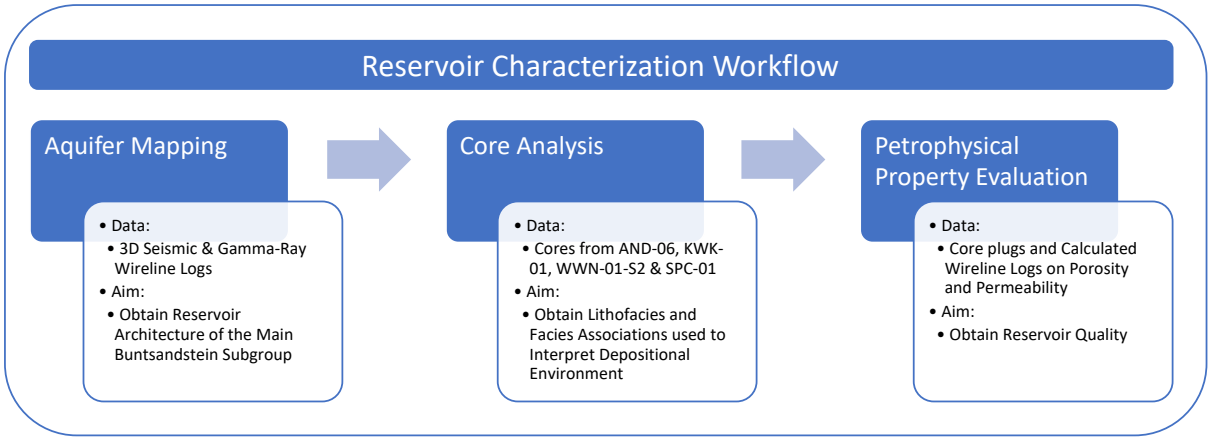

Figure 4: Workflow chart displaying the reservoir characterization approach of the study including the necessary data and the research aim to obtain.

A 3D seismic cube, that is stored under the SEG convention, is used during the seismic interpretation process as well as the different wells that are located inside the seismic area. The aim of this analysis is to obtain information on geometry, size, and shape of the reservoir/aquifer at Subgroup scale. Since the seismic dataset is already converted into the depth domain, no time to depth conversion needs to be applied. During this process, the top and the base of the Main Buntsandstein Subgroup are interpreted as well as the faults that cut through. Interpretation of the stratigraphy is done with the use of the well data and imported well tops. The horizon interpretation is started at the well locations since well tops can be tied directly to the seismic. From the wells, the horizons can be interpreted away from the wells when knowing the seismic response of that specific horizon. For this process, the guided auto tracking and/or manual picking are used. 3D seismic survey In- and X-lines were interpreted on with an increment of 10, increasing the frequency when a higher resolution was necessary. The results provide depth and isopach maps of the Main Buntsandstein Subgroup as well as interpreted cross sections throughout the area.

In order to avoid uncertainties regarding picking the right reflector for that specific horizon, the acoustic impedance at the well location is calculated from the corresponding well logs. The difference in acoustic impedance in the subsurface between rock layers directly affects the reflection coefficient of the seismic reflector. A seismic reflector with a positive amplitude (red) represents an acoustic hardening in the subsurface. The reverse is applicable for a reflector with a negative amplitude (Veeken, 2007). The acoustic impedance of the top and bottom of the Main Buntsandstein, as well as the internal formation boundaries inside the Subgroup are provided in the results chapter of the seismic study. The quality of the seismic

generally decreases with increasing depth throughout the dataset. At depths of 3000 – 3500 m, the top and bottom reflectors of the Subgroup are thus sometimes more difficult to pick due to the lower seismic quality. Figure 5 displays the area of the 3D seismic dataset, as well as the different wells that are used for this study. From Figure 5 it can be seen that the 3D cube covers the town of Tilburg, which is the focus area of this study. Seismic- and well log interpretation is conducted with the use of the Petrel E&P Software.

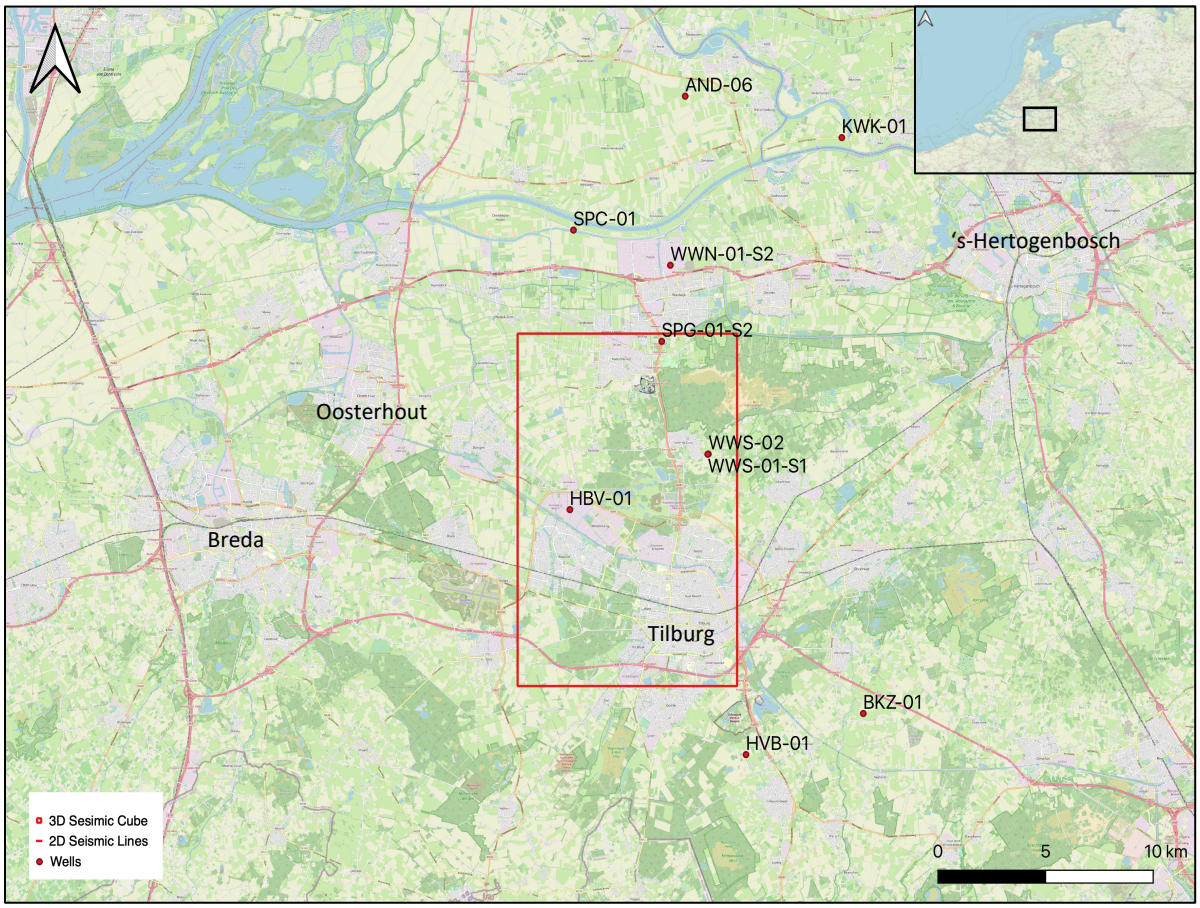

Figure 5: Map of the study area displaying the different wells that penetrate (partly) the Triassic Main Buntsandstein as well as the 3D seismic cube. The study area is predominantly focused inside the 3D seismic cube, which is located around the town of Tilburg. The cored wells analyzed for the study are the AND-06, KWK-01, SPC-01 and WWN-01-S2, respectively. Furthermore, the larger cities in the area are displayed with their names.

Ten different wells that penetrate (partly) the Triassic Main Buntsandstein are used during the well analysis for this study. Their locations are also shown in Figure 5. The locations, depths, deviation, well logs, and horizon markers of these ten wells are retrieved from NLog.nl (TNO, 2016). From the ten wells, only four wells contain available core data of the Main Buntsandstein to evaluate its reservoir sedimentology. These wells are the AND-06, KWK-01, SPC-01 and WWN-01-S2, respectively. Core material has been logged on a 1:10 or 1:25 scale to describe the grain sizes, sedimentary structures, and other visible structures/texture. Based on these core descriptions, different lithofacies are established which are grouped into several facies association types. From the facies associations together with the literature, the depositional setting associated with RBM sediments can be inferred. The lithofacies scheme in this thesis follows similar principles as that of the Bunter Atlas which is based on the classification of the RGD-Nogepa lithofacies coding system presented in Reijers et al. (1993). This system displays a lithofacies code that consists of a code for the lithology (grain size)

followed by codes for the present sedimentary structures and characteristics. Upper case letters are used for the lithology codes and are separated from other characteristics by a “”,” (comma). Lower case letters represent the sedimentary structures and characteristics of the specific lithofacies. The complete lithofacies classification modified from de Reuver (1994) can be found in Appendix A. A core description conducted by BP Exploration for the wells WWN-01-S2 (Cade, 1989) and SPC-01 (Adamson, 1987) are used for their lithofacies and facies association interpretation.

During the last stage of the reservoir characterization process, core plugs and well log measurements are used to assess the reservoir quality at these well locations. The multiple heterogeneity scales will be plotted versus the porosity and permeability in order to see the influence of the different heterogeneity scales on the reservoir property parameters. Table 1 shows a more detailed scheme of the available data for each well in the study area.

Table 1: Summary of all the well data in the study area. The abbreviations used refer to: MD is measured depth along the borehole, TVD is the true vertical depth, RBMH is Hardegsen Formation, RBMD is Detfurth Formation and RBMV is Volpriehausen Formation. All data is retrieved from Nlog.nl (TNO, 2016).

Well Number	Well Name	MD (m)	TVD (m)	Penetrating Stratigraphic Intervals	Interval (MD) Penetrating the Main Buntsandstein (m)	Available Main Buntsandstein Cores	Total Core Thickness (m)	Cored Intervals (According to NLog)	Cored Depths (MD)	Gamma Ray	Density	Sonic	SP	Neutron	Induction	Resistivity
AND-06	Andel-06	3136	2666.84	RBMH, RBMD & Partly RBMV	2862.5 - 3136	Yes	14.5	Upper Detfurth Lower Detfurth	2894 - 2904 2906 - 2910.5	Yes	Yes	Yes	Yes	Yes	Yes	No
BKZ-01	Broekzijde-01	2702	2689.33	RBMH, RBMD & RBMV	2416 - 2679	No	-	-	-	Yes	Yes	Yes	Yes	Yes	Yes	Yes
HBV-01	Huibeven-01	2350	2217.46	RBMH, RBMD & RBMV	2113 - 2292	No	-	-	-	Yes	Yes	Yes	Yes	Yes	No	No
HVB-01	Hilvarenbeek-01	2621	2546.01	RBMH, RBMD & Partly RBMV	2388 - 2621	No	-	-	-	Yes	Yes	Yes	Yes	Yes	Yes	Yes
KWK-01	Kerkwijk-01	3281	3110.13	RBMH, RBMD & RBMV	2543 - 2754	Yes	53.6	Hardegsen Upper Detfurth Lower Detfurth	2548 - 2572 2572 - 2598 2598 - 2601.6	Yes	Yes	Yes	Yes	Yes	No	Yes
SPC-01	Sprang Capelle-01	3180	2865.55	RBMH, RBMD & RBMV	2597 - 2756.50	Yes	27.5	Lower Detfurth Upper Volpriehausen	2647 - 2664 2664 - 2674.5	Yes	Yes	Yes	Yes	Yes	No	No
SPG-01-S2	Sprang-01-Sidetrack2	3214	3026.31	RBMH, RBMD & Partly RBMV	3116 - 3208	No	-	-	-	Yes	Yes	Yes	Yes	Yes	No	No
WWN-01-S2	Waalwijk Noord-01-Sidetrack2	3377	2982.41	RBMH, RBMD & RBMV	3164 - 3355	Yes	136.5	Hardegsen Upper Detfurth Lower Detfurth Upper Volpriehausen Lower Volpriehausen	3169 - 3182 3182 - 3200 3200 - 3224 3224 - 3287.5 3287.5 - 3305.5	Yes	Yes	Yes	Yes	Yes	Yes	Yes
WWS-01-S1	Waalwijk South 01-Sidetrack1	3486	3054.28	RBMH, RBMD & RBMV	3228 - 3433.5	No	-	-	-	Yes	Yes	Yes	Yes	Yes	Yes	Yes
WWS-02	Waalwijk South-02	4850	2950.36	RBMH, RBMD & RBMV	4564 - 4801	No	-	-	-	Yes	Yes	Yes	Yes	Yes	Yes	No

3. Results

3.1 Aquifer Mapping

3.1.1 Horizons

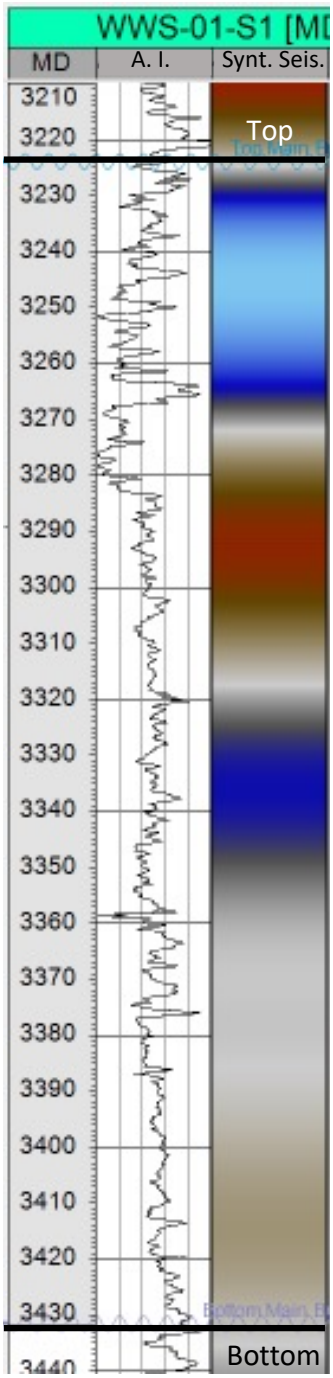

The seismic study consists of two parts, namely the description and interpretation of the horizons and the faults. The reflectors of the top and bottom Main Buntsandstein show the size and shape of the aquifer at Subgroup scale (Figures 7 and 8). The acoustic impedance at the well location is retrieved by dividing the density-log values by sonic-log values. The acoustic impedance allows us to create a synthetic well seismogram (Figure 6). The synthetic seismogram is used to distinguish the top and bottom of the Main Buntsandstein as well as to test the well tops retrieved from NLog. The top and bottom of the Subgroup are located near the base of the upper most and lower most hard kick reflectors respectively (Figure 6), with the top reflector showing a better quality compared to the bottom reflector (Figures 6, 7 and 8; Table 2).

During the first stage of the seismic interpretation, the top of the Chalk Group horizon, which shows as a distinct hard kick reflector, is picked with the use of NLog well tops (Figures 7 and 8). The character of this reflector is caused by transition from sand- and claystones in the overlying North Sea Group to carbonates in the Chalk Group (TNO-GSN, 2021a). The seismic reflector appears to be excellent around the dataset.

Secondly, the top of the Posidonia Shale Formation is tracked in the seismic cube. The top of the Posidonia Shale Formation displays a strong 'hard kick' reflector which is clearly present around the whole dataset. Its reflectors quality is therefore considered as excellent. The character of the Posidonia Shale Formation is likely to be caused by a transition from an overlying distinct limestone unit to a claystone unit in the concerned Formation (TNO-GSN, 2021b).

The top of the Triassic stratigraphy is represented by the Keuper Formation. This Formation, comprising of predominantly claystones and anhydrite, appears as a strong hard-kick reflector on the seismic dataset. The quality of the seismic reflector is commonly

Figure 6: Screenshot of a well section window displaying the depths (measured depth) of the top and bottom of the Main Buntsandstein from well WWS-01-S1. The shown well logs are the Acoustic Impedance on the left and the synthetic seismic on the right. The figure indicates the seismic character of the Subgroup boundaries.

good throughout the dataset, but sometimes loses quality at deeper located places in the area (Figures 7 and 8). If this is the case, the Posidonia Shale reflector is used as a guide to track the top of the Triassic as this horizon is located circa 500 meter deeper than the top of the Posidonia Formation.

The top of the Main Buntsandstein, known as the transition from the Sölling to Hardegsen Formation appears as a moderate hard kick and is on average located circa 100 – 150 m deeper than the top of the Triassic horizon (Figures 7 and 8). The quality of the reflector varies per location, which is most likely caused by the Hardegsen/Sölling Unconformity, but also by a loss of seismic quality due to the increasing depth (Figures 7 and 8).

The bottom of the Main Buntsandstein, that is represented by the transition of the Volpriehausen to Rogenstein Formation, is on the seismic characterized by the transition of a weak hard kick reflector to a soft kick (Figures 6, 7 and 8). The quality of the reflector is relatively low to moderate caused by the significant depth (> 2500 m) of this horizon (Figures 7 and 8). Hence, the bottom of the Subgroup is often tracked by knowing that the Main Buntsandstein has an average thickness of circa 200 m inside the Roer Valley Graben (Geluk, 2005).

Internal formation boundaries inside the Main Buntsandstein Subgroup are not tracked on the seismic cube as these are not clearly apparent. Hence, the results of the seismic study are limited to Subgroup scale. Overall, the quality of the reflectors varies in the seismic data set and is commonly controlled by the depth of the reflector: shallower reflectors show better quality reflectors than deeper located reflectors (Figures 7 and 8; Table 2).

Table 2: Summary showing the polarity and quality of the interpreted reflectors

Stratigraphic Interval	Polarity	Quality
Top Chalk	Strong hard kick	Excellent
Top Posidionia Shale	Strong hard kick	Excellent
Top Triassic	Strong hard kick	Good
Near Top Main Buntsandstein	Hard kick	Moderate
Near Bottom Main Buntsandstein	Hard kick	Poor to moderate

3.1.2 Faults

Picking and tracking of faults is conducted when a clear offset of seismic reflectors is visible on the seismic data. For this process, the above-mentioned horizons are used to see whether any offset appears in their seismic reflectors. The faults cutting through the Main Buntsandstein are of most relevant as this research is limited to possible geothermal applications in this stratigraphic Subgroup.

Several faults are observed from the cross sections (Figures 7 and 8). The first observation shows that nearly all of the visible faults cut to cross through all of the previous observed seismic horizons, with exception of the reflector of the top Chalk Group (Figure 7). Only the

larger apparent faults, that have lengths of circa 1500 – 2500 m, cut through the top Chalk at some places. These faults show commonly offsets of circa 100 – 400 m, with outliers of up to 800 m (see left fault Figure 8). Since the blocks above all the faults has moved downward relative to the blocks below, all these faults are considered as normal faults and have fault angles of around 60 degrees and steeper (Figures 7 and 8).

The smaller faults, that do not reach the top of the Chalk horizon, terminate in between the Posidonia horizon and top of the Chalk horizon. These have lengths of around 1000 – 1500 m and generally show offsets of around 100 – 200 m with exceptions of up to 500 m (Figures 6 and 7). Similar to the larger faults, the above fault block has moved downward relative to the bottom blocks suggesting normal fault movement (Figures 7 and 8).

The orientation of these two fault sets is observed from the structural depth maps of the top and bottom Main Buntsandstein: the larger faults have an NNW-SSE orientation whereas the smaller faults are NE-SW orientated (Figure 9). Moreover, the maps show that the NNW-SSE orientated faults commonly cut the NE-SW orientated faults indicating that the latter mentioned set of faults is relatively younger than the NNW-SSE faults.

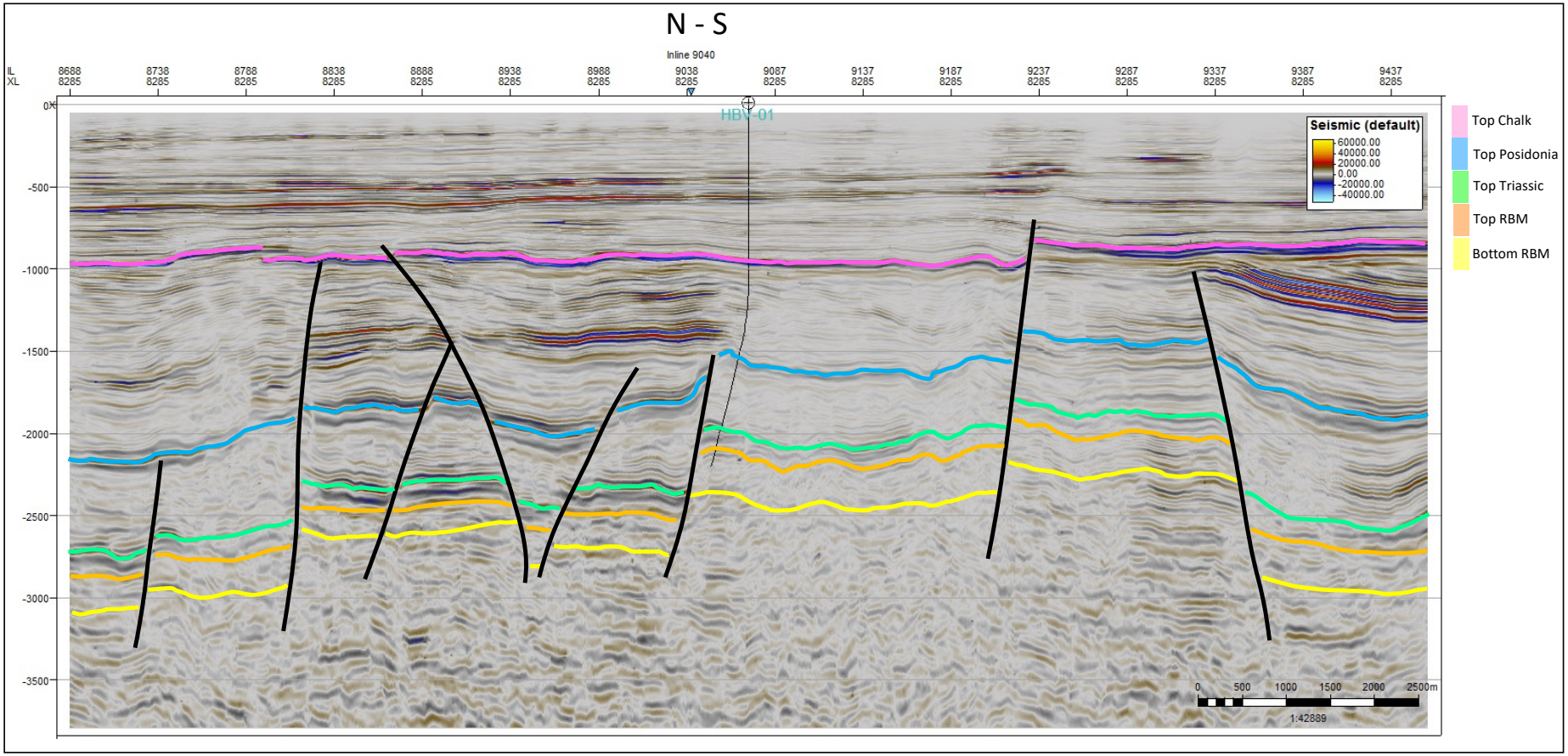

Figure 7: Interpreted seismic cross section along the North-South direction of the study area. The interpreted horizons are (from top to bottom) the top Chalk, top Posidonia, top Triassic, top Main Buntsandstein and bottom Main Buntsandstein. Faults are indicated by the black solid lines. All apparent faults show normal movement. The cross section indicates a horst and graben structure in the study area where the Main Buntsandstein is generally located at depths of 2000 – 3000 m. The projected well is HBV-01.

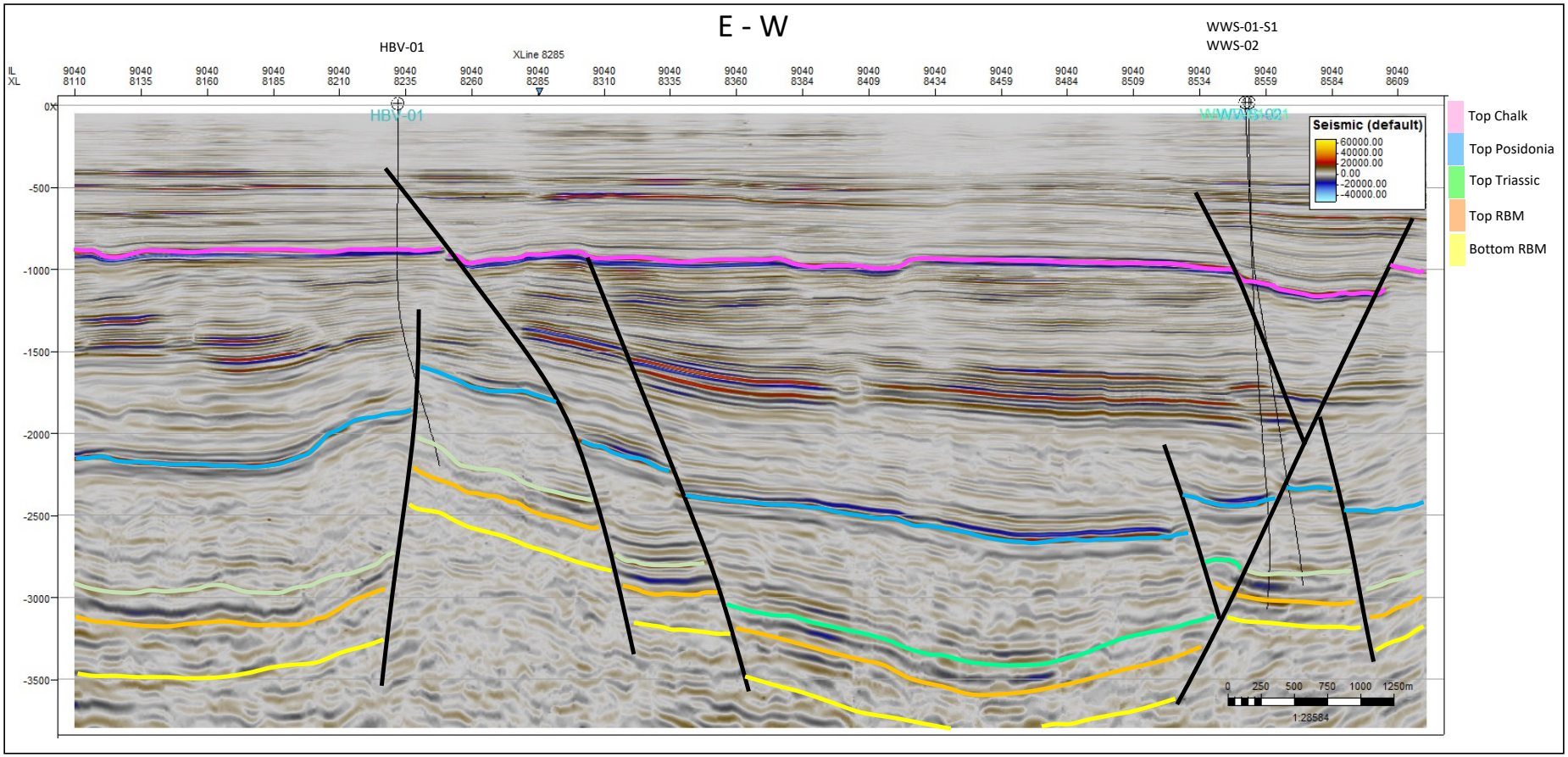

Figure 8: Interpreted seismic cross section along the East-West direction of the study area. The interpreted horizons are (from top to bottom) the top Chalk, top Posidonia, top Triassic, top Main Buntsandstein and bottom Main Buntsandstein. Faults are indicated by the black solid lines. All apparent faults show normal movement. The cross section indicates a horst and graben structure in the study area where the Main Buntsandstein is generally located at depths of 2500 – 3500 m. The projected wells are the HBV-01. WWS-01-S1 and WWS-02.

3.1.3 Depths and Thickness Maps

Depth maps and cross sections display the split up of the study area into structural highs and lows by the NNW-SSE orientated normal faults indicating a horst- and graben structure. The shallowest parts of the Subgroup (for the top boundary) are located at depths of ca. 1900-2500 m on the structural highs, whereas the deepest parts are situated at depths ranging from 3000-3500 m in the structural lows. The bottom boundary of the Main Buntsandstein is located at depths of 2500 – 3000 m for the structural highs and 3500 – 3800 for the structural lows, respectively. The width of the horst and grabens ranges from circa 3000 to 4000 meters.

By extracting the bottom depth of the top depth of the Main Buntsandstein maps, the thickness of the Subgroup in the study area is obtained. The Main Buntsandstein has an average thickness of around 200 meters, with a standard deviation of circa 20 m according to the thickness map (Figure 9). However, due to the moderate to poor seismic quality throughout the data set, the thickness map displays a considerable number of artefacts which is for example visible around well WWS-02 (purple spot in Figure 9). True stratigraphic thickness of the Main Buntsandstein at wells HBV-01, WWS-01-S1 and WWS-02 is added to the thickness map to improve the thickness observation at these well locations. These thicknesses are derived from the GR-logs of these wells.

Thickness variations are observed between the horsts- and grabens in the area, where thicker packages of the Subgroup are located in the grabens compared to the horsts. This suggests faults were active at time of deposition (during the Triassic) and caused a difference in accommodation space in the basin. The thickness of the Subgroup in the grabens is around 220 – 230 meters, whereas the horsts display a thickness of around 180 – 200 meters (Figure 9).

Well log correlations are created in order to give a more general understanding on the thickness distribution at Subgroup scale from well to well. The top and bottom of the Main Buntsandstein are correlated with the use of the well tops depths retrieved from Nlog.nl (TNO, 2016). The bottom boundary is represented by a distinct transition from high gamma-ray values (due to claystones in the Rogenstein) to low values caused by the sandstones within the Volpriehausen Formation. Top of the Main Buntsandstein displays a distinct change from low gamma-ray (from sandstones within the Hardegsen Formation) to high gamma-ray values caused by claystones of the Sölling Formation. A structural map (Figure 10) shows that all wells are located on a structural high. This is evident from the fact that the faults intersecting the Jurassic horizons are located at the inside of a fault block, whereas the intersection with Triassic horizons appear at the outside of a similar fault block.

Considering the well correlation panels, displayed in Figures 10B, 10C and 10D, some indications on thickness trends of the Subgroup can be identified. First, the southern wells, BKZ-01 and HVB-01, show a considerable thicker package of Main Buntsandstein. The wells clustered in the North, named AND-06 and KWK-01, again display a significant thick RBM package of around 200 – 220 meters. The middle cluster of wells (HBV-01, SPC-01, WWN-01-S2, WWS-01-S1 and WWS-02; Figure 10C), show a thinner package of RBM of around 160 – 200 m, compared to the southern and northern cluster.

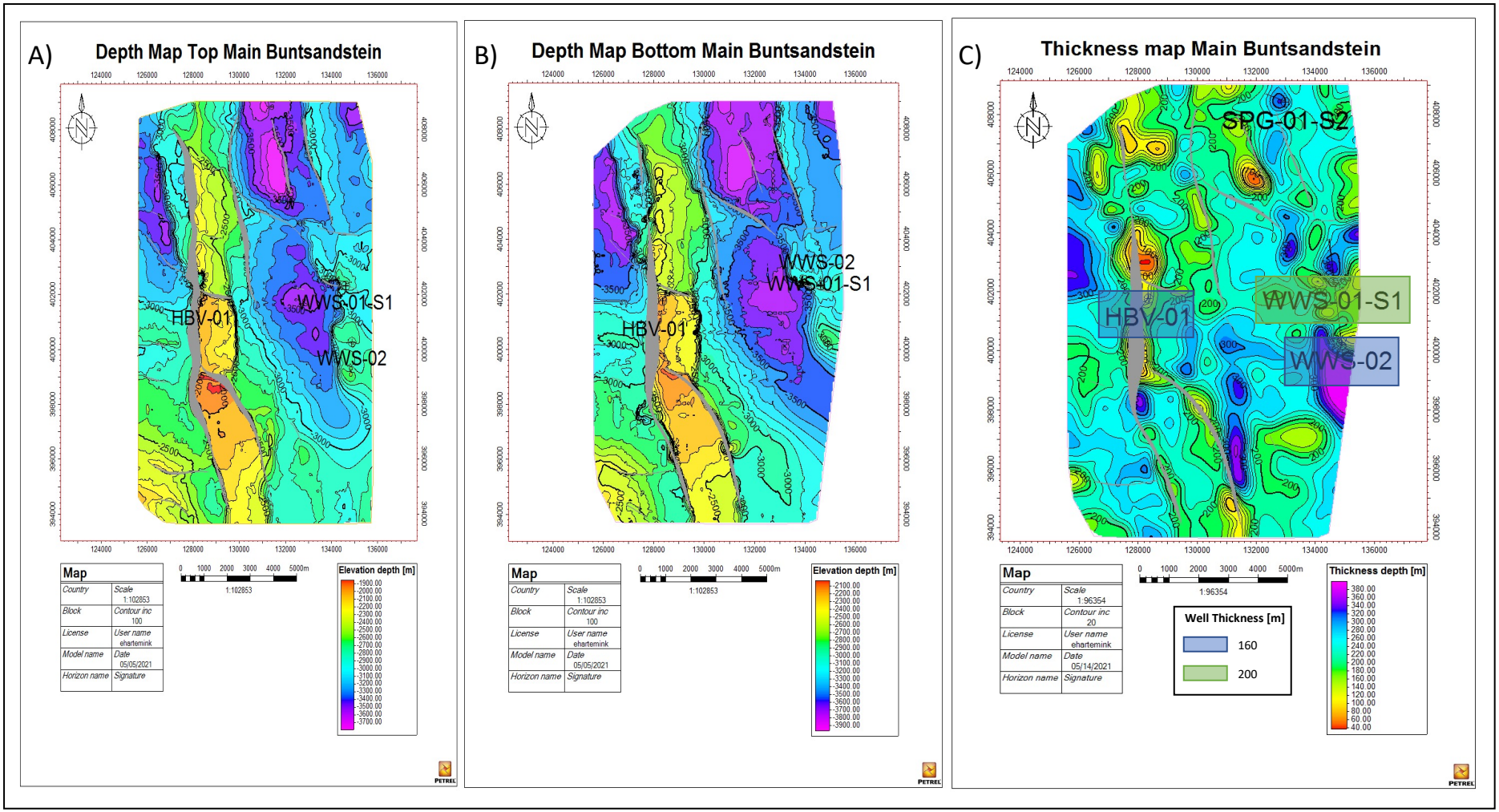

Figure 9: Depth and thickness maps of the Main Buntsandstein including the interpreted faults shown in light-grey and wells penetrating (partly) the Main Buntsandstein. The top is represented by the boundary between the top of the Hardegsen- and the overlying Sölling Formation whereas the bottom corresponds to the boundary between the underlying Rogenstein- and bottom of the Volpriehausen Formation. A) depth map of the top. B) depth map of the bottom. C) thickness map of the Main Buntsandstein created from the depth maps. Faults are predominantly orientated NNW-SSE. Rarely, NW-SE orientated faults exist. The map shows some artifacts (for example the thick purple spot around WWS-02), which is most likely created by the poor quality of seismic in this area. The color boxes display the thickness of the RBM taken from the well logs in true vertical thickness.

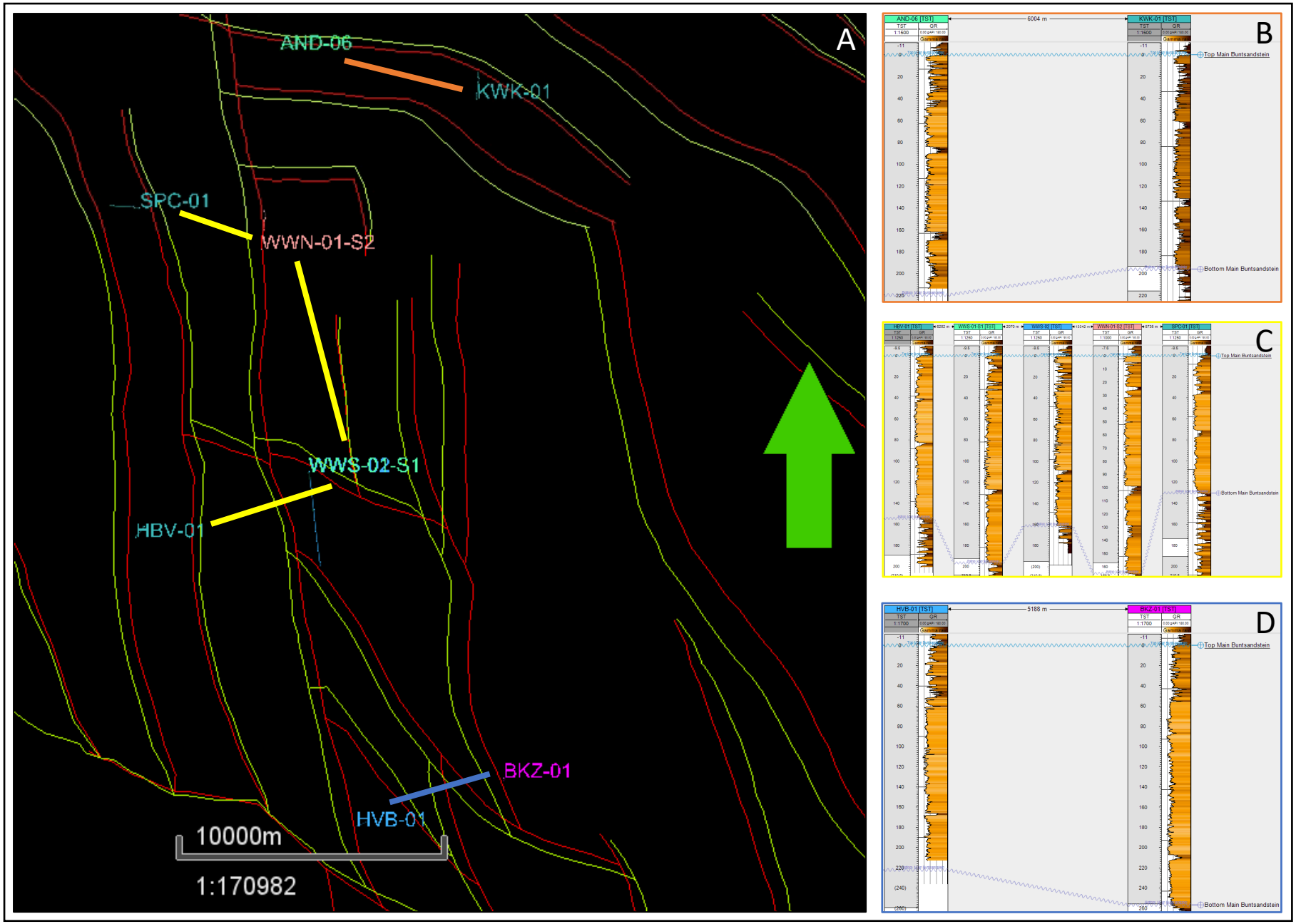

Figure 10: Structural map and regional well correlations (in true stratigraphic thickness) used to evaluate thickness trends across the basin. The structural map (A) suggests all wells are located on a structural high. The well correlations (B, C and D) indicate that the southern cluster (B) shows considerable thicker Main Buntsandstein deposits, which is also true for the northern cluster (D). The middle cluster of wells (C) displays a varying thickness.

3.2 Reservoir Sedimentology

Four different wells are studied for the reservoir sedimentology part of the research, namely: AND-06, KWK-01, SPC-01 and WWN-01-S2. A lithofacies and facies association scheme is constructed in order to describe the different heterogeneities encountered in the cores. Table 1 in the materials chapter displays the information that is covered by the different cores. Note that not the whole Main Buntsandstein Subgroup is cored in each well, but only specific stratigraphic intervals. The objective of the core study is: (1) to characterize the lithofacies and facies associations of the Main Buntsandstein according to the available core sections; (2) to interpret the depositional environment of the different facies associations and (3) to present a stratigraphic framework of the study area (i.e., an interpretation on the depositional environment of the stratigraphy). The latter is proposed in order to build a facies architectural model at well scale spacing in the Tilburg area.

3.2.1 Lithofacies Classification

The KWK-01, SPC-01 and WWN-01-S2 were logged at a scale of 1:25 whereas the AND-06 was logged at a scale of 1:10. The full core description logs are shown in Appendix A. Ten separate lithofacies are distinguished and are shown in Table 3 below including a short description and picture. The total lithofacies distribution is shown in Figure 11, whereas Figure 12 displays the lithofacies occurrence per well. Lithofacies **S1/2,w/l** ("Wavy/Subparallel Bedded Very Fine to Fine Sandstones") is the dominant present lithofacies found within the studied cores (Figure 11).

The lithofacies table show some of the results conducted during the petrophysical properties analysis as the mean ("$\bar{x}$") and median ("*$\tilde{x}$"*) value for both the porosity and (horizontal/vertical) permeability is given according to the number of measurements ("#") for each measurement type. A more detailed analysis on the petrophysical properties is provided later in this report.

*Medium to Coarse Sandstones with Clasts: **S3/4,m/l***

This lithofacies comprises of medium- to coarse-grained sandstones with high amount (>30 %) of clay (grey; 7/2-5YR) and dolomite (brown; 6/4-5YR) clasts. The clasts, that range in size of around 1 – 10 mm, are locally imbricated and scour surfaces are often found at the base by displaying an irregular surface between the underlying lithofacies and **S3/4,m/l**. Overall, this lithofacies is poorly sorted due to the high number of clasts. It is encountered in the cores of wells AND-06 and KWK-01 only.

*(Sub)Parallel Laminated Sandstones with Clasts: **S2/3,l***

This lithofacies consists of fine- to medium-grained, (sub)parallel laminated sandstones. It includes a high amount of subangular to subrounded clay and dolomite clasts (with sizes of ca. 0.5 – 10 mm) and is therefore poorly sorted. The clasts are predominantly oriented with

the long axis along the bedding plane. Overall, this lithofacies is strongly cemented and can be found in the cores of AND-06 and KWK-01.

*Massive Sandstones: **S2/3,m***

This lithofacies consists of fine- to medium-grained homogeneous sandstones. It has a homogeneous appearance, but locally includes clay (grey; 7/2-5YR) and/or dolomite (brown; 6/4-5YR) clasts. Their size ranges from 1 to 5 mm and are commonly subrounded. The lithofacies is moderately to strongly cemented by calcite minerals. It is present in the cores of wells AND-06, KWK-01 and SPC-01.

*(Sub)Parallel Laminated Sandstones: **S2/S3,l***

This lithofacies consists of (sub)parallel-laminated, fine- to medium-grained sandstones. Fining-upward structures are locally present as well as mica laminae. Scour surfaces, which have an irregular surface appearance, can sometimes be found on top of this lithofacies. Dolomite clasts, with sizes of 1 – 5 mm, appear locally in this lithofacies. **S2/3,l** is encountered in wells AND-06 and KWK-01 only.

*Fine to Medium Cross-Stratified Sandstones: **S2/S3,xl-xh***

This lithofacies consists of fine- to medium-grained sandstones showing cross-stratifications. Commonly, the cross-stratifications comprise of alternations of fine to medium grained sands with mica laminae and its size ranges from around 30 to 90 centimeters. The laminae generally steepen upwards from low to high angle cross-stratifications. Dolomite and/or clay clasts are also present locally within this lithofacies. It is present within the cores of wells AND-06 and KWK-01.

*Very Fine Cross-Stratified Sandstones: **S1/2,xl-xh***

This lithofacies is made up of very-fine to fine-grained, cross-stratified sandstones. It is moderately sorted and comprises of centimeter to decimeter bedding of the cross sets. Laminae seems to steepen upward from a bottomset at the base into foresets on top of a sequence. Finally, clay clasts, of 1 to 10 mm, are locally present within this lithofacies. **S1/2,xl-xh** is encountered in wells SPC-01 and WWN-01-S2, respectively.

*Wavy/Subparallel Bedded Very Fine to Fine Sandstones: **S1/2,w/l***

This lithofacies is made up of very-fine to fine sandstones alternated with clays/silts. Commonly, the scale of these alternations is a few mm's to centimeters. The bedding is wavy to subparallel in character. Locally, clay flakes, with sizes of 1 – 10 mm, are present in this lithofacies. It is encountered in the cores of wells SPC-01 and WWN-01-S2, respectively.

Mud Alternated with Fine Sands: ***M/S1,w,i***

This lithofacies comprises of dominantly mud alternated with (very) fine sands. These mud and sand layers are commonly a few mm's to 10 cm thick. Laminations are wavey in character and locally a strong influence of bioturbation is visible in the form of burrows, especially within the mud layers where mud is replaced by sand in the burrow. Furthermore, desiccation cracks and red oxidized layers, are sometimes present, especially within the muddy parts of this lithofacies. This lithofacies is located in the cores of well WWN-01-S2.

Mudstones: ***M/J,m/l***

This lithofacies consists of (sub)parallel laminated to massive shales and/or silts. It is often bounded by scour surfaces, usually on top of the lithofacies. Locally oxidation has affected the mudstones causing a reddish appearance. The mudstones are found in different colors (4/1-5YR; 5/1-5YR). They are encountered in all of the cores.

Paleosols: ***M/J,An***

This lithofacies is made up of shales/silts only that are strongly affected by pedogenic/soil forming processes. Oxidized layers and anhydrite nodules are common in this lithofacies. Anhydrite nodules have a greyish to whitish appearance and are ranging in size of 1 mm to up to 2 cm. Due to the presence of oxidized layers, the paleosols generally have a reddish appearance in the cores. This lithofacies is only encountered in the cores of wells AND-06 and KWK-01, respectively.

Table 3: lithofacies Tables A & B established from the core analysis from wells AND-06, KWK-01, WWN-01-S2 and SPC-01. The first row displays the lithofacies name and its corresponding Bunter Atlas code. The second row shows the key features and a small table displaying the number of measurements (#) for porosity and horizontal permeability for each lithofacies as well as the mean ("$\bar{x}$") and median ("$\tilde{x}$") of these properties. The bottom row shows a picture of the lithofacies including the scale.

Lithofacies Table A

Medium to coarse grained sandstones with clasts (S3/S4,m/l)	(Sub)parallel laminated sandstones with clasts (S2/3,l)	Massive sandstones (S2/3,m)	Sub)Parallel laminated sandstones (S2/S3,l)	Fine to medium cross-stratified sandstones (S2/S3,xl-xh)
• Med. to coarse grained • High % of clay (grey; 7/2-5YR) and dolomite (brown; 6/4-5YR) clasts • Poorly sorted • Locally imbrication • Often scour surface at base	• Fine to medium grained • Poorly sorted • High % of subangular to subrounded clasts (clay & dolomite) • Clasts are mostly imbricated • Strongly cemented •	• Fine to medium grained • Homogeneous • Locally clay (grey; 7/2-5YR) and/or dolomite (brown; 6/4-5YR) clasts • Moderately to strongly cemented (by calcite)	• Fine to medium grained • (Sub)parallel lamination • Locally presence of: - Fining upward structures - Scour surface on top - Dolomite clasts	• Fine to medium grained • Cross-stratified • Cm to dm bed scale • Laminae steep upwards • Locally dolomite and/or clay clasts present

Property Measurement	#	$\bar{x}$	$\tilde{x}$
Porosity [%]	19	3.57	3.5
Hor. Perm. [mD]	-	-	-

Property Measurement	#	$\bar{x}$	$\tilde{x}$
Porosity [%]	23	5.65	5.8
Hor. Perm. [mD]	1	0.02	0.02

Property Measurement	#	$\bar{x}$	$\tilde{x}$
Porosity [%]	20	8.84	6.2
Hor. Perm. [mD]	9	31.4	16.3

Property Measurement	#	$\bar{x}$	$\tilde{x}$
Porosity [%]	55	5.25	5.3
Hor. Perm. [mD]	9	0.058	0.04

Property Measurement	#	$\bar{x}$	$\tilde{x}$
Porosity [%]	24	6.02	6
Hor. Perm. [mD]	2	0.03	0.03

Lithofacies Table B

Very fine cross-stratified sandstones (S1/2,xl-xh)	Wavy/subparallel bedded (very) fine sandstone (S1/2,w/l)	Mud alternated with fine sands (M/S1,w,i)	Mudstones (M/J,m/l)	Paleosols (M/J,An)
• Very fine to fine grained • Cross-stratified • Cm to dm bed scale • Moderately sorted • Laminae steepen up • Locally presence of clay clasts	• Very fine to fine sands alternated with silts/mud • Poorly sorted • Irregular wavy lamination	• Alternations of (very) fine sands with mud • Ripple lamination of mud • Wavey lamination in sands • Heavily bioturbated • Local oxidized mud layers	• Shales/silts • (Sub)parallel to massive appearance • Locally bounded by scour surfaces • Found in different colors (4/1-5YR; 5/1-5YR)	• Shales • Strongly affected by pedogenesis • Locally oxidized • Anhydrite nodules are common

Property Measurement	#	$\bar{x}$	$\tilde{x}$
Porosity [%]	379	8.51	8.6
Hor. Perm. [mD]	332	3.15	0.15

Property Measurement	#	$\bar{x}$	$\tilde{x}$
Porosity [%]	177	12.02	12.1
Hor. Perm. [mD]	172	19.77	2.3

Property Measurement	#	$\bar{x}$	$\tilde{x}$
Porosity [%]	42	2.5	2.1
Hor. Perm. [mD]	20	0.25	0.09

Property Measurement	#	$\bar{x}$	$\tilde{x}$
Porosity [%]	10	4.23	3.2
Hor. Perm. [mD]	4	0.098	0.01

Property Measurement	#	$\bar{x}$	$\tilde{x}$
Porosity [%]	28	3.19	3.35
Hor. Perm. [mD]	3	0.023	0.01

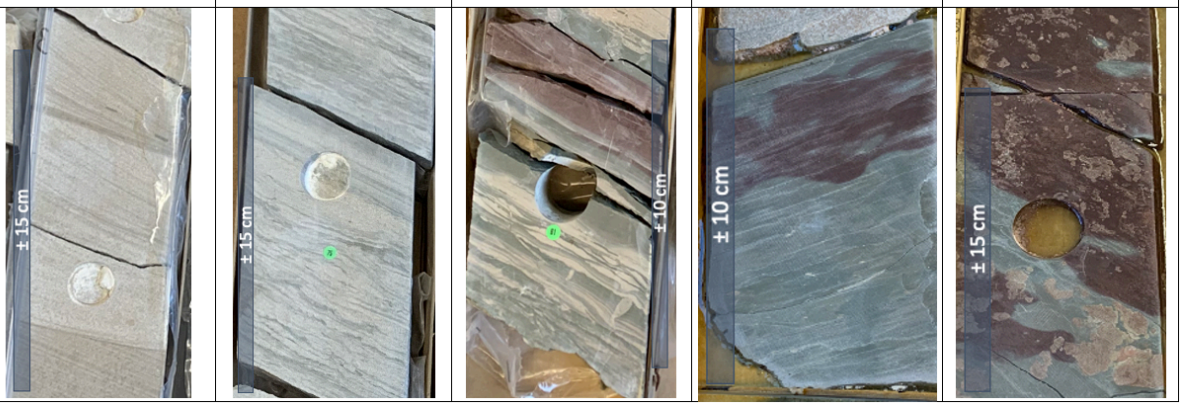

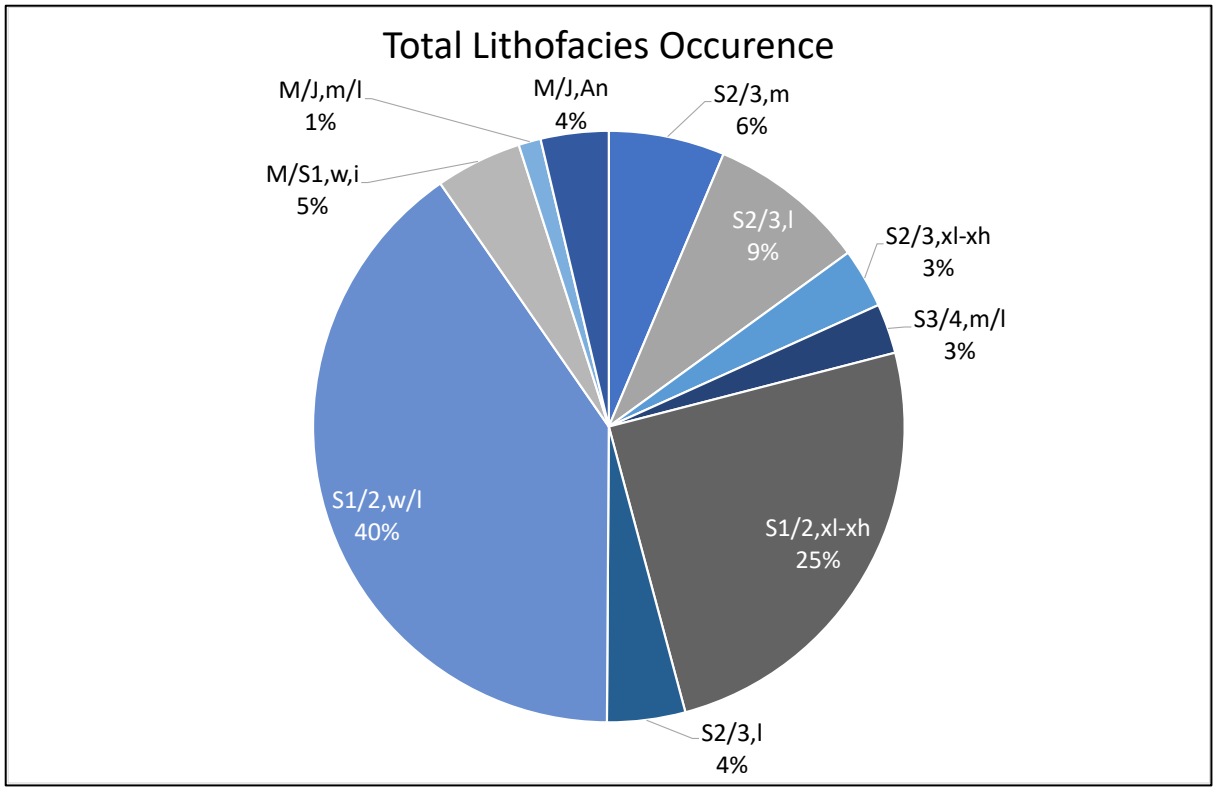

Figure 11: Total lithofacies occurrence of all the studied cores.

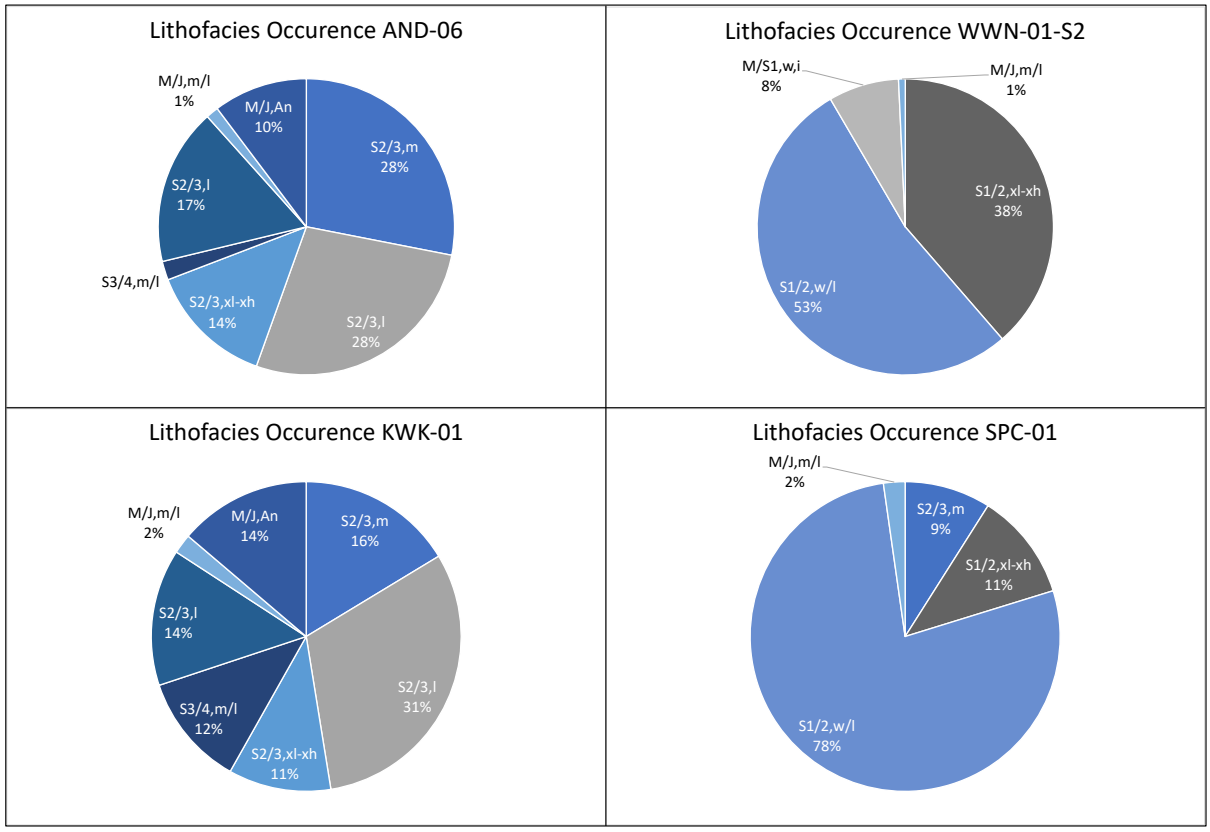

Figure 12: Lithofacies occurrence per cored well.

3.2.2 Facies Association Classification

The lithofacies are grouped into four facies associations (FA1 to FA4) that describe an architectural element within the depositional system of the area. The classification is based on lithology, contacts, and depositional structures. Table 4 below displays the four separate facies associations including a picture, key features, a table of petrophysical property measurements, and finally an interpretation on its depositional environment. The facies associations (FA1 – FA4) are named as follow:

- FA1: Braided Channel Element Facies
- FA2: Fluvial Fan Dominated Facies
- FA3: Playa Lake Facies
- FA4: Overbank/Floodplain Facies

Figure 13 shows the total occurrence of all facies encountered in the core study, whereas Figure 14 displays the occurrence of these facies in each individual cored well. Wells AND-06 and KWK-01, that belong to the Detfurth and Hardegsen Formations according to NLOG (see Table # in materials chapter), only consist of the FA1 and FA2. The cores from SPC-01 are from the Detfurth and Volpriehausen Formations according to NLOG whereas the WWN-01-S2 cores penetrate all formations of the Main Buntsandstein (see Table 1 in materials chapter), and both only comprise of facies associations three and four.

The facies association tables show some of the results conducted during the petrophysical properties analysis as the mean ("$\bar{x}$") and median ("*$\tilde{x}$")* value for both the porosity and (horizontal/vertical) permeability is given according to the number of measurements ("#") for each measurement type. A more detailed analysis on the petrophysical properties is provided later in this report.

FA1: Braided Channel Element Facies

Description:
This facies association comprises of the following lithofacies massive sandstones ("**S2/3,m**"), medium to coarse grained sandstones with clasts ("**S3/4,m/l**"), fine to medium cross-stratified sandstones ("**S2/3,xl-xh**"), (sub)parallel laminate sandstones ("**S2/3,l**"), mudstones ("**M/J,l**") and paleosols ("**M/J,An**").

It is often characterized by the presence of an erosive base and top. The bottom of FA1 often consists of a basal lag of medium to coarse grained sandstones with clasts ("**S3/4,m/l**"), containing an high amount of (dolomite/clay) clasts followed by finer cross-stratified sands from **S2/3,xl-xh** lithofacies which make up the bottom- and foresets of a dune. Usually, the cross-stratifications steepens upwards from the bottom to the foresets and are sometimes topped by a fine grained parallel laminated sandstone ("**S2/3,l**") containing an high amount of mud.

In case when the bottom sets are significantly thick, aggradation of the dune happened vertically rather than laterally. The variation in this bottom set thickness can be explained by

a change in flow strength in the channels. Scour surfaces are often found on top of the foresets of this facies association. Furthermore, clay flakes are rarely present in FA1 as well as thin mud layers (< 50 cm). This facies association displays considerable low gamma-ray values and sometimes shows fining upward sequences (Table 5).

Interpretation:
Erosive based, commonly fining upward and presence of cross-stratifications suggest high energy, fluvial dominated deposits in confined braided channels as stacked channel fill units. The abundance of cross-stratified sandstones indicates the formation of barforms in the channel as bottom- and foresets of a migrating river dune. However, the variation in bottom set thickness may be explained by a change in flow strength. Overall, the fining upward structure of FA1 suggests a loss in flow strength, which could be caused by either migration of the channel and/or internally change in hydrodynamics of the river.

The fact that scouring surfaces combined with basal lag deposits containing a significant number of clasts, are often found at the base of this facies, indicates migration/avulsion of the fluvial braided channels. Presence of clay and/or dolomite flakes/nodules suggest erosion of the levees/banks by the rivers whereas the rare existence of thin mud layers indicate channel plug deposits as the result of channel migration.

FA2: Fluvial Fan Dominated Facies

Description:
This facies association comprises dominantly of the lithofacies very-fine cross-stratified sandstones ("**S1/2,xl-xh**") and in lesser extent of wavy/subparallel bedded (very) fine sandstones ("**S1/2,w/l**") and mudstones ("**M/J,l**"). It is characterized by fine-grained sandstones showing parallel- to cross-stratified laminations with locally wavy bedding structures. Occasionally, decimeter- to meter-scale fining upward structures occur in this facies association. Often, a sequence is topped by an interval (10-30 cm) of significant finer sands and/or mud drapes whereas clay flakes locally appear in FA2. Furthermore, scour surfaces are rare within these facies. This facies association shows significant low values on the gamma-ray wireline log with a blocky character (Table 5).

Interpretation:
Parallel to cross-stratified sandstones record deposition under a variety of weakly channel-confined conditions whereas the presence of wavy-parallel sandstone suggest periodically deposition under unconfined conditions. This difference is predominantly determined by the availability of water, the amount and type of sediment being carried by the flow and the gradient of the surface (Nichols, 2009). The abundance of clay flakes either indicates channel erosion of the overbank/levee muds or channel reworking of mud drapes. The fact that it consists of predominantly fine-grained sandstones implies a relatively distal setting from the source in an arid to semi-arid environment.

FA3: Playa Lake Facies

Description:
This facies association (FA3) only comprises of the lithofacies mud alternated with fine sands ("**M/S1,w,l**") and mudstones ("**M/J,l**"). It is characterized by heterolithic deposits consisting of millimeter- to centimeter-scale alternations of mudstones and very fine to fine-grained sandstones. Overall, the playa-lake facies display meter-scale fining upward. Wave-ripple and current-ripple lamination are abundant, as well as desiccation fabrics and oxidized mud layers. Evidence of bioturbation (in the form of burrows) are rarely present. The top of this facies is commonly characterized by a scour surface. This facies association predominantly shows high gamma-ray values on the wireline log due to the presence of mudstones. Locally, thin layers with low gamma-ray values occur caused by the presence of sandy intervals (Table 5).

Interpretation:
These muddy dominant deposits display low-energy deposition in a playa environment. It is characterized by irregular sand deposition and erratic water table conditions that fluctuated between subaqueous and subaerial conditions, as is visible from the oxidized mud layers. Sands were deposited when the run-off and thus energy to the playa-lake was larger compared to the deposition of the mud. Sediments were deposited by a distal fluvial/alluvial fan system terminating in a playa lake environment.

FA4: Floodplain Facies

Description:
Facies association (FA2) displays floodplain deposits that solely consists of lithofacies mudstones ("**M/J,m/l**") and paleosols ("**M/J/An**"). Commonly FA4 comprises of solely mudstones and little amount of very fine sands. Pedogenic mudstones are locally present and show intensive mottling of the sediments, which gives them a reddish to brown-greyish appearance. Anhydrite nodules are frequently present as well. Traces of bioturbation are visible in the form of burrows; however, no specific animals can be detected. Lastly, desiccation cracks are locally detected in FA4. This facies association is represented by high gamma-ray values (Table 5).

Interpretation:
the presence of (pedogenic) mudstone suggest soil formation in a low energy vegetated floodplain environment. Deposition happened by flooding of the channels resulting in predominantly muddy deposits. The existence of sandy layers in FA4 implies breaching of the fluvial channels, leaving crevasse splay deposits behind on the floodplain. Presence of anhydrite nodules suggests the formation of initial gypsum on the floodplain that transformed into anhydrite during the burying process whereas the presence of scour surfaces on top of this facies indicates frequent avulsion of the channels through the floodplain environment, leaving a distinct erosional boundary (scour surface) between FA4 and FA1.

Table 4: facies association Tables A & B established from the core analysis from wells AND-06, KWK-01, WWN-01-S2 and SPC-01. The first row displays the lithofacies name and its corresponding Bunter Atlas code. The second row shows the key features and a small table displaying the number of measurements (#) for porosity and horizontal permeability for each lithofacies as well as the mean ("$\bar{x}$") and median ("$\tilde{x}$") of these properties. The bottom row shows a picture of the facies association including a scale. The yellow dashed line represents the bottom, whereas the grey-whitish dashed line represents the top of a facies sequence.

Facies Associations Table A

FA1 Braided Channel Element: *S3/4,m/l S2/S3,xl-xh S2/S3,l S2/3,m M/J,l*

- Poorly to medium sorted
- Fine to medium grained with often high % of clasts at the base
- Erosive base and top
- Locally displays bottom- and foresets of migrating bedforms

Property Measurement	#	$\bar{x}$	$\tilde{x}$
Effective Porosity [%]	162	5.46	5.50
Hor. Permeability [mD]	13	0.04	0.03
Ver. Permeability [mD]	-	-	-

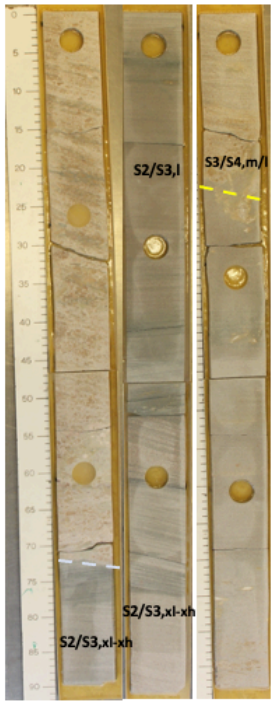

FA2 Fluvial Fan Dominated Deposits: *S1/2,xl-xh S1/2,w/l M/J,l*

- Dominantly low to high angle cross-stratifications with some horizontal wavy beddings
- Set thickness varies from cm to dm scale
- Local presence of clay clasts
- Often topped by a 1 – 20 cm thick mudstone unit

Property Measurement	#	$\bar{x}$	$\tilde{x}$
Effective Porosity [%]	562	9.70	9.40
Hor. Permeability [mD]	510	9.27	0.28
Ver. Permeability [mD]	204	13.08	0.35

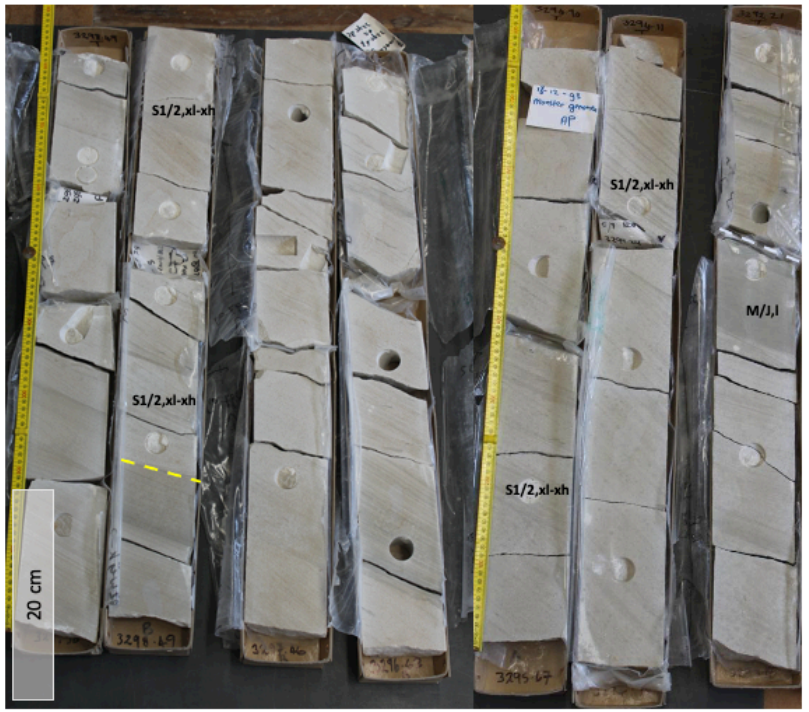

Facies Associations Table B

FA3 Playa Lake Deposits: *M/S1,w,i M/J,l*

- Heterolithic deposits: alternations of shales/silts with fine sands
- Wavy bedding
- Locally desiccation cracks and oxidized layers
- Indications of bioturbation: presence of burrow traces
- Erosive top

Property Measurement	#	$\bar{x}$	$\tilde{x}$
Effective Porosity [%]	42	2.50	2.10
Hor. Permeability [mD]	20	0.25	0.09
Ver. Permeability [mD]	10	0.02	0.01

FA4 Floodplain Deposits: *M/J,m/l M/J,An*

- Dominantly shales and silts
- Locally affected by pedogenesis (Image I & II) and oxidation (Image I)
- Anhydrite nodules are common
- Locally indications of bioturbation

Property Measurement	#	$\bar{x}$	$\tilde{x}$
Effective Porosity [%]	33	3.48	3.30
Hor. Permeability [mD]	5	0.09	0.01
Ver. Permeability [mD]	1	0.01	0.01

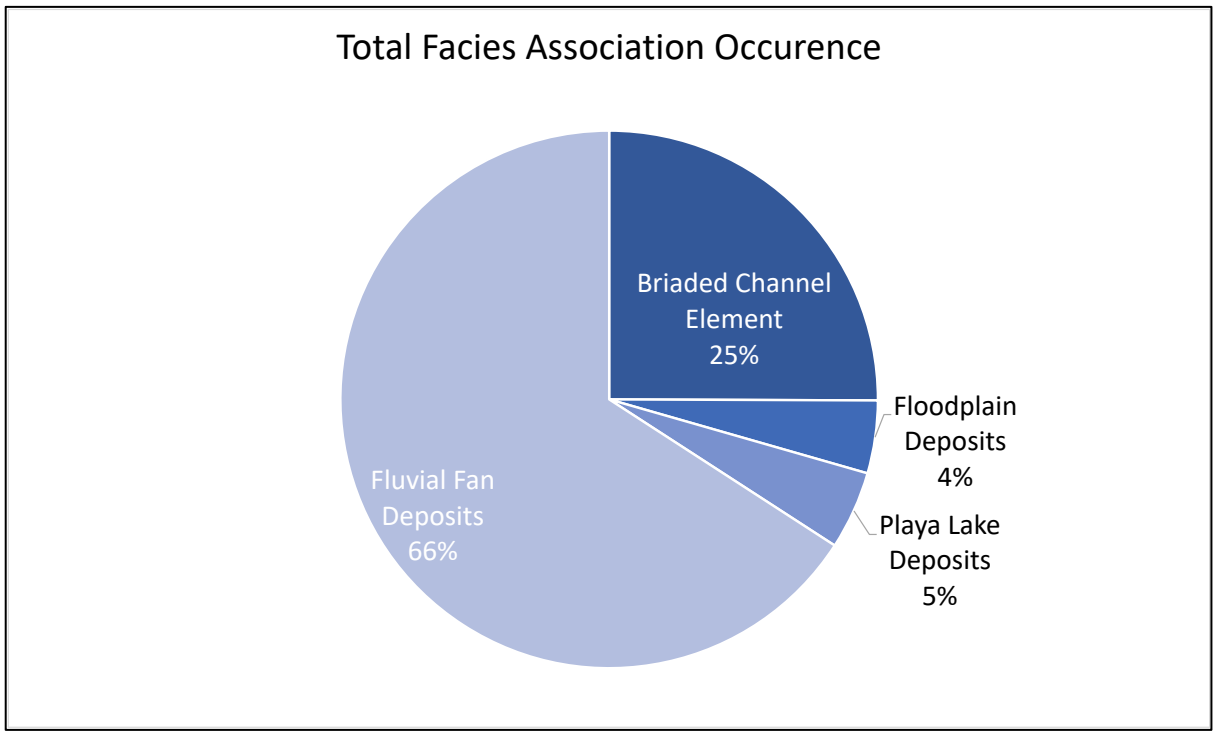

Figure 13: The total occurrence of the facies associations encountered in all studied cores (AND-06, KWK-01, SPC-01 and WWN-01-S2.

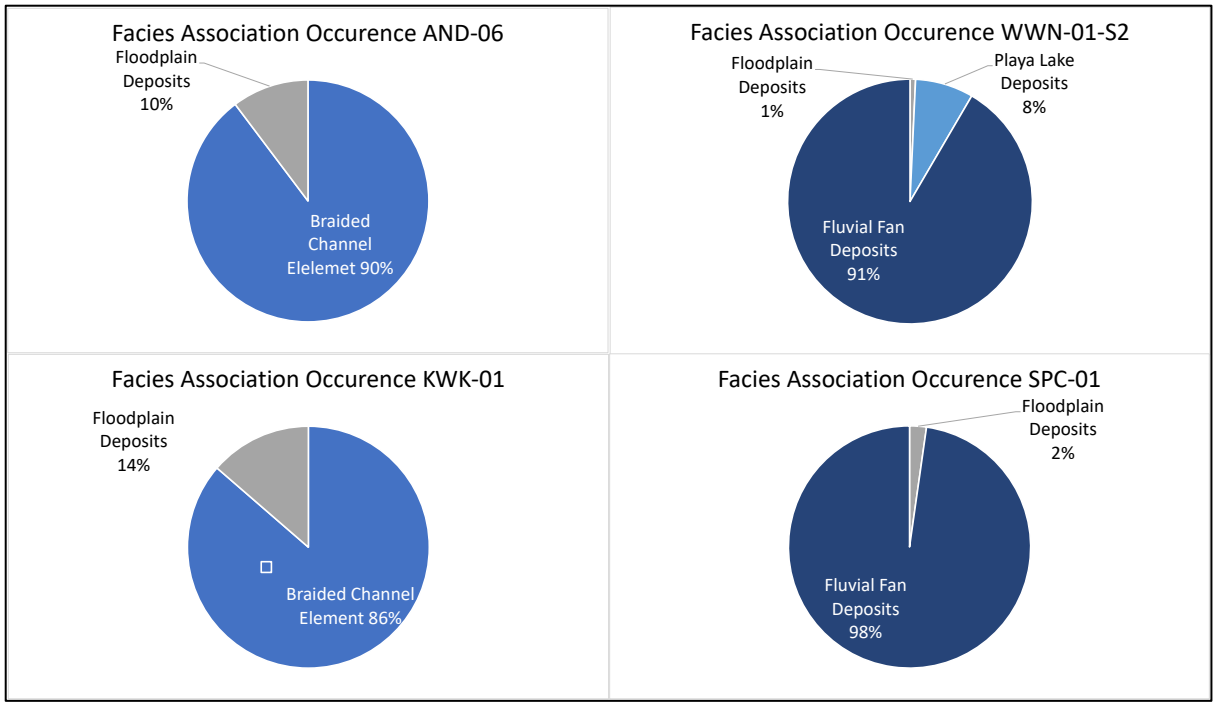

Figure 14: The occurrence of all facies associations per studied cored well (AND-06, KWK-01, WWN-01-S2 and SPC-01).

Facies Association Log Response

The classification of the lithofacies and facies associations in the cores allows it to describe the reservoir sedimentology in each well, which is in the next paragraph used to build the facies architecture model of the full Main Buntsandstein Subgroup at well scale. Each facies association is associated with a specific gamma-ray signature on the wireline log, which is described in the previous paragraph for FA1 to FA4. Table 5 displays these different signatures as well as a description and depositional architecture of the facies association, which are needed to build the facies architecture model provided in the discussion.

Table 5: Gamma-ray wireline signature and description of each facies association together with the interpreted depositional architecture.

Facies Association	Gamma-Ray Signature	Gamma-Ray Description	Depositional Architecture
FA1	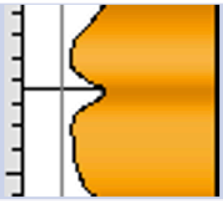	Bell shape gamma-ray wireline response.	Single (sometimes fining-upward) braided fluvial sandstones, often bounded by FA3.
FA2	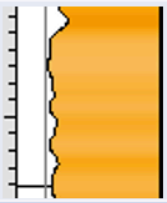	Blocky gamma-ray wireline response.	Stacked (horizontally and vertically) amalgamated pattern of fluvial-fan sandstone bodies.
FA3	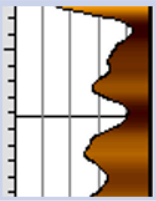	Irregular gamma-ray wireline response, predominantly displaying high values.	Widespread playa-lake mudstones. Regional correlation marker on wireline logs.
FA4		High gamma-raywireline values.	Floodplain mudstone intervals encountered between braided channel facies (FA1).

The cores of well WWN-01-S2 (3169 – 3305.5 m) consist predominantly of FA2 and in lesser extent of FA1, FA3 and FA4 (Figure 15). The bottom part, with depths of 3305.5 to 3193 meter are characterized by predominantly fluvial fan facies deposits (FA2). In between, at depths of 3279 - 3287.5 m, a low net-to-gross layer of playa-lake facies deposits (FA3) exists, which is also the case on top of the fluvial fan facies from depths 3194 – 3197 m. Upon the above playa-lake deposits, the stratigraphy is controlled by braided channel deposits (FA1) with minor floodplain intervals (FA4). Overall, the net-to-gross of this well is relatively high.

The cores from SPC-01 (2647 – 2674.5 m) are solely composed of stacked fluvial-fan facies (FA2). Its net-to-gross is therefore considerably high (Figure 15).

Cores taken from well KWK-01 (2548 – 2601.6 m) are composed of alternations of braided channel facies (FA1) and overbank/floodplain facies (FA4). The net-to-gross of this cored section is relatively lower due to the significant presence of mudstones in the floodplain facies (Figure 15).

The core of AND-06 (2894 – 2910.5 m) comprises of alternations of braided channel facies (FA1) and floodplain facies (FA4). Net-to-gross of the core is considered as intermediate (Figure 15).

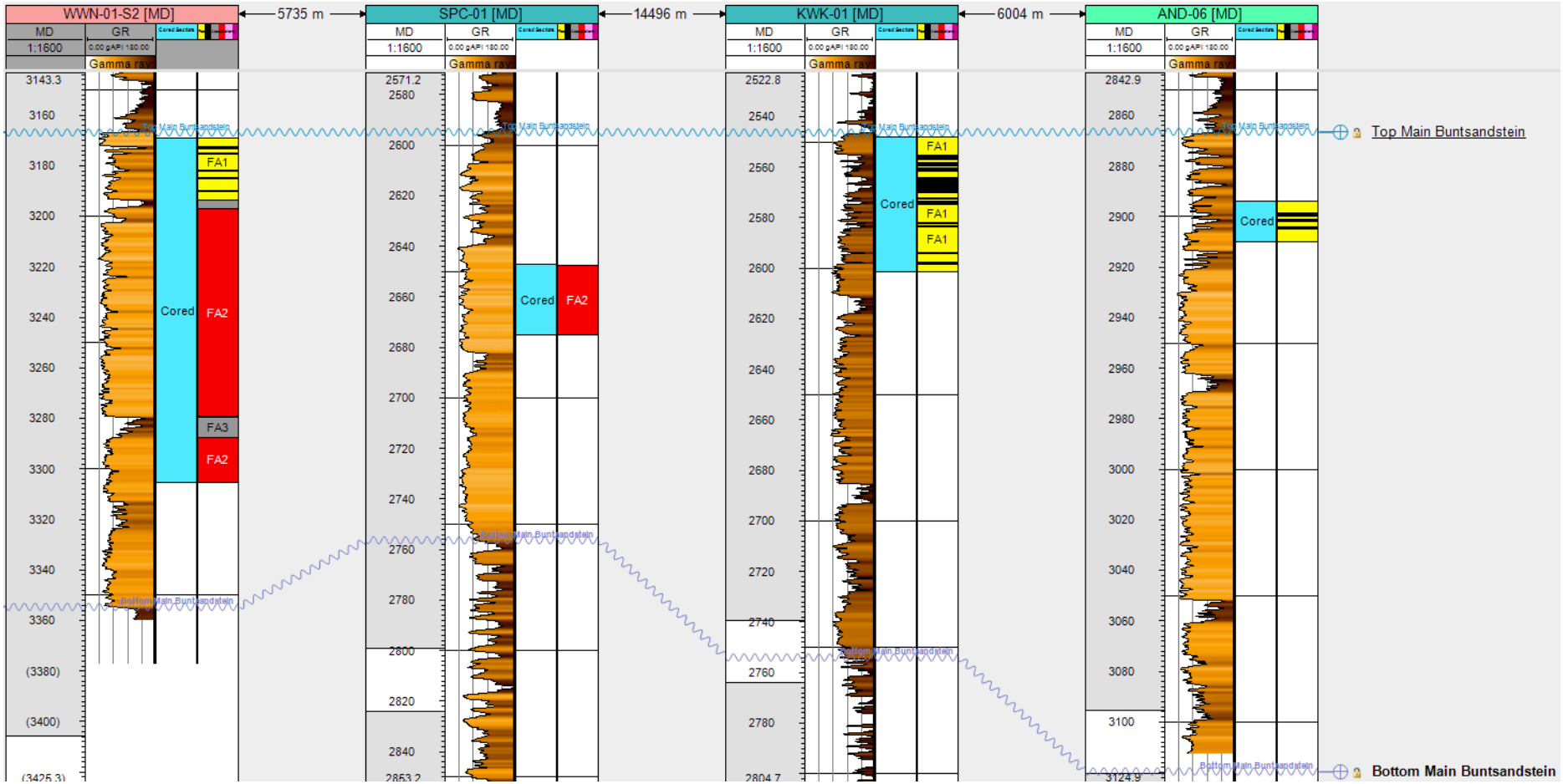

Figure 15: Well log panel of the cored wells (AND-06, KWK-01, SPC-01 and WWN-01-S2) displaying the gamma-ray wireline response, cored section, and interpreted facies association versus the measured depth (MD). FA1 is the braided channel element facies (yellow), FA2 is the fluvial fan dominated facies (red), FA3 the playa-lake facies (grey) and FA4 is the floodplain facies association (black).

3.3 Petrophysical Property Evaluation

3.3.1 Cored Wells

Figures 16 and 17 display all of the porosity and permeability measurements from the four wells that contain core plug measurements on porosity and permeability (AND-06, KWK-01, SPC-01 and WWN-01-S2). It shows highly variable porosity and permeability values ranging from circa 1 - 22 % for the porosity and 0.01 to circa 500 mD for the permeability, respectively. Moreover, no relationship with present-day depth can be distinguished.

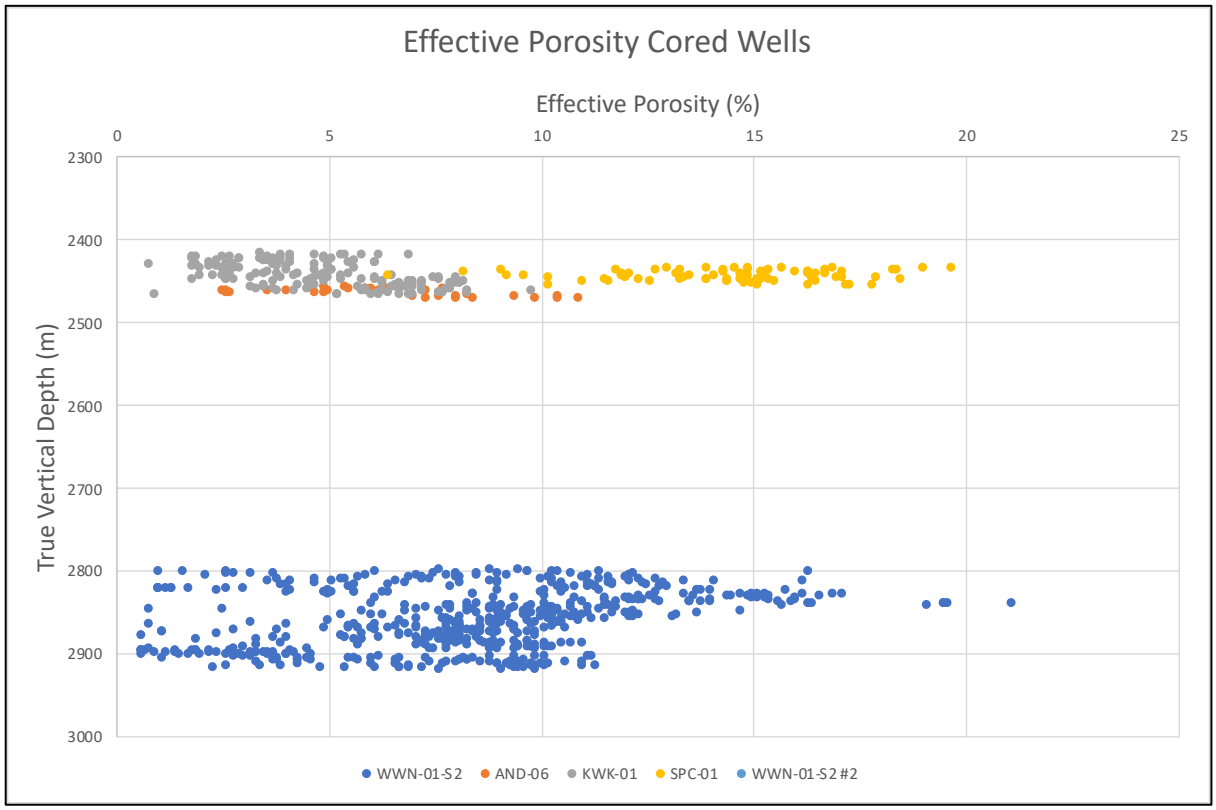

Figure 16: Porosity (%) measurements taken from the core plugs plotted versus the true vertical depth. The results indicate highly variable porosity measurements ranging from circa 1 – 21%. Horizontal permeability results also display highly variable values ranging from 0.01 to ca. 500 mD. No relationship with present-day depth can be distinguished. The different colors represent the separate data sets from the cored wells that are taken from NLOG.nl

Porosity (effective) and permeability core plugs measurement are used to study the controls on aquifer quality of the Main Buntsandstein for the cored wells. A positive relationship between the porosity and permeability of the cored wells is established, indicating higher permeability values for higher porosity values (Figure 18).

Some core plugs from the SPC-01 and WWN-01-S2 wells have measurements on both the horizontal and vertical permeability, such that permeability anisotropy ratio (kv/kh) can be inferred. Figure 19 shows that this ratio is just a bit below 1. This indicates that the horizontal permeability is commonly a bit higher than the vertical permeability, which is likely caused by the horizontal layering of the sediments at bedding scale.

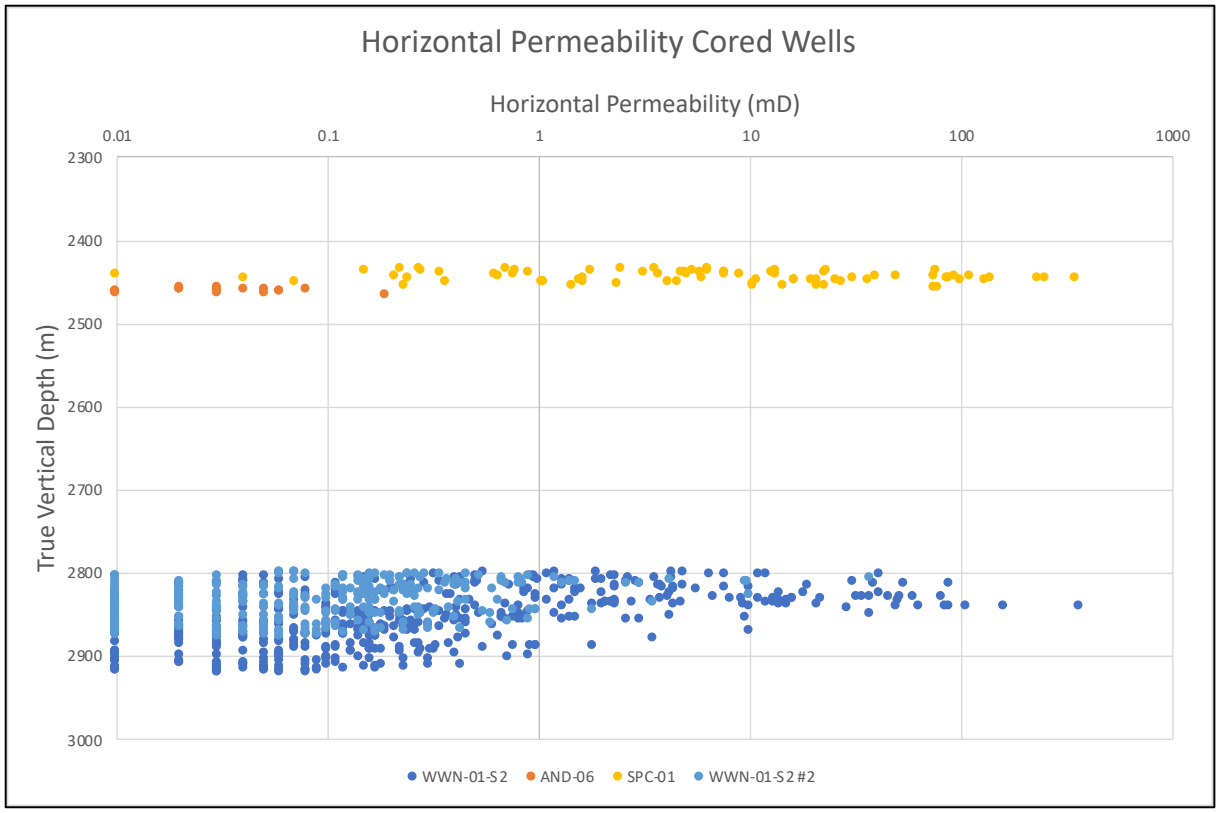

Figure 17: Horizontal permeability (mD) measurements taken from the core plugs plotted versus the true vertical depth. The results display highly variable values ranging from 0.01 to ca. 500 mD. No relationship with present-day depth can be distinguished. The different colors represent the separate data sets from the cored wells that are taken from NLOG.nl

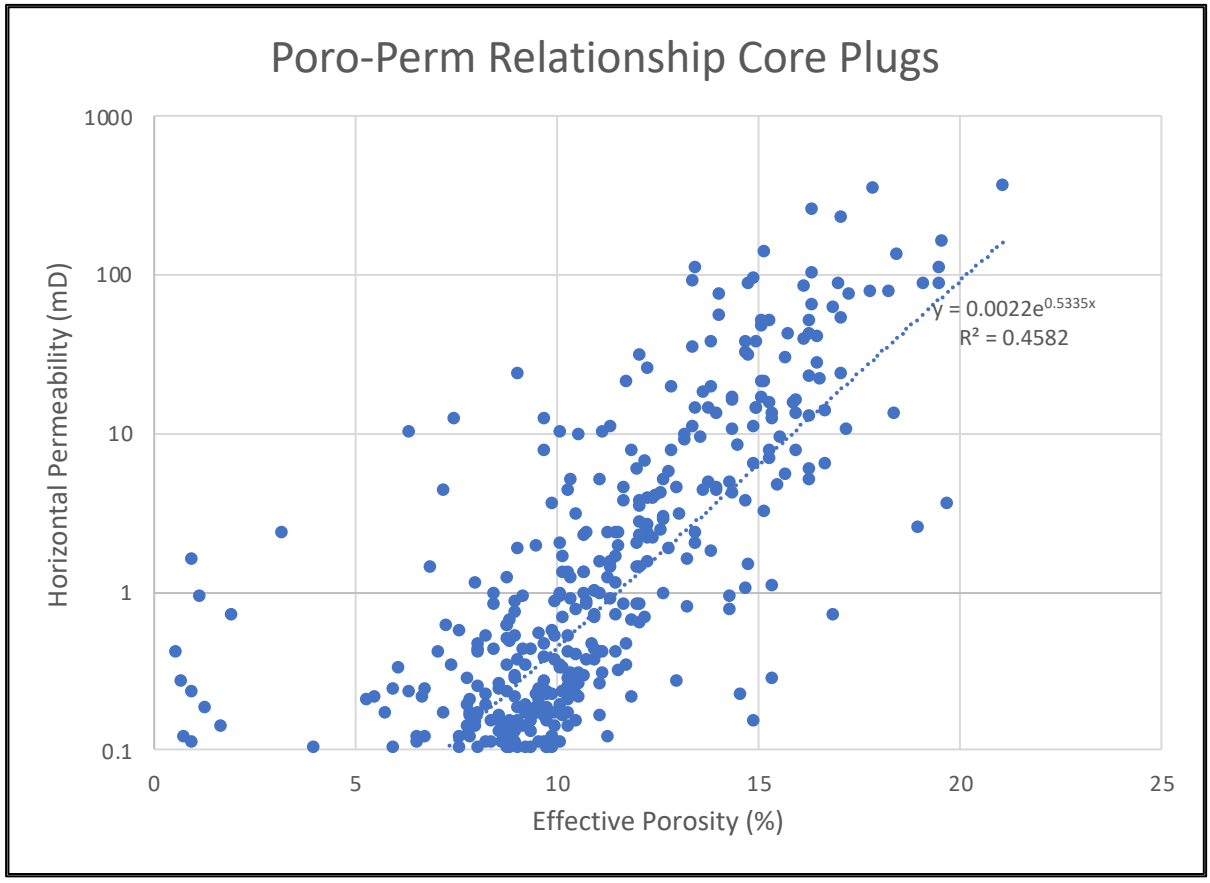

Figure 18: Porosity versus permeability plot of the cored wells. The graph clearly shows a positive relationship between the two petrophysical parameters. The core plug data is taken from NLOG.nl

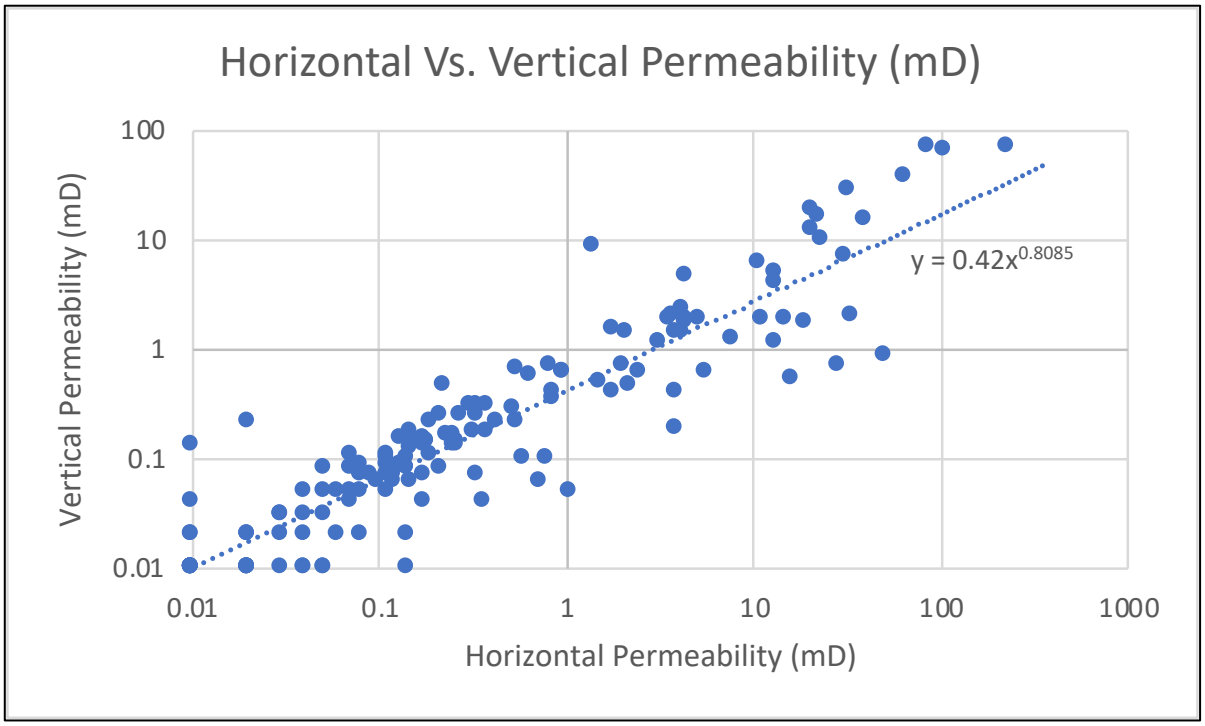

Figure 19: Horizontal versus vertical permeability plot showing that the kv/kh values is slightly below 1 indicating in higher horizontal permeability values than vertical. Most likely caused by initial horizontal layering of the sediments during deposition. Core plug measurements are taken from NLOG.nl

As the present-day depth lacks a control on the aquifer quality, a deeper inside into the control on reservoir sedimentology is conducted by plotting the data versus (1) the lithofacies scale and (2) facies association scale (Figure 20 and 21). Plug measurements at lithofacies scale show highest mean porosity is found within the wavy/subparallel bedded (very) fine sandstone lithofacies ("**S1/2,w,l**"), whereas the highest mean permeability belongs to the massive sandstones ("**S2/3,m**"). The results indicate that the lithofacies containing a significant amount of mud commonly have poorer reservoir quality potential than lithofacies containing sand. Very fine cross-stratified sandstones ("**S1/2,xl-xh**") and wavy/subparallel bedded (very) fine sandstone lithofacies ("**S1/2,w,l**") appear to have the optimal combination in porosity and permeability values, with mean porosity values of around 10%. Permeability data is highly scattered with mean values of 3.15 mD and 19.8 mD, respectively. The number of data points per lithofacies can be found in Table 3.

Petrophysical measurements for the facies associations (Figure 21) show highest mean values, for all three measurements, for the fluvial-fan facies association which counts to 9.70%, 9.27mD and 13.08mD for the effective porosity, horizontal permeability, and vertical permeability, respectively (plot of the vertical permeability is given in Appendix B). However, the median (namely 0.28 and 0.35) of both permeability measurements deviates significantly of the mean due to strongly scattering of the dataset. Scattering of this facies is most likely caused by smaller sedimentary internal heterogeneities such as local sand cementation. Measurements on FA1, FA2 and FA3 display mean (horizontal) permeability of below 1 mD and mean porosity values below 6 %, indicating poor reservoir quality potential. The number of data points per facies association can be found in Table 4.

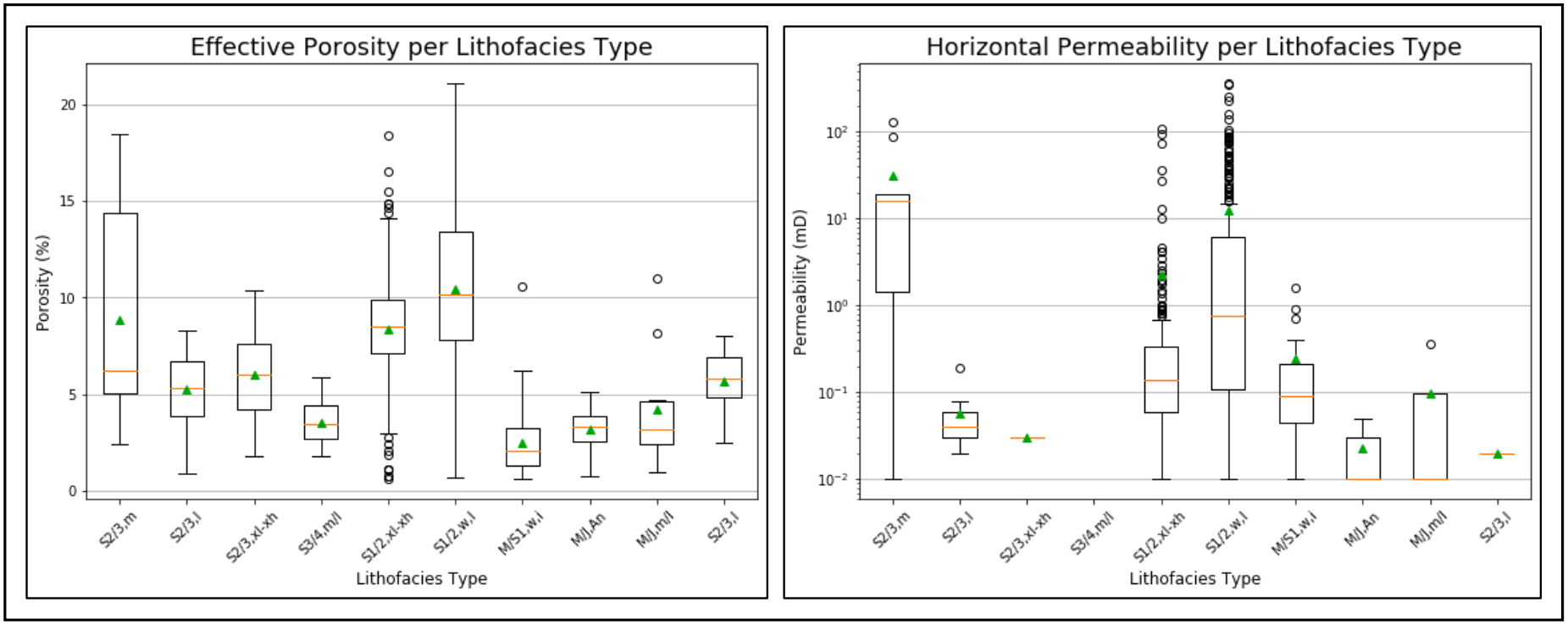

Figure 20: Box-cross plots displaying the effective porosity and permeability of the different lithofacies encountered in the cored wells. The box refers to the main body of the boxplot showing the lower and higher quartiles and the median (yellow line). The green triangle represents the means of each dataset. Individual points display the outliers, whereas the whiskers refer to the minimum and maximum of each dataset. The number of measurements per lithofacies are shown in Table 3.

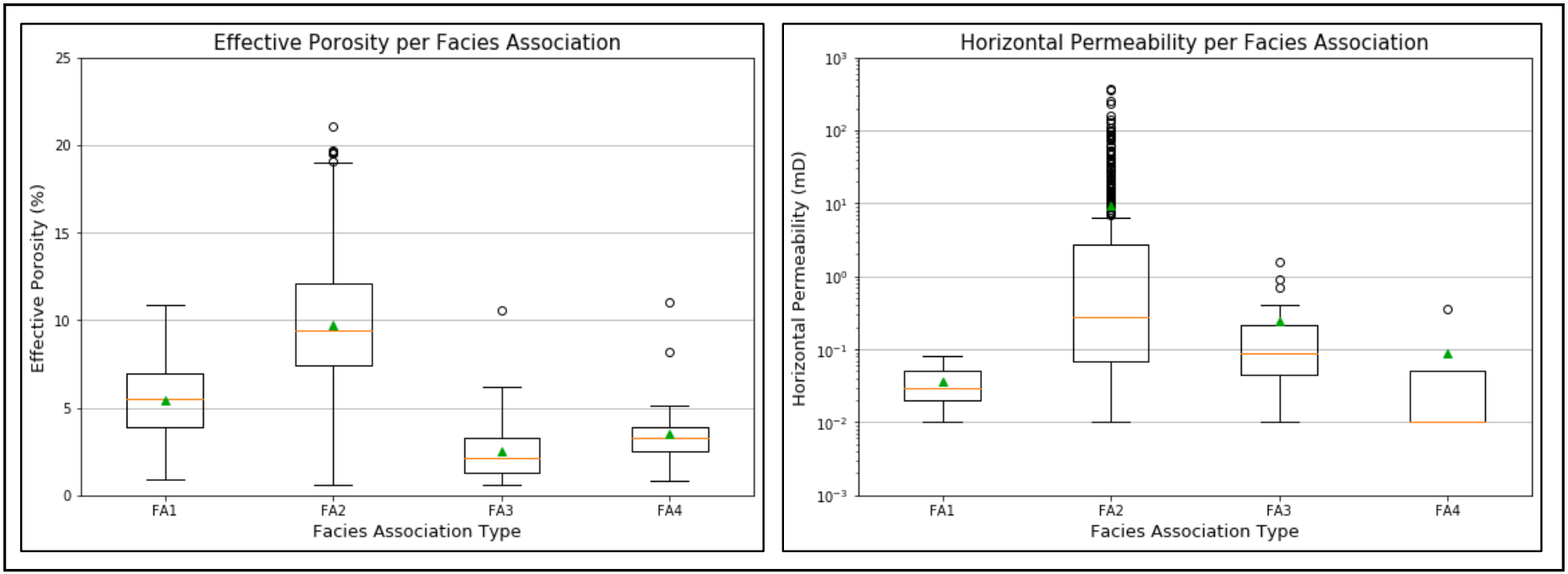

Figure 21: Box-cross plots displaying the effective porosity and horizontal/vertical permeability of the different facies associations encountered in the cored wells. The box refers to the main body of the boxplot showing the lower and higher quartiles and the median (yellow line). The green triangle represents the means of each dataset. Individual points display the outliers, whereas the whiskers refer to the minimum and maximum of each dataset. The number of measurements per facies association are displayed in Table 4.

3.3.1 Uncored Wells

Calculated well logs are used to study the petrophysical properties of the wells that do not contain direct core plug measurements. These corresponding wells are the BKZ-01, HVB-01, WWS-01-S1, WWS-02 and the calculated properties are the effective porosity, total porosity, and horizontal permeability. The plots for the effective porosity and horizontal permeability per well are plotted versus the measured depth in Figures 22 and 23. Total porosity plots are displayed in Appendix B. At first, the porosity measurements derived from the logs are compared to the direct measurements taken from the core plugs. The results show a nearly 1 to 1 correlation between the two measurement types suggesting no correction cutoff needs to be applied for the petrophysical data derived from the well logs (Figure 22).

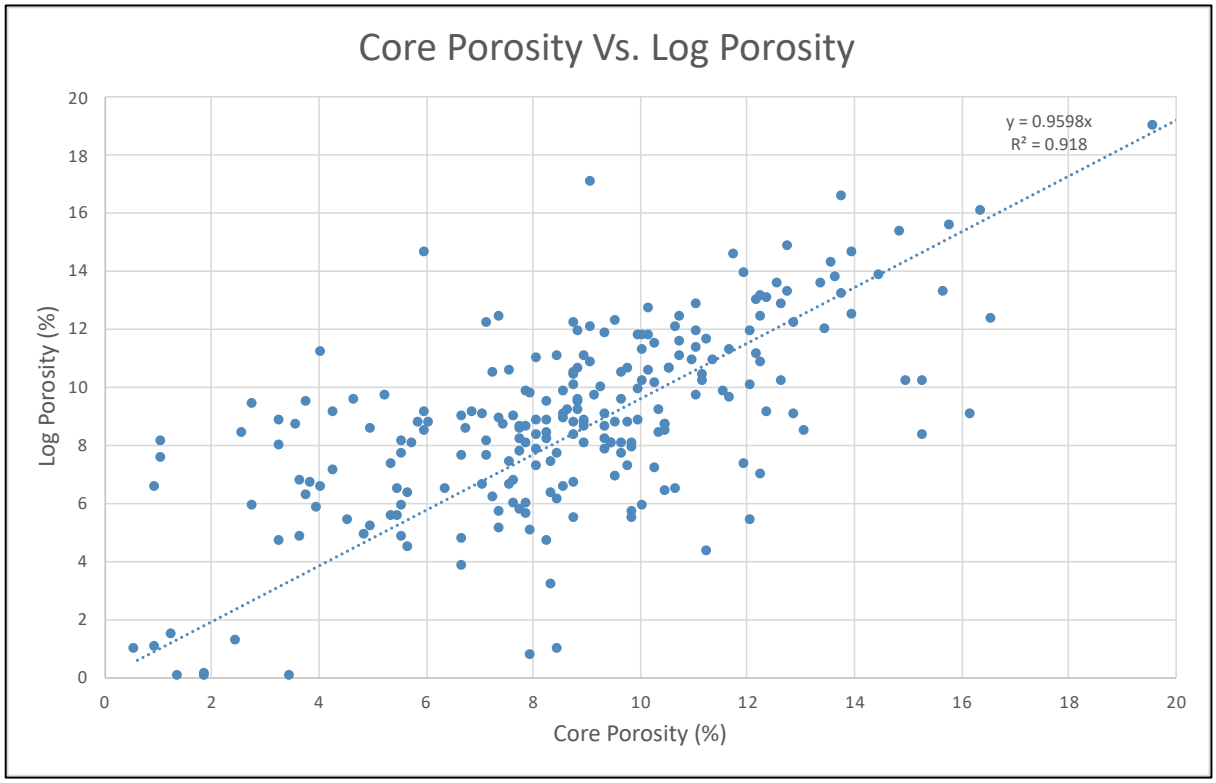

Figure 22: Core porosity versus well log porosity displaying a nearly 1 to 1 correlation of the two measurement types indicating no correction factor needs to be applied for the log measurements. The number of measurements amount to 235.

The effective porosity and permeability plots indicate a lack in relationship with present-day depth (Figures 23 and 24). Highest mean values of the effective porosity and horizontal permeability are encountered in well HBV-01 with values of 12.9 % and 148 mD, respectively. Wells WWS-01-S1, WWS-02 and BKZ-01 show mean values of 7.3 %, 7.2 % and 9.0 % for the effective porosity and < 1 mD, 8.9 mD and 56.0 mD for the horizontal permeability.

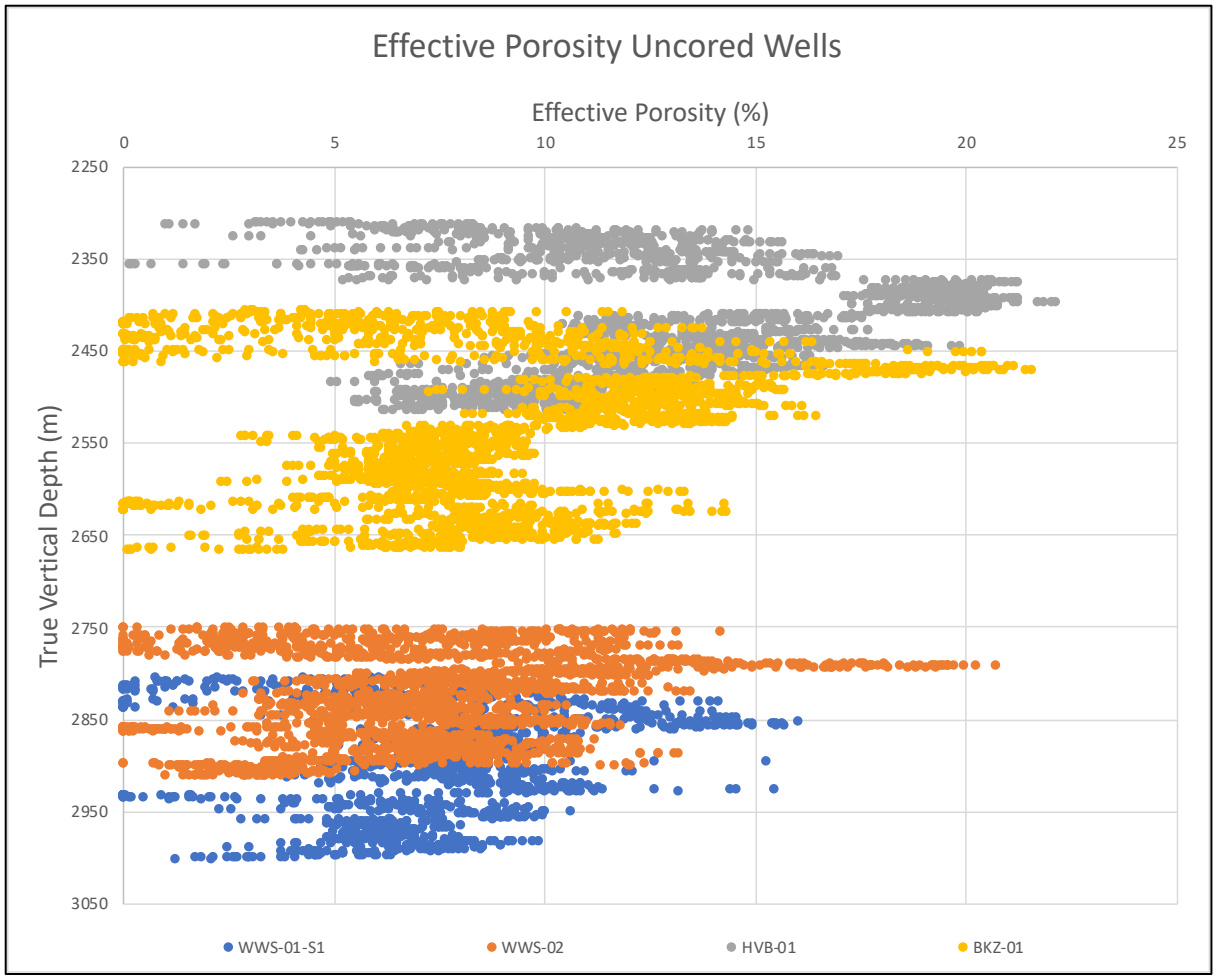

Figure 23: Effective porosity plot for the uncored wells WWS-01-S1, WWS-01, HBV-01 and BKZ-01. The graph indicates a lack in relationship between the petrophysical property and present-day depth.

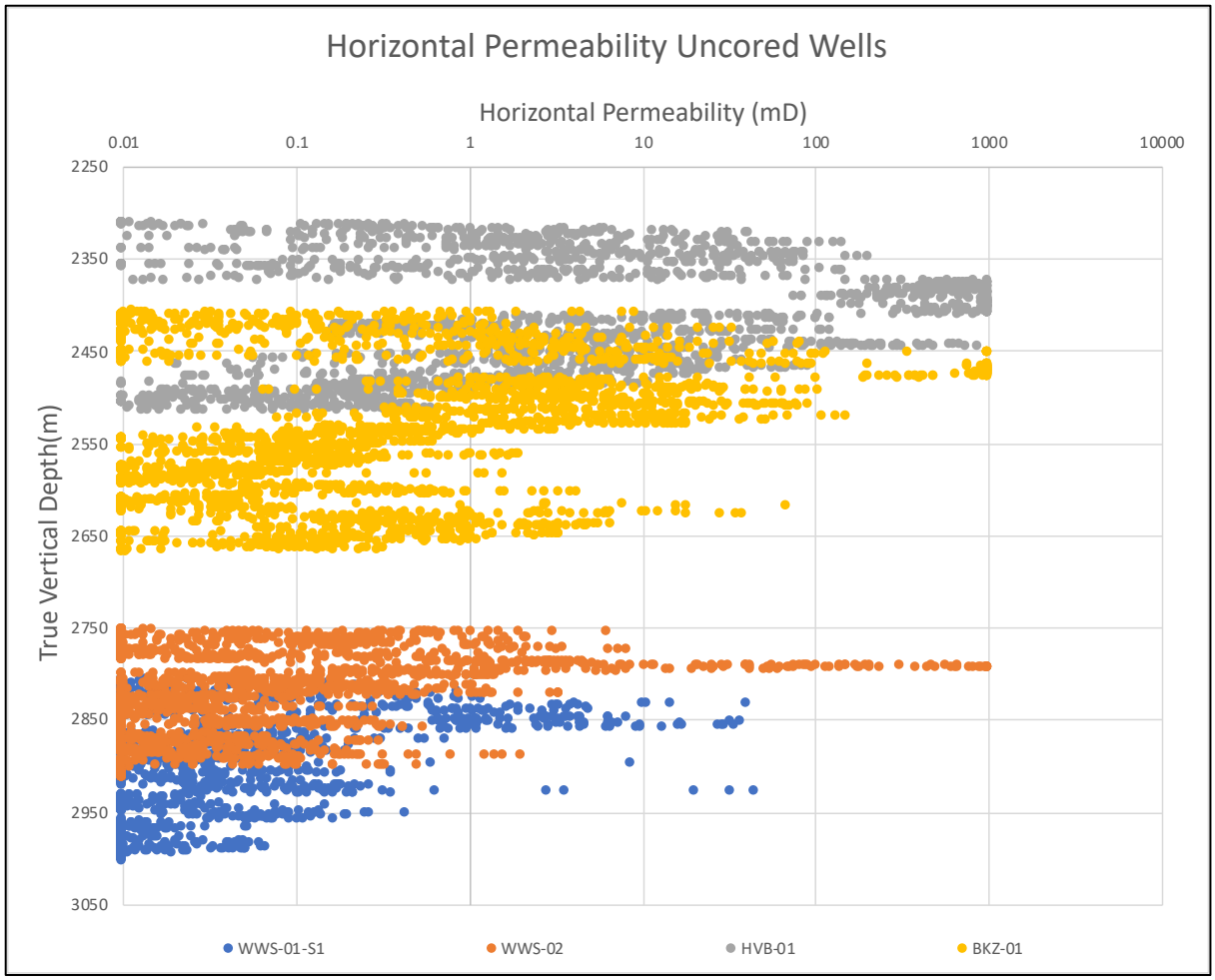

Figure 24: Horizontal permeability plot for the uncored wells WWS-01-S1, WWS-01, HBV-01 and BKZ-01. The graph indicates a lack in relationship between the petrophysical property and present-day depth.

4.1 Discussion

4.1 Main Buntsandstein Mapping

Regional mapping of the Main Buntsandstein, using 3D seismic data and well correlations, shows that the Subgroup is present in the whole study area. The presence and thickness of the Subgroup changes throughout the area which can be attributed to the existence of a horst- and graben fault system that distributed thickness differences of the Main Buntsandstein. Hence, the ratio between accommodation space and sediment supply changed within the study area/basin. The Main Buntsandstein shows significant thickness variations in the study area around Tilburg ranging from circa 160 to 220 m, where commonly thicker RBM deposits are located within the grabens. This suggests better geothermal potential for the grabens compared to the horsts as these are located at greater depths, and thus higher in-situ temperatures, as well as higher transmissivity values due to the thicker deposits according to Mijnlieff (2020). Considering a geothermal gradient of around 30° Celsius per kilometer and a surface temperature of 10° Celsius, reservoir temperatures of up to 100 ° Celsius may be expected in the grabens where the RBM is located at depths of 3000 m and greater (Stegers et al., 2018). The normal faults, that are responsible for the horst- and graben tectonic system in the study area, were likely formed by the reactivation of pre-existing faults in the RVG (de Jager, 2003). However, no clear evidence of inversion structures is found in the seismic data set.

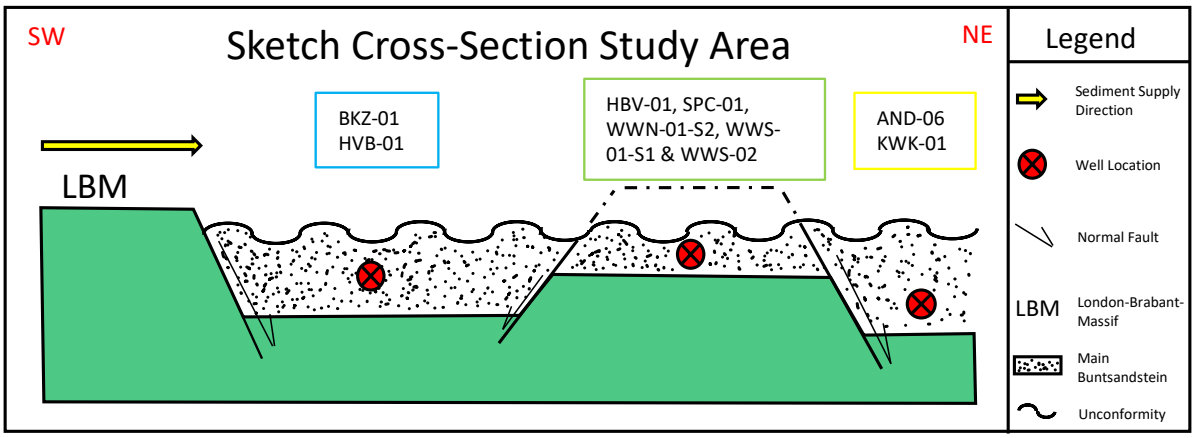

Figure 25: General sketch of a cross-section through the study area displaying the interpreted thickness differences encountered in the wells. The figure indicates the presence of the Hardegsen unconformity that strongly affected the thickness of the Main Buntsandstein, especially in the areas where a horst was present. Note that the figure is not scaled.

Considering the well correlations, the southern wells, BKZ-01 and HVB-01 (Figure 10D), show a considerable thicker package of Main Buntsandstein compared to the middle cluster of wells (HBV-01, SPC-01, WWN-01-S2, WWS-01-S1 & WWS-02; Figure 10C). As the seismic data lacks evidence on synsedimentary tectonics in the RBM, a likely explanation for the thickness differences within the study area might be related to the presence of normal faults that were active at the end/after deposition of the RBM such that a horst- and graben system was formed. Here, RBM packages were partly eroded on the structural highs resulting in the present-day thickness differences. This interpretation coincides with the fact that the

pronounced Hardegsen unconformity is placed upon the RBM, which was a basin wide unconformity related to extensional tectonics triggering erosion of the Main Buntsandstein Subgroup (Geluk, 2005). The thickness of the RBM in the northern cluster, where AND-06 and KWK-01 are located, again shows a thicker package (Figure 10B). This might also be related to the fact that this area is located more to the basin center, suggesting stronger subsidence and thus more space for sediments to accumulate. Figure 25 displays a general sketch of a cross-section through the study area showing the existence of the Hardegsen unconformity that strongly triggered the thickness of the RBM at the structural highs in the horst- and graben tectonic system. A thickness map of the RBM formed from the well correlations is added in Appendix D.

4.2 Depositional Environment

The interpretation on the four established facies associations allows us to construct a regional conceptual depositional model. This sedimentological model defines an alluvial/fluvial fan system terminating in a playa-lake environment, also known as a terminal fluvial system. Figures 26 and 27 depicts the different depositional environments that describe the stratigraphy and observed facies associations in the study area. Figure 26 shows a setting of more confined flow on the alluvial plain, dominated by a high-energy braided fluvial system bounded by vegetated floodplains, whereas Figure 27 represents a lower-energy unconfined terminal fluvial-fan system. Overall, the interpretation on the depositional environment shows strong similarities to the interpretation on the Judy sand unit within the Triassic Skagerrak Formation described by McKie (2011).

Figure 26 captures the model in which facies associations 2 and 3 were deposited. It marks a setting where unconfined to confined fluvial channels were active on the alluvial-plain that terminated into a playa-lake environment. The interaction between these two processes were dominantly determined by the availability of water, the amount and type of sediment being transported from the source as well as the sediment availability in the inland, and the gradient of the alluvial plain (Nichols, 2009). Furthermore, the ratio of evaporation downstream might have played a role too. The climate was likely to have been relatively arid, which is evident from the fact that fine grained floodplain deposits lacked during this period.

Figure 27 displays a strongly confined braided fluvial system. This is evident from the abundance of fining-up barforms comprising of massive to cross-stratified and parallel fine to medium grained sandstones (FA1) scouring through vegetated floodplains (FA4). Hence, it marks a change in fluvial style compared to Figure A, that is related to the increase of water availability in the system. Due to frequent avulsion of the channels combined with mudstone dominated overbank floodplain deposits, this system resulted in much lower N/G deposits than the arid to semi-arid system captured in Figure 26. Similar to Figure 26, this depositional system also terminated into a playa-lake environment. The playa-lake facies (FA3) were deposited as a result of several regional transgression and regression periods of the lake.

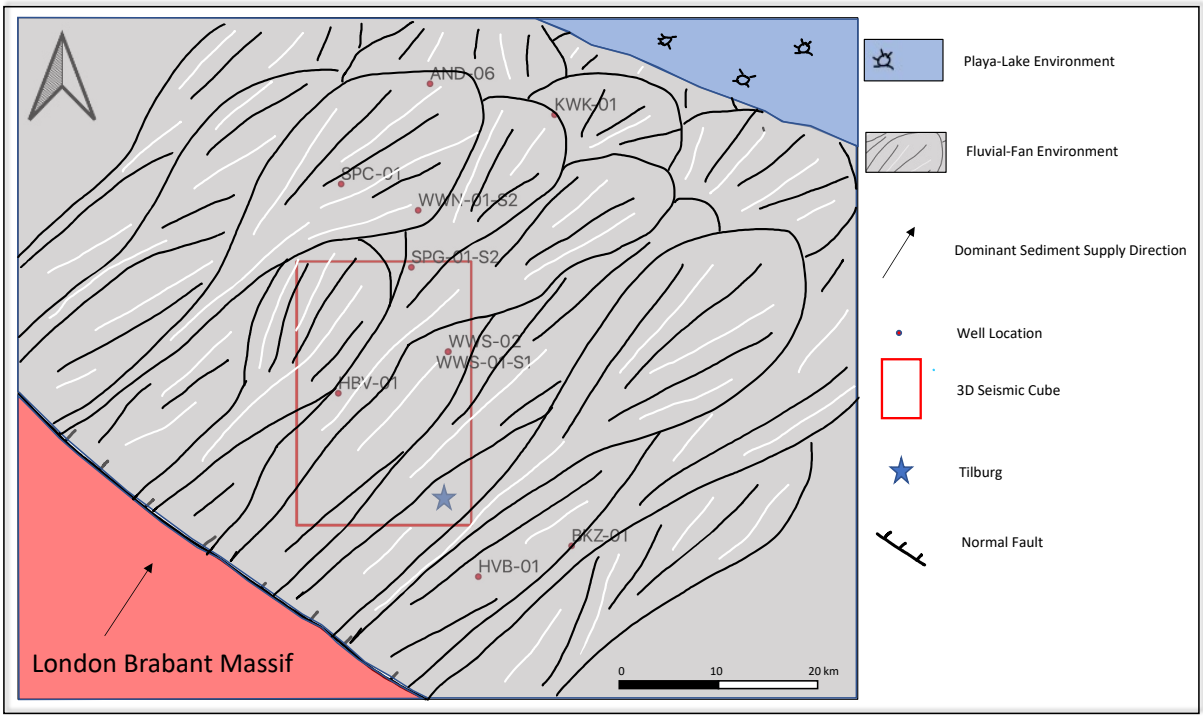

Figure 26: Conceptual depositional model of the study area for FA2 and FA3. The sketch captures the unconfined fluvial fan system terminating into a playa-lake environment. In this sort of setting, fluvial-fan sandstone facies (FA2) and playa-lake mudstone facies (FA4) are deposited.

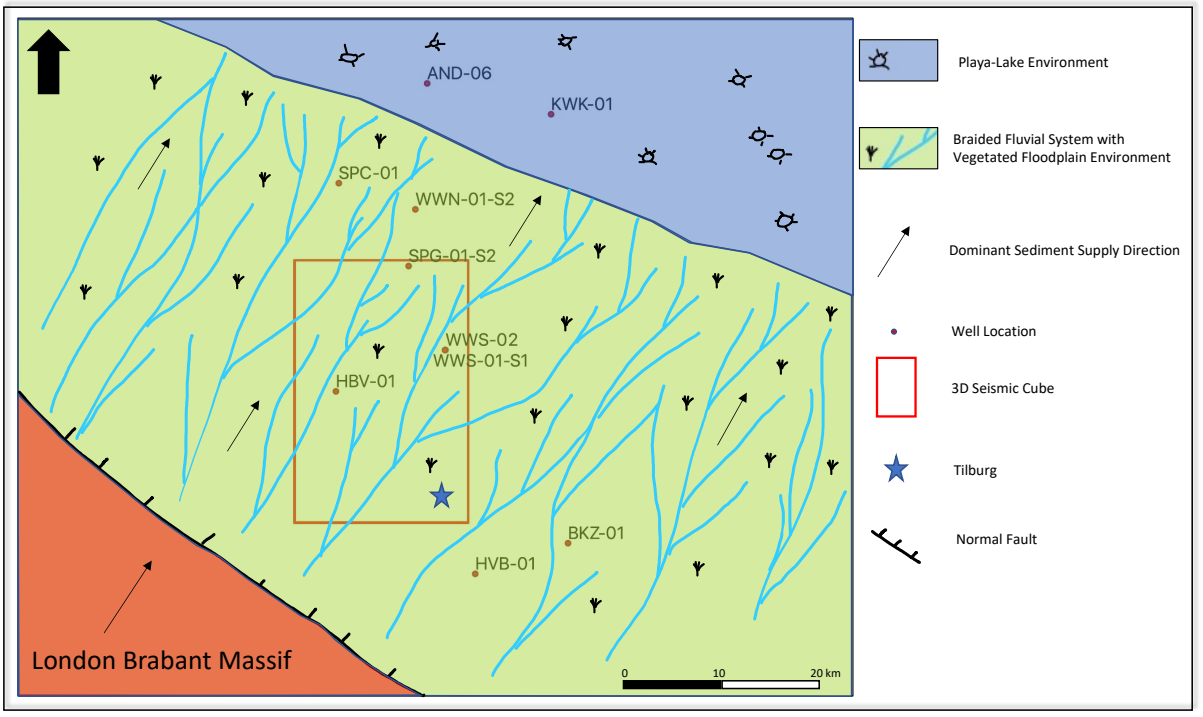

Figure 27: Conceptual depositional model of the study area for FA1, FA3 and FA4. The sketch displays a braided fluvial system together with surrounding vegetated floodplains terminating in a playa-lake environment. It captures the braided channel facies (FA1), floodplain facies (FA4) and playa-lake facies (FA3).

4.3 Facies Architecture and Stratigraphy

The results of the core study combined with gamma-ray wireline well logs allow us to provide a facies architecture model and stratigraphic framework of the study area. A facies architecture model is created in order to predict reservoir- and non-reservoir sediments bodies at well spacing scale. Figure 28 displays the distribution of the four difference facies associations across wells AND-06, KWK-01, WWN-01-S2 and SPC-01, respectively. The facies architecture model provides information on the horizontal and vertical connectivity of potential geothermal aquifer reservoirs, which is further discussed in a later paragraph. Besides, the facies architecture, Figure 28 displays the stratigraphic framework of the Main Buntsandstein which is discussed at Member and Formation scale. The full stratigraphic framework and facies architecture model, containing all studied wells, are provided in Appendix C.

The lower part of the section is predominantly characterized by low gamma-ray values that can be correlated across the different wells and show a thickness of circa 10 to 50 meters. Based on the core interpretation, these sandstones are associated with the fluvial-fan facies. Furthermore, the lower section comprises of some alternations of high gamma-ray values, that are correlated across all wells with a thickness of up to 10 meters. The core results suggest these are connected with playa-lake mudstone facies.

The upper section comprises of a more heterogeneous gamma-ray pattern compared to the lower part. Here, low gamma-ray wireline responses have a thickness of up to 12 meters and are associated with braided channel facies sandstones. Based on the channel sand thickness, the channel depth and channel belt width of braided fluvial systems can be guessed with the use of the model of Fielding and Crane (1987). This results in channel belt widths of up to ca. 5 kilometers. Since the four wells in the facies architecture model are located more than 5 km apart from each other, it is likely that braided facies sandstones do not interfere with each other (Figure 28). High gamma-ray values in the upper section are associated to over bank floodplain mudstone facies that punctuate the braided channel facies (Figure 28).

Considering the facies architecture, a clear subdivision can be made between the lower, which consists in terms of stratigraphy of the Volpriehausen and Lower Detfurth Formations, and upper (Upper Detfurth and Hardegsen Formations) sections of the Main Buntsandstein. This is visible from the correlation panel that shows a clear difference in its facies architecture, which is related to a change in depositional environment over time, likely influenced by tectonic and climatic conditions in the basin. The depositional environment of the lower section is dominated by an environment as sketched in Figure 26 whereas the lower section reflects the architecture formed during an environment as displayed in Figure 27.

4.3.1 Lower Volpriehausen Sandstone Member

The bottom part of the Main Buntsandstein is represented by the Lower Volpriehausen Sandstone Member (from Base Main Buntsandstein to Volpriehausen Claystone Member). It consists of the fluvial-fan facies associations and shows a high N/G ratio on the gamma-ray log. However, in the northern part of the area, well logs (AND-06, KWK-01, SPC-01 & WWN-

01-S2) show thin packages of higher gamma-ray values suggesting some local expansion of the playa-lake as is visible on the well correlation. The high N/G values (i.e., low gamma-ray) on the gamma-ray log represents the amalgamated stacking pattern of the sandy-rich facies. This corresponds to the interpretation by Geluk (2005), who stated that the Lower Volpriehausen Sandstone Member mainly consists of fluvial origin in the Southern parts of the Netherlands. Thickness of this member is rather constant in the area, suggesting that differential subsidence and sediment supply was rather constant at time of its deposition. The bottom boundary is taken where the transition of high gamma-ray values of the Rogenstein Formation to low gamma-ray values occurs. See Figure 28.

4.3.2 Volpriehausen Claystone Member

The Volpriehausen Claystone Member represents a part in the stratigraphy during which the playa-lake expanded and resulted in the deposition of the fine-grained mudstone dominated playa-lake facies association. On the well logs, it is characterized as a regional correlation marker by displaying a distinct low N/G stratigraphic interval, which supports the findings conducted by (Geluk and Rohling, 1997). From the full well correlation panel (Appendix C), it can be seen that the member thickens towards the North, which is most likely caused by the fact that the lake margin was located near the center of the basin, thus resulting in thicker deposits to the North. However, Geluk (2005) argued that the considerable variations in thickness of the Volpriehausen claystone are attributed to erosion prior to deposition of the Detfurth Formation. The bottom boundary is based upon the significant increase in gamma-ray response. See Figure 28.

4.3.3 Lower Detfurth Sandstone Member

The Lower Detfurth Sandstone Member displays a similar character as the Lower Volpriehausen Sandstone Member in terms of facies association and corresponding high N/G well log character. It comprises solely of the fluvial-fan facies sandstones in the area displaying an amalgamated stacking pattern, according to the core study. The bottom boundary is based upon the distinct transition of high- to low gamma-ray values. See Figure 28.

4.3.4 Detfurth Claystone Member

The Detfurth Claystone Member has a similar sedimentary character as the Volpriehausen Claystone Member and solely consists of the playa-lake facies. It represents the expansion of the lake in the area during a more humid period. The member thickens towards the North and has a strong expression on the gamma-ray logs. However, the full correlation panel, shown in Appendix C, shows that the southern wells do not contain this member. A possible explanation for this might be that the lake transgression did not reach these areas and that it was limited to the northern part of the basin. The bottom boundary is based upon the significant increase in gamma-ray response. See Figure 28.

4.3.5 Upper Detfurth & Hardegsen Formation

The uppermost part of the stratigraphy of the Main Buntsandstein consist of alternations of clean sandstones with mudstones. It comprises entirely of the braided fluvial channel facies and overbank facies and displays a distinct change in depositional environment compared to the older stratigraphic units. On the logs it is commonly characterized by the alternations of high and low gamma-ray values. The N/G of this Formation decreases towards the North, which is likely caused due to the fact that it is further away from the source.

The Upper Detfurth Member and Hardegsen Formation are taken together as there lacks a strong marker in the stratigraphy. Hence, the top of the Detfurth Claystone Member, which is a strong pronounced regional correlation marker on the well logs, is taken as the bottom boundary. This approach corresponds to the stratigraphic model established by Geluk and Röhling (1997) that also combined the Upper Detfurth and Hardegsen Formations together as one. This stratigraphic unit shows a significant variation in thickness throughout the basin, caused by the pronounced Hardegsen unconformity that is located between the top of this Formation and base of the Sölling (Geluk, 2005). The bottom boundary is based upon the distinct transition of high gamma-ray values of the Detfurth Claystone Member to lower gamma-ray values, whereas the top boundary is based upon the significant increase in gamma-ray response (due to the presence of mudstones in the overlying Sölling Formation). See Figure 28.

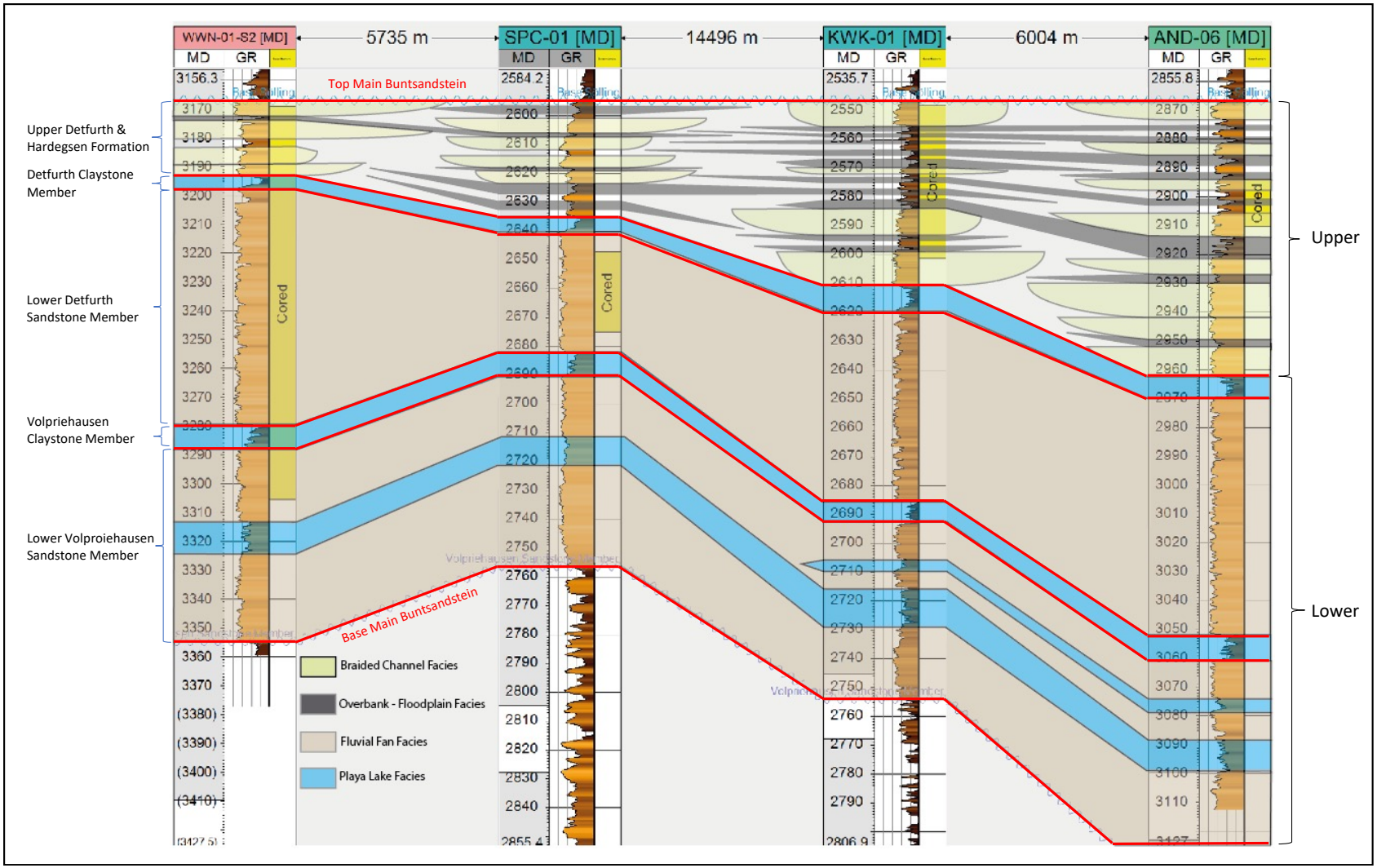

Figure 28: Facies architecture model and stratigraphic framework of the Main Buntsandstein across wells WWN-01-S2, SPC-01, KWK-01 and AND-06 (from south to north). Gamma-ray is the shown log versus the measured depth. Thickness changes can be attributed to local erosion caused by the Hardegsen unconformity and/or difference in sediment deposition due to local differential subsidence. Facies correlation is conducted with respect to the gamma-ray wireline response. The overall architecture shows alternations of fluvial fan and playa-lake expansions in the lower section that comprises of the Lower Volpriehausen Sandstone & Claystone Member as well as the Lower Detfurth Sandstone & Claystone Member. Main floodplain shale intervals are dominating in the upper section (Upper Detfurth & Hardegsen Formation), which punctuate the braided channel facies

4.4 Reservoir Architecture Model

4.4.1 Reservoir Compartmentalization

Considering the facies correlation across the wells, the Main Buntsandstein Subgroup shows evidence of stratigraphic compartmentalization by mudstones. The mudstones in the Main Buntsandstein differ from its origin, ranging from playa-lake mudstones in the lower section to overbank-mudstones in the upper part, with the latter being deposited across floodplains forming a variety of paleosol maturity and oxidation. These shale-rich layers, that are thick enough to be visible on the gamma-ray log, appear to be correlatable over many tens of kilometers across well spacing scale and have the potential to form vertical flow barriers in the subsurface of Tilburg. This is also supported in the paper by Geluk and Rohling (1997) who stated the cyclic character of the Main Buntsandstein which allows a very good correlation across different wells in the Netherlands. In this case, the Upper Detfurth and Hardegsen Formation (see upper section in Figure 28) especially show intense vertical stratigraphic compartmentalization by floodplain shales. This could negatively block subsurface flow vertically. Considering the horizontal connectivity of the upper section, which is the main subsurface flow direction during geothermal operations, would be affected less strongly by these mudstone intervals. Although pinching out of these braided channel sandstone bodies would still be crucial for horizontal connectivity during geothermal operations.

Lower scale sedimentary heterogeneities, such as bar tops/mud drapes in the channel and fluvial fan facies, may also act as baffles/barriers to flow but their lateral extent and ability to block flow in the subsurface is difficult to determine. However, previous conducted research performed by McKie (2011) stated that in terminal fluvial systems, playa, floodplain, and bar-top shales have kilometer-scale dimensions that are often greater than the size of a subsurface reservoir and as the Main Buntsandstein in the Tilburg area is deposited in a similar depositional setting, these mudstone-rich facies strongly have the potential to act as a vertical barrier to flow.

The lower section (Figure 28), consisting of the Volpriehausen and Lower Detfurth Formations, displays a stacked amalgamated stacking pattern of the fluvial-fan facies, whereas the Upper Detfurth and Hardegsen Formation displays a compartmentalized structure consisting of braided fluvial channel deposits alternated with floodplain shales. Hence, the lower section appears to have the better horizontal connectivity compared to the upper section. However, predictions on well correlations and thus reservoir compartmentalization remains to be strongly speculative without a high-resolution chronostratigraphic framework. Moreover, since all wells are located on a horst, and geothermal energy exploitation is preferred in the grabens due to higher in-situ temperatures (greater depths) and usually greater grain sizes, well data from the grabens should be collected to make better predictions reservoir compartmentalization.

Besides the presence of stratigraphic reservoir compartmentalization, compartmentalization formed by faults could play a role as well as they potentially can block subsurface fluid flow (Jolley et al., 2010). This is especially important since the study area is characterized by a considerable number of faults (Figures 7 and 8). Furthermore, reactivations of faults and

related seismicity is another crucial aspect that could happen during geothermal operations. Therefore, a fault seal analysis is recommended to study the sealing potential of the faults as well as possible appearance of induced seismicity during geothermal operations.

4.4.2 Reservoir Quality

Results of the petrophysical property studies shows highly variable porosity and permeability values within the Main Buntsandstein, for both the core plug measurements as well as calculated properties. The Main Buntsandstein lacks a correlation with depth and stratigraphic interval in the study area (Figures 23, 24, 30 & 31). Both findings match the results of Kunkel et al. (2018), who studied the sedimentology and its corresponding reservoir properties of the Main Buntsandstein in Erfurt, Germany. However, the studied Main Buntsandstein of Kunkel et al. (2018) is located at much shallower depths (694 – 913 m). She concluded that the reservoir quality of the Main Buntsandstein is dominantly controlled by grain size and diagenetic evolution.

Similar to the core plug measurements, plots of the porosity and permeability from the uncored wells show a lack in correlation between the petrophysical properties and increasing depth (Figures 30 & 31). Moreover, no specific relationship with stratigraphic interval can be determined (Figures 30 and 31). Overall, the Lower Detfurth Formation shows highest mean values of 10.9 % and 105 mD for the effective porosity and horizontal permeability, although the data is highly scattered. A histogram of the porosity and permeability data for the Lower Detfurth is added into Appendix B. The highest mean effective porosity and permeability are encountered in the Lower Detfurth Formation of well HVB-01, which count to 15.6 % and 279 mD, respectively. The Lower Detfurth Formation in well BKZ-01 also displays considerable high mean effective porosity and permeability of 10.2 % and 89 mD. Besides measurements on porosity and permeability, the considerable high amount of sand, as is visible on the logs, the net-to-gross of the Lower Detfurth seems high promising. Net sand, gross thickness of the member and a N/G map are shown in Figure 29, which are created with the use of Hydreco shale volume data with a cutoff of 40% for the net sand. The results suggest significant high geothermal potential considering the net/gross of the Lower Detfurth member.

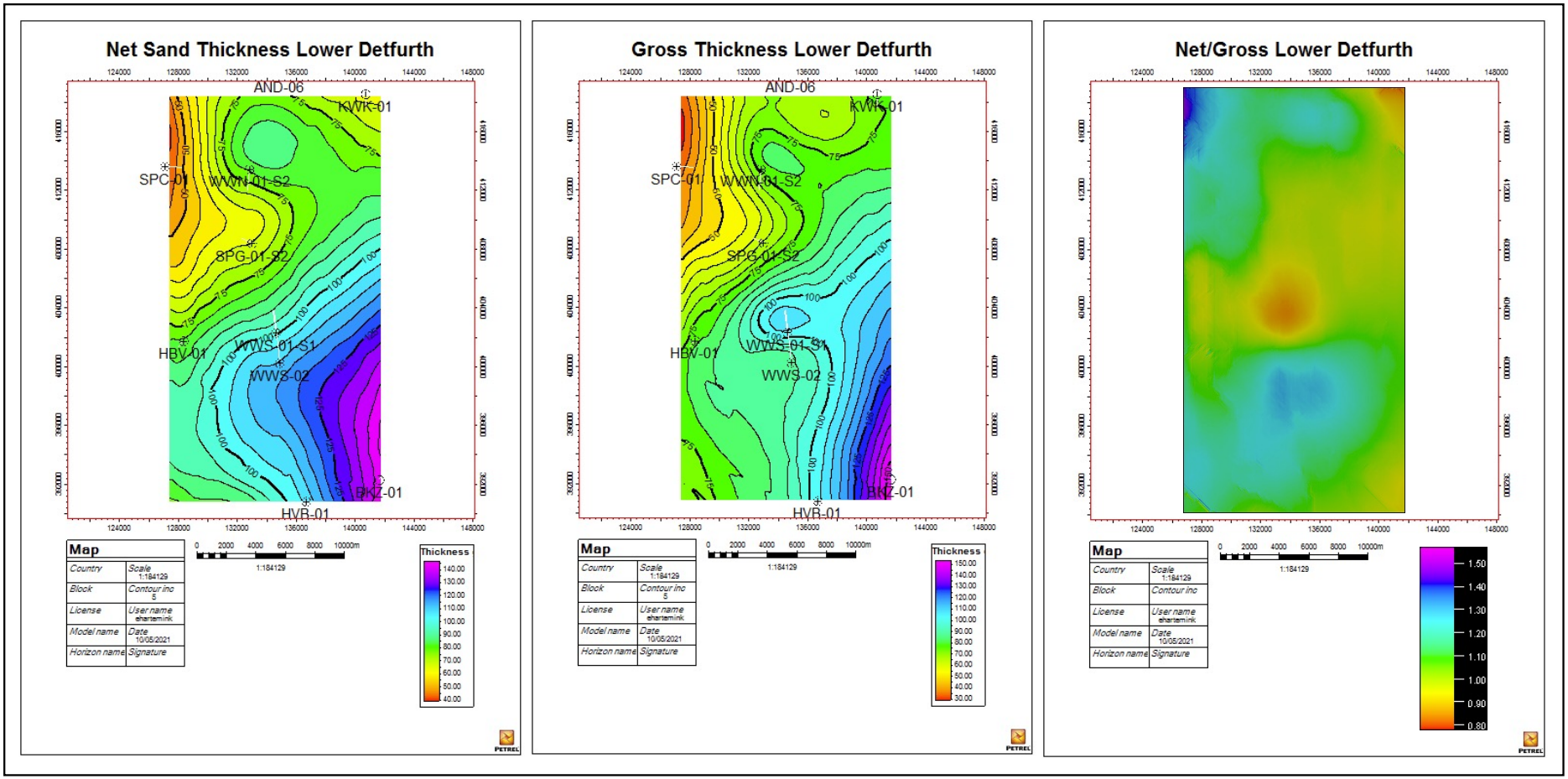

Figure 29: Net sand thickness, gross thickness and net/gross maps of the Lower Detfurth Member from left to right. The net/gross map shows significant number of artifacts which are likely caused by the fact that the net sand thickness is generally as thick as the gross thickness of the member as a whole. Overall, the results suggest good geothermal potential considering the net/gross due to the general high values.

Core analysis conducted by Panterra Geoconsultants B.V., did show that shallower wells (SPC-01 and BKZ-01) in the Tilburg Noord area have better reservoir quality (Main Buntsandstein as well as the overlying Röt Formation) compared to wells with deeper located Main Buntsandstein intervals (WWK-01 and WWS-01-S1). However, it remains to be unclear whether this is related to the degree of compaction and/or degree of cementation (Böker and Brautigam, 2017).

Core plug measurements used for this study show a positive relationship between the porosity and permeability, which is comparable to the upper located Röt Formation in the WWN-01-S2 studied by (Loveless et al., 2013). Measurements from this Formation show a similar petrophysical character as to the studied Main Buntsandstein core plugs with predominantly low porosity (< 15 %) and permeability (< 100 mD) values where most of these very low petrophysical property values can be correlated with silt- and or claystones intervals.

The lithofacies plots indicate a correlation between grain size and porosity/permeability, where highest mean values are found within lithofacies wavy/subparallel bedded (very) fine sandstone ("**S1/2,w,l**") and massive sandstones ("**S2/3,m**"). Similar conclusions were drawn by Kunkel et al. (2018) who stated that best aquifer potential occurs in parallel to cross bedded- and massive sandstones of fluvial to sandflat origin. The facies association plot indicates best reservoir potential within the fluvial-fan facies, located in the Lower Volpriehausen and Detfurth Formations. These findings are supported by the calculated petrophysical properties of the uncored wells, that also show optimal reservoir quality within the Lower Detfurth Formation.

A reservoir study conducted by Panterra Geoconsultants B.V. showed a base average porosity and horizontal permeability of 15.6 % and 93 mD in the Tilburg Noord area for the Main Buntsandstein and overlying Sölling Formation, according to measurements from wells HBV-01, HVB-01, SPC-01 and BKZ-01. A quick look evaluation on regional well tests showed that in-situ permeabilities are not higher than the petrophysical base case averages for this area (Böker and Brautigam, 2017).

The calculated petrophysical properties of the uncored wells (located in the southern part of the study area) display considerable higher reservoir properties (porosity as well as permeability) compared to the cored wells, which are located in the northern part of the basin. The average porosity and permeability of the cored wells is 8.2 % and 7.7 mD, whereas for the uncored wells it amounts to 8.3 % and 88.8 mD. A possible explanation might be related to the fact that the Triassic strata in the center (to the north) of the basin is buried deeper than the sediments at the basin fringe (southwards), resulting in better reservoir properties at the wells along the basin edge (Brautigam and Veeningen, 2018).

Finally, the variation of aquifer potential within stratigraphic formations is often explained by spatial facies variations and its associated lithofacies. Especially, differences in lithology (e.g., amount of mud layers and variations in grain size) influence petrophysical properties. However, the reservoir quality of the Triassic sediments in the Tilburg area are not only controlled by its depositional environment but also by the diagenetic history (Brautigam and Veeningen, 2018). Therefore, further studies using thin sections of different wells across the study area is recommended to obtain valuable information on the mineralogy and any

presence of diagenesis in the Main Buntsandstein, which again improves the prediction on reservoir quality across the basin.

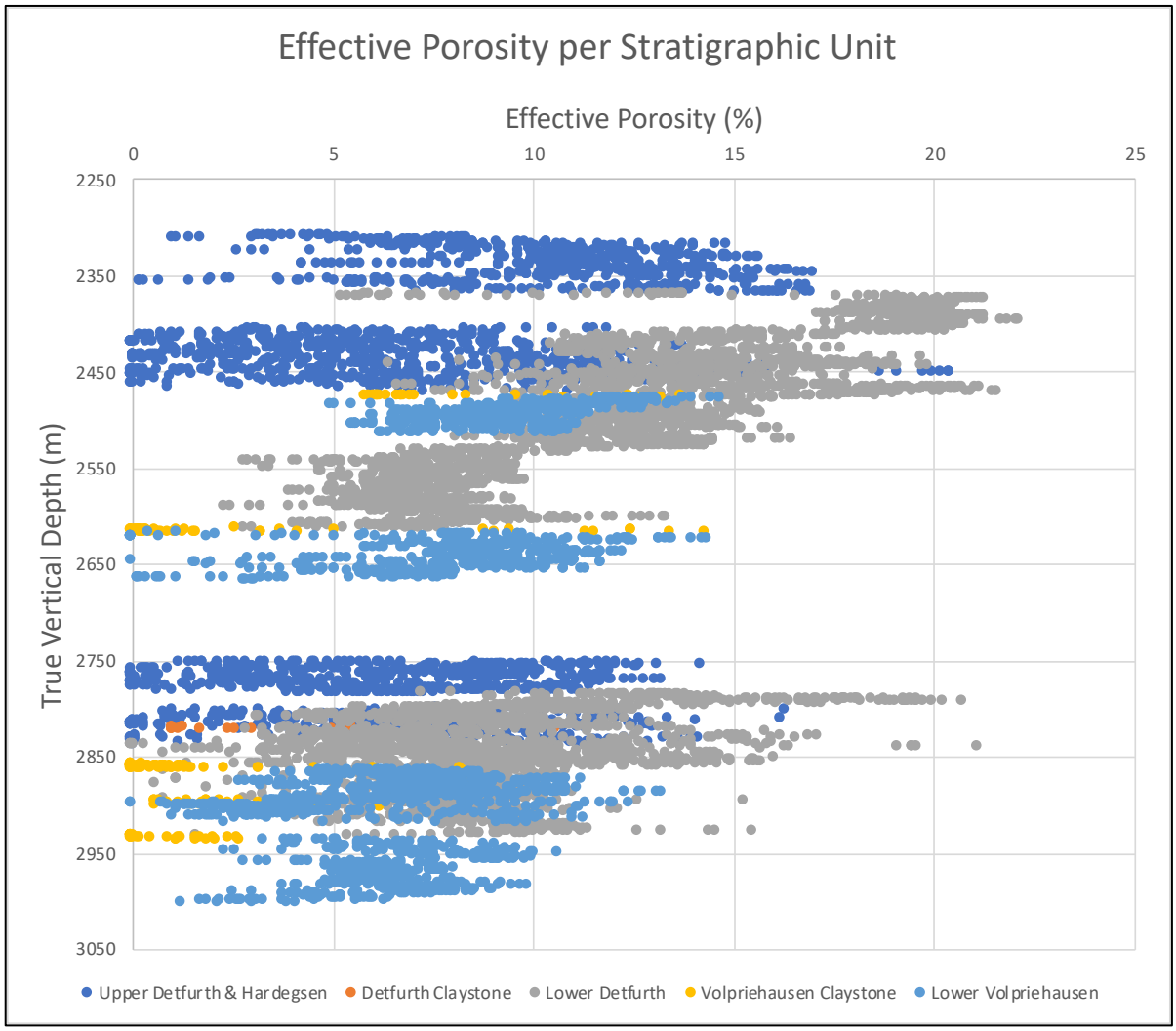

Figure 30: Effective porosity for each stratigraphic unit plotted versus the true vertical depth. Measurements derive both from core plugs as well as calculated well logs. Data derives from the following wells: AND-06, BKZ-01, HBV-01, KWK-01, WWN-01-S2, WWS-01-S1 and WWS-02.

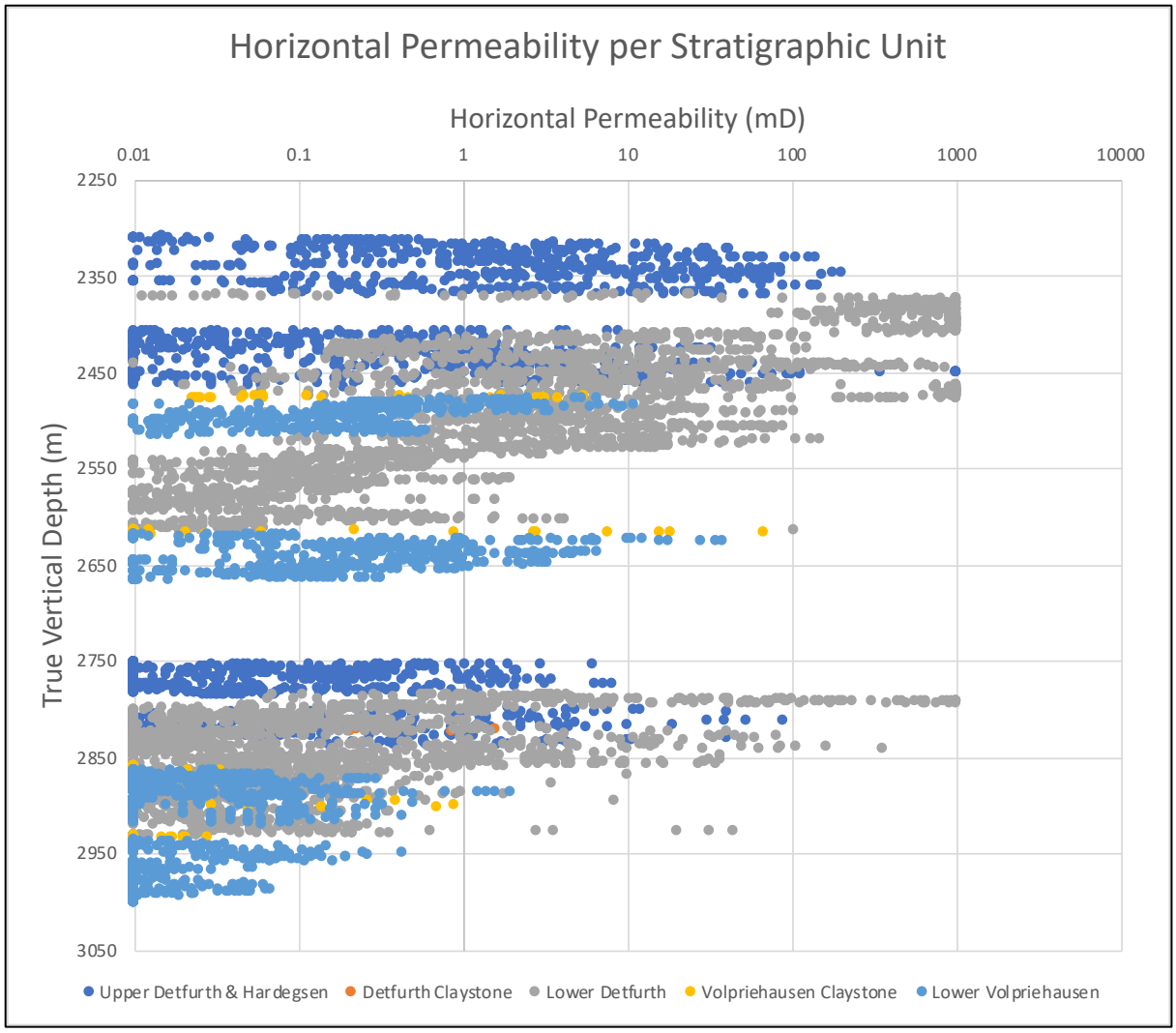

Figure 31: Horizontal permeability for each stratigraphic unit plotted versus the true vertical depth. Measurements derive both from core plugs as well as calculated well logs. Data derives from the following wells: AND-06, BKZ-01, HBV-01, KWK-01, WWN-01-S2, WWS-01-S1 and WWS-02.

5. Conclusions

A multi-scale reservoir characterization workflow is conducted for this study to evaluate the Main Buntsandstein in the Tilburg area for potential geothermal operations. For this, seismic data, well log data, core plugs and calculated petrophysical property data are used to provide a qualitative and quantitative description of the subsurface. The following conclusions can be drawn regarding the results of this study:

- It was found that the study area comprises of a horst- and graben fault system where the top of the Main Buntsandstein is located at depths of ca. 1900 – 2100 m on the structural highs, and at ca. 3300 – 3500 m in the structural lows.
- Major fault orientation in the Tilburg area is NNW-SSE for the larger faults, while the smaller faults predominantly have an NW-SE orientation. The latter often being cut by the larger faults suggesting that the NNW-SSE faults are relative younger.
- Isopach maps of the Subgroup shows average thickness of around 200 meters in the study area. Well log correlations display similar results but indicate local thickness variations across the wells, which is a result of either the presence of local strong depocenters and/or non-deposition and/or local strong erosion.
- Thicker RBM deposits are commonly encountered in the grabens, suggesting better geothermal potential due to greater depths (thus higher in-situ temperatures) and higher transmissivity values.
- Ten different lithofacies and four separate facies associations are established from the core study. The distinguished facies are braided channel element facies (FA1), fluvial-fan sandstone facies (FA2), over bank floodplain facies (FA3), and playa-lake mudstone facies (FA4).
- Results from the core study suggested the existence of a terminal fluvial (fan) system. Here, deposition was dominated on the alluvial plain which terminated into a playa-lake environment. Transgression periods resulted in the widespread deposition of the playa-lake facies. Fluvial-fan facies were deposited during a relative dry period whereas the presence of braided channel and floodplain facies suggested a wet climate.
- Stratigraphic compartmentalization inside the Main Buntsandstein by mudstones is evident from the facies architecture, which is especially visible within the Upper Detfurth & Hardegsen Formation where over bank floodplain mudstones punctuate braided channel sandstones.
- Optimal reservoir connectivity is, according to the facies architecture, expected in the Lower Detfurth and Lower Volpriehausen Members due to its stacked amalgamated pattern of fluvial fan sandstone facies.
- Poor reservoir connectivity is, according to the facies architecture, expected in the Upper Detfurth and Hardegsen Formations due to punctuation of floodplain facies with braided fluvial sandstone facies that possibly pinch out.
- Core plug measurements on porosity and permeability show best reservoir quality within the wavy/subparallel fine sandstones (**S1/2,w,l)** and massive sandstone (**S2/3,m)** lithofacies. The facies association plot indicates best reservoir potential

within the fluvial-fan facies, located in the Lower Volpriehausen and Detfurth Formations.

- Petrophysical properties of the uncored wells suggest optimal reservoir quality within the Lower Detfurth Formation. In this Formation, highest porosity and permeability are found at well HVB-01 where mean values of 15.6 % and 279 mD are encountered.
- Southern wells display better reservoir properties. This might be related to the fact that the Triassic sediments in the northern part, towards the basin center, have been buried deeper, resulting in better reservoir properties along the basin edge (to the south) and thus better geothermal potential in the Tilburg area.

References

Adamson, J.L., 1987. Integrated Core Anlysis Well Sprang-Capelle-01, BP Exploration.

Adrichem-Boogaert, H.A. and Kouwe, W., 1993. Stratigraphic nomenclature of the Netherlands; revision and update by RGD and NOGEPA. TNO-NITG, Mededelingen Rijks Geologische Dienst. Haarlem, 50.

Böker, U. and Brautigam, K., 2017. Petrophysical Evaluation Tilburg Noord, Panterra Geoconsultants B.V.

Brautigam, K. and Veeningen, R., 2018. Diagenesis study of the Germanic Trias Group sediments near Tilburg., PanTerra Geoconsultants B.V.

Cade, C., 1989. Summary Sedimentological Logs WWN-01-S2, BP Exploration.

de Jager, J., 2003. Inverted basins in the Netherlands, similarities and differences. Netherlands Journal of Geosciences - Geologie en Mijnbouw, 82(4): 339-349.

de Reuver, F., 1994. Lithofacies Atlas for Bunter and Buntsandstein Deposits, GAPS Nederland B.V.

Fielding, C.R. and Crane, R.C., 1987. An Application of Statistical Modelling to the prediction of Hydrocarbon Recovery Factors in Fluivial Reservoir Sequences. SEPM (Society for Sedimentary Geology): 321 - 327.

Geluk, M.C., 2005. Stratigraphy and tectonics of Permo-Triassic basins in the Netherlands and surrounding areas, Utrecht University, 171 pp.

Geluk, M.C., 2007. Triassic. In: T.E. Wong, D.A.J. Batjes and J. De Jager (Editors), Geology of the Netherlands, Royal Netherlands Academy of Arts and Sciences, pp. 85 - 106.

Geluk, M.C., Duin, E.J.T., Dusar, M., Rijkers, R.H.B., Van Den Berg, M.W. and Van Rooijen, P., 1994. Stratigraphy and tectonics of the Roer Valley Graben. Geologie en Mijnbouw, 73(2-4): 129-141.

Geluk, M.C., Plomp, A. and van Doorn, T.H.M., 1996. Development of the Permo-Triassic succession in the basin fringe area, southern Netherlands. In: H.E. Rondeel, D.A.J. Batjes and W.H. Nieuwenhuijs (Editors), Geology of Gas and Oil under the Netherlands: Selection of papers presented at the 1983 Iternational Conference of the American Association of Petroleum Geologists, held in The Hague. Springer Netherlands, Dordrecht, pp. 57-78.

Geluk, M.C. and Rohling, H.G., 1997. High-resolution sequence stratigraphy of the Lower Triassic 'Buntsandstein' in the Netherlands and northwestern Germany. Geologie en Mijnbouw, 76(3): 227-246.

Jager, J.d., 2007. Geological Development. In: T.E. Wong, D.A.J. Batjes and J.d. Jager (Editors), Geology of the Netherlands. Royal Netherlands Academy of Arts and Sciences, pp. 5 - 26.

Jolley, S., Fisher, Q. and Ainsworth, R.B., 2010. Reservoir compartmentalization: An introduction. Geological Society of London Special Publications, 347: 1-8.

Kortekaas, M., Böker, U., Van Der Kooij, C. and Jaarsma, B., 2018. Lower Triassic reservoir development in the northern Dutch offshore, Geological Society Special Publication, pp. 149-168.

Kunkel, C., Aehnelt, M., Pudlo, D., Kukowski, N., Totsche, K.U. and Gaupp, R., 2018. Subsurface aquifer heterogeneities of Lower Triassic clastic sediments in central Germany. Marine and Petroleum Geology, 97: 209-222.

Lokhorst, A. and Wong, T.E., 2007. Geothermal Energy, Geology of the Netherlands. Royal Netherlands Academy of Arts and Sciences, pp. 341-346.
Loveless, S., Eggenkamp, H., Laenen, B., Lagrou, D. and Rombaut, B., 2013. Diagenetic study of Triassic Sandstones in the Roer Valley Graben, Vito.
McKie, T., 2011. Architecture and Behavior of Dryland Fluvial Reservoirs, Triassic Skagerrak Formation, Central North Sea. SEPM (Society for Sedimentary Geology)(97): 189 - 214.
Michon, L. and Van Balen, R., 2005. Characterization and quantification of active faulting in the Roer Valley Graben based on high precision digital elevation models. Quaternary Science Reviews, 24: 455-472.
Mijnlieff, H.F., 2020. Introduction to the geothermal play and reservoir geology of the Netherlands. Netherlands Journal of Geosciences, 99: e2.
Nichols, G., 2009. Sedimentology and Stratigraphy. Blackwell Science Ltd.
Reijers, T.J.A., Mijnlieff, H.F. and Pestman, P.J., 1993. Lithofacies and their interpretation: a guide to standardised description of sedimentary deposits. 55.
Ringrose, P.S., Martinius, A.W. and Alvestad, J., 2008. Multiscale geological reservoir modelling in practice, Geological Society Special Publication, pp. 123-134.
Slatt, R.M., 2013. Chapter 1 - Basic Principles and Applications of Reservoir Characterization. In: R.M. Slatt (Editor), Developments in Petroleum Science. Elsevier, pp. 1-38.
Stegers, D.P.M., Edelman, S. and Pieterse, K., 2018. Geological study into the geothermal potential near fault zones in the Roer Valley Graben and West Netherlands Basin, T&A Survey BV.
TNO, 2016. NLOG: Nederlandse Olie- en Gas Portaal.
TNO-GSN, 2021a. Chalk Group. In: Stratigraphic Nomenclature of the Netherlands, TNO – Geological Survey of the Netherlands.
TNO-GSN, 2021b. Posidonia Shale Formation. In: Stratigraphic Nomenclature of the Netherlands, TNO – Geological Survey of the Netherlands.
TNO-GSN, 2021c. Upper Germanic Trias Group, Stratigraphic Nomenclature of the Netherlands, TNO – Geological Survey of the Netherlands.
Veeken, P.C.H., 2007. Chapter 2 - The Seismic Reflection Method and Some of Its Constraints. In: P.C.H. Veeken (Editor), Handbook of Geophysical Exploration: Seismic Exploration. Pergamon, pp. 7-109.
Ziegler, P.A., 1990. Geological atlas of Western and Central Europe. Shell Internationale Petroleum Maatschappij ; Distributed by Geological Society Pub. House, [The Hague?]; Bath.

Appendix

A. Core Study

Codes for the lithofacies classification from the Bunter Atlas following the coding system presented by Reijers et al. (1993). Table modified from de Reuver (1994)

1. Lithology and Grain size	
M	Claystone
J	Siltstone
S	Sandstone
S1	Very fine grained sandstone
S2	Fine grained sandstone
S3	Medium grained sandstone
S4	Coarse grained sandstone
S5	Very coarse grained sandstone
C	Conglomerate (clast-supported)
CE	Extraclast conglomerate
CI	Intraclast conglomerate
2. Sedimentary Structures and Other Characteristics	
A. Sedimentary Structures	
l	Horizontal and subhorizontal lamination (dip of beds (<5°)
xl	Low-angle crossbedding (dip of beds is approx. 5-15°)
xhp	High-angle crossbedding, (foreset dip >15°)
xht	Trough crossbedding
r	Ripples, general
ro	Wave/oscillation ripples
rc	Current ripples and crosslamination (set-heights <3cm)
rcl	Climbing current ripples
rd	Adhesion ripples
w	Wavy bedding, general
wt	Wavy bedding, textural (bimodal grain size) lamination
d	Soft sediment deformation, general
dc	Contorted bedding
df	Flame structures
m	Homogeneous, general
mf	Homogenised, by fluidisation
ml	Homogenised, by liquefaction
or	Common rootlets
i	Common bioturbation
B. Diagenetic Features	
An	Diagenetic nodules, general
Anan	Anhydrite nodules
Ando	Dolomite nodules

Core Description AND-06 (Logged at 1:10 Scale)

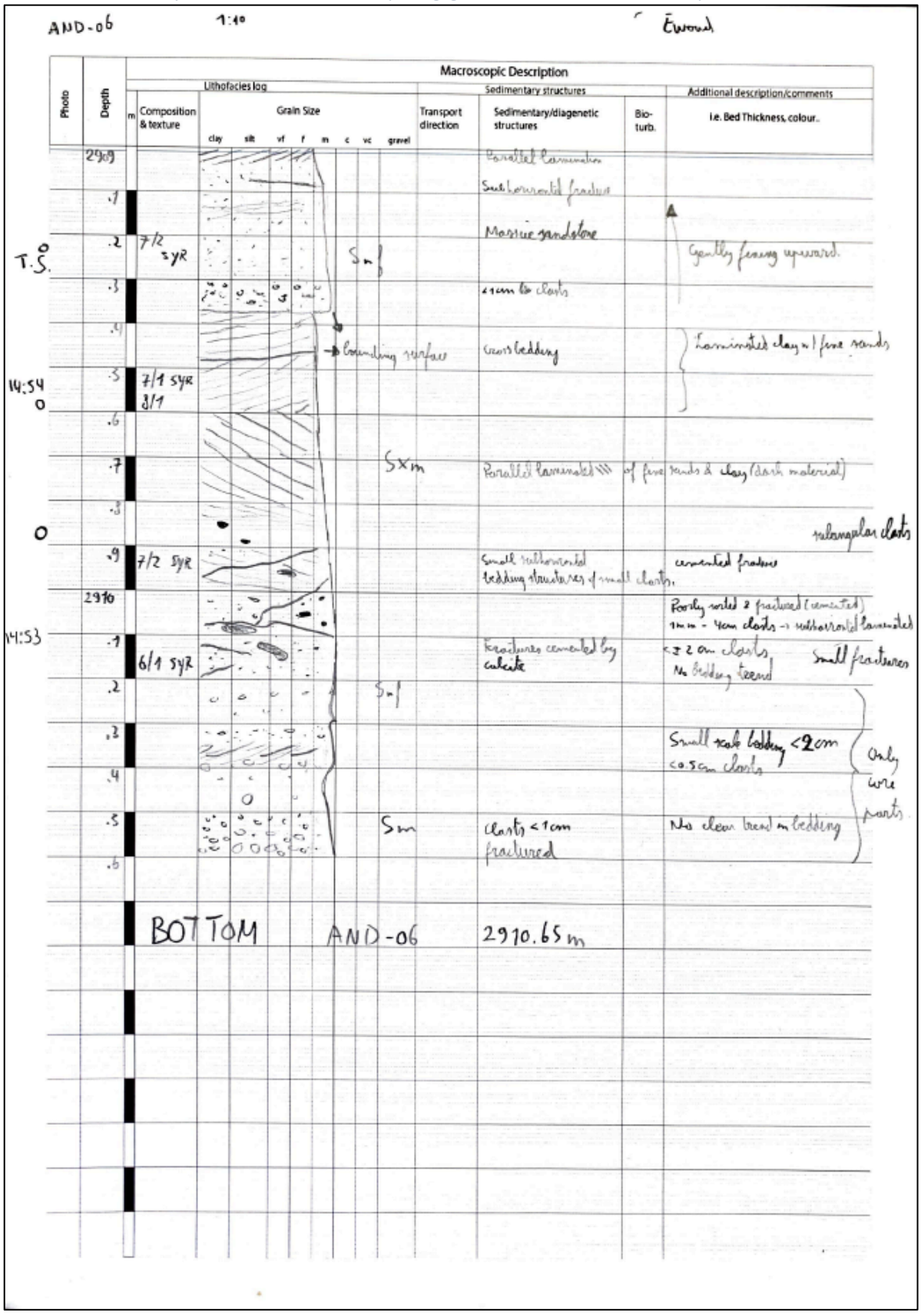

Core description #1 of AND-06 (2910.65 – 2909 m)

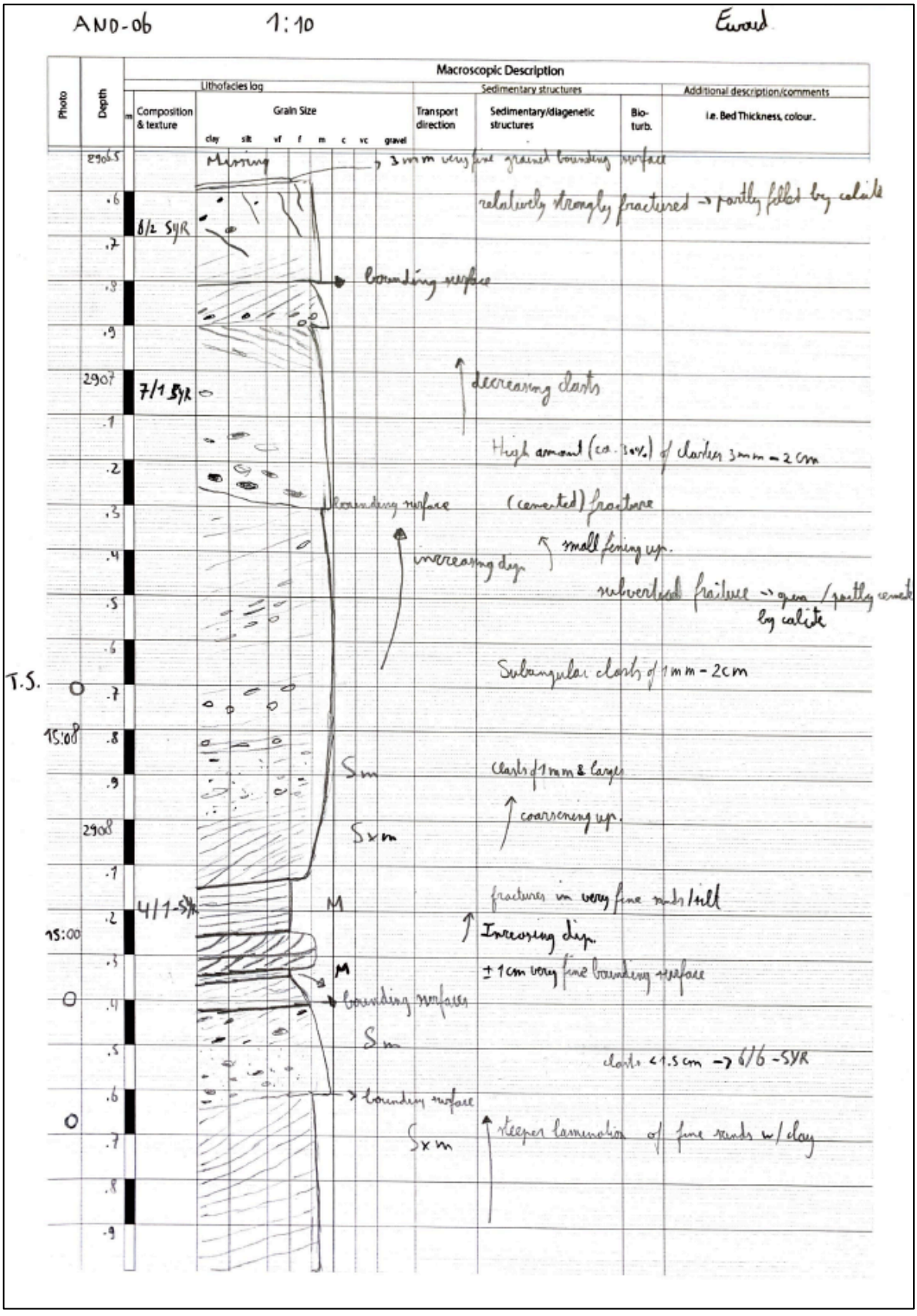

Core description #2 of AND-06 (2909 – 2906.5 m)

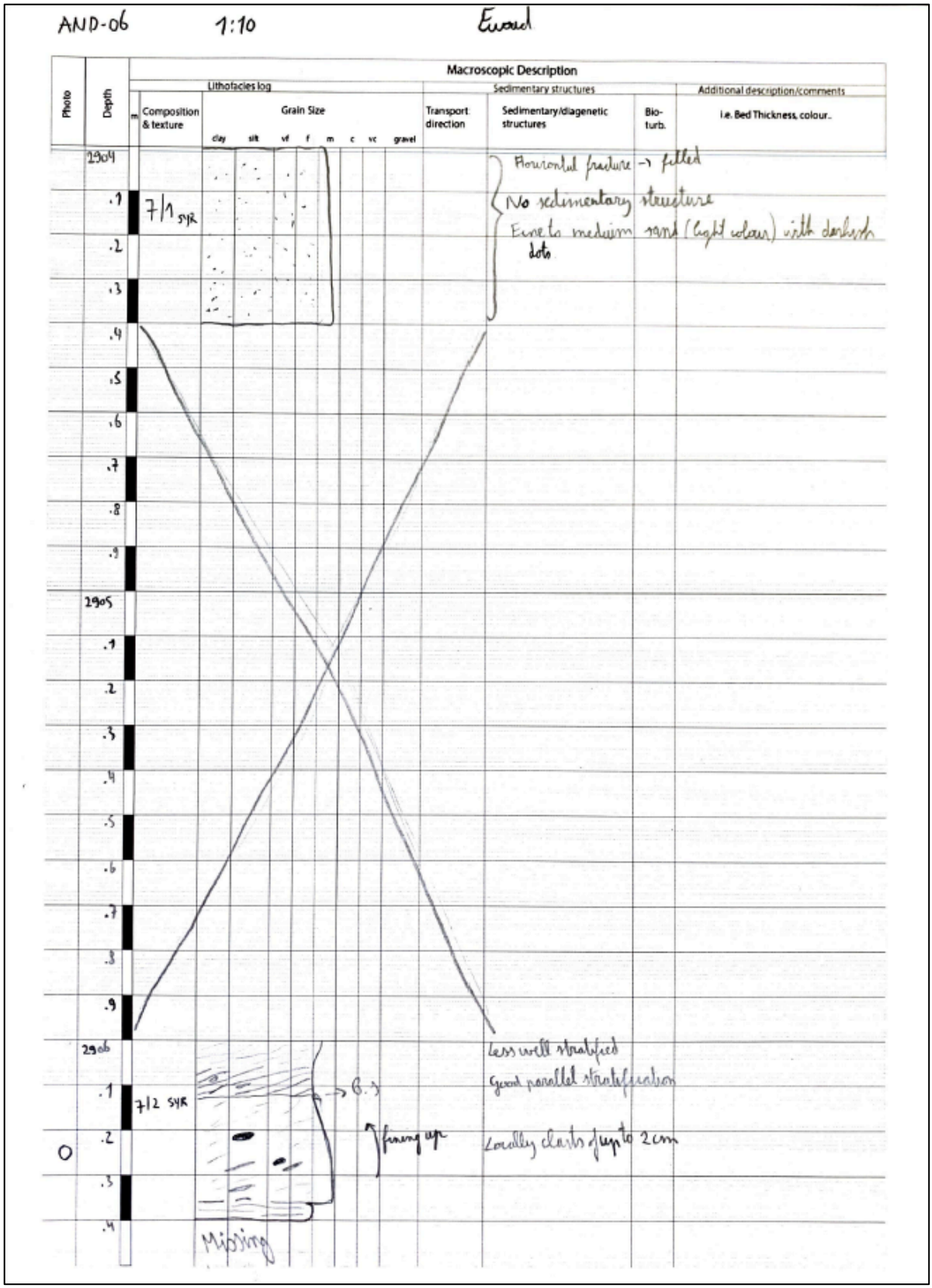

Core description #3 of AND-06 (2906.5- 2904 m)

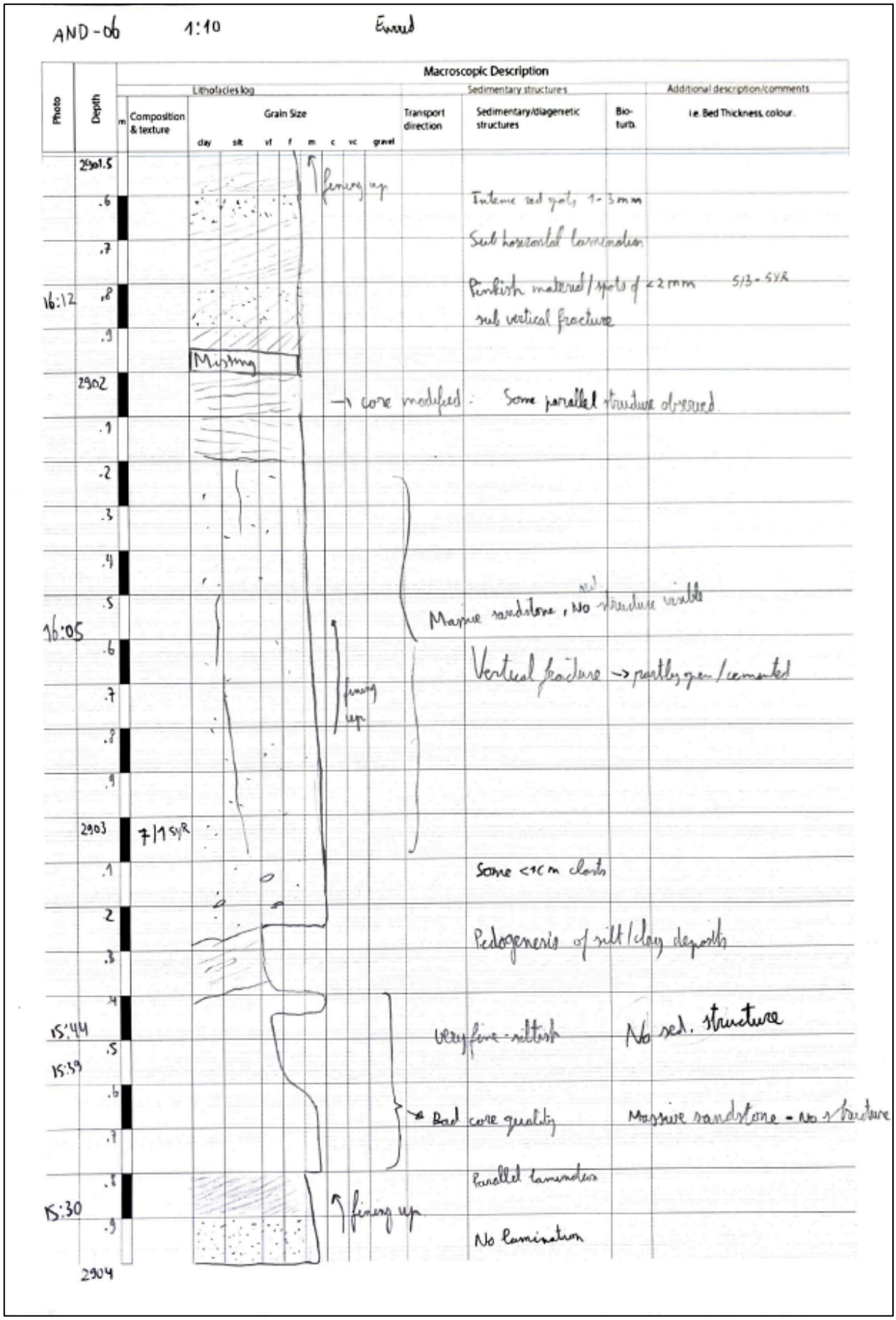

Core description #4 of AND-06 (2904 – 2901.5 m)

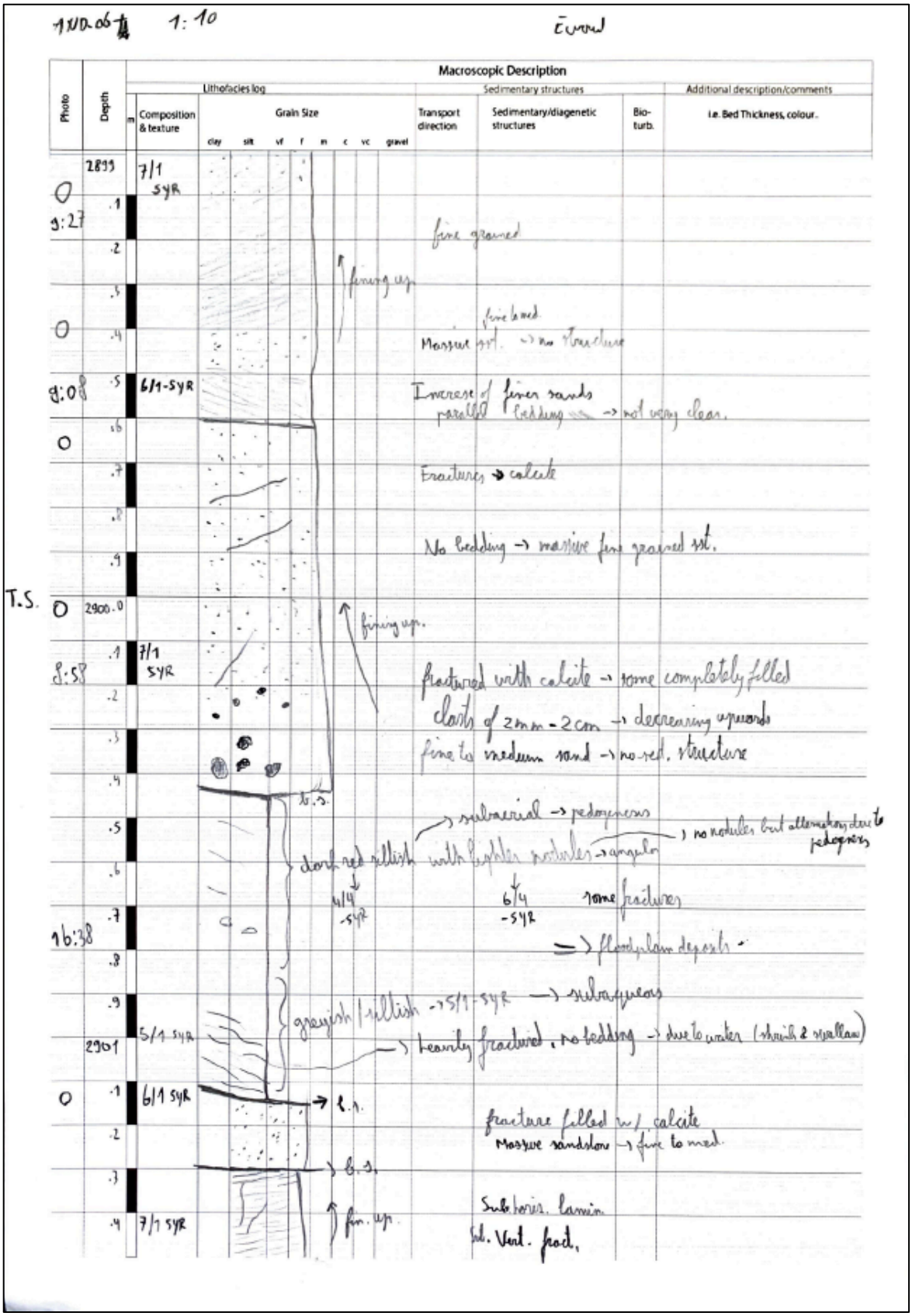

Core description #5 of AND-06 (2901.5- 2899 m)

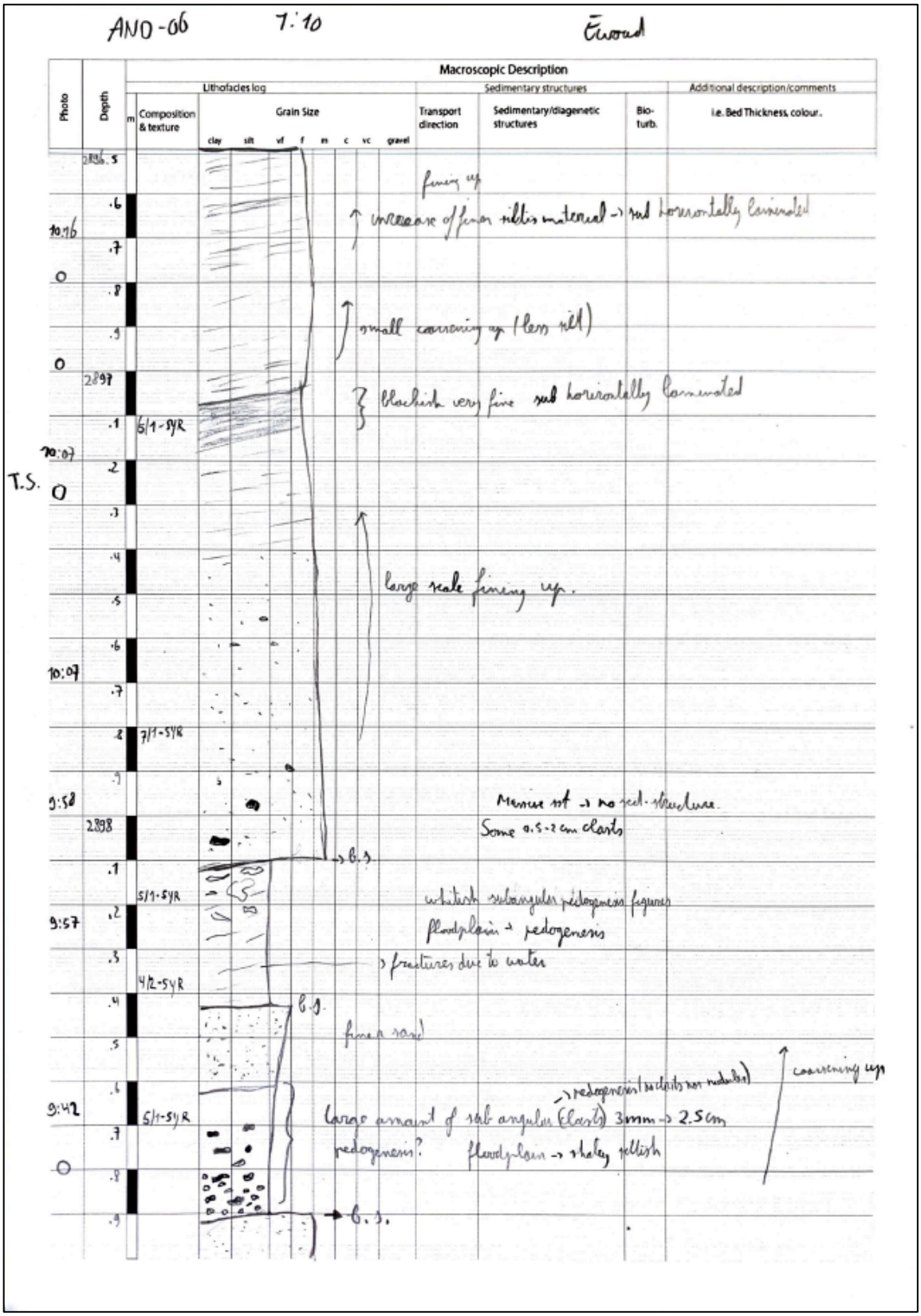

Core description #6 of AND-06 (2899 – 2896.5m)

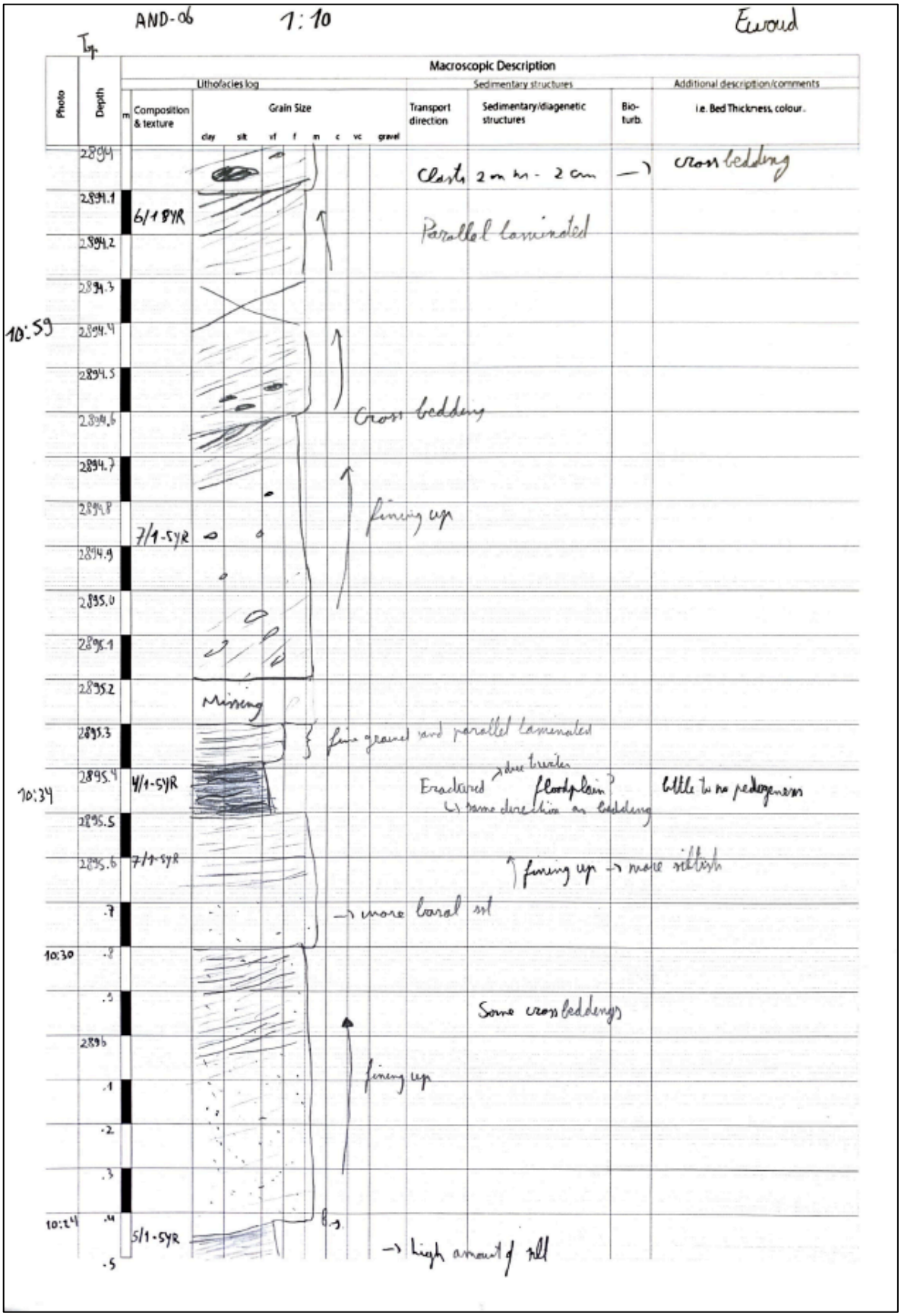

Core description #7 of AND-06 (2896.5 – 2894 m)

Core Description KWK-01 (Logged at 1:25 Scale)

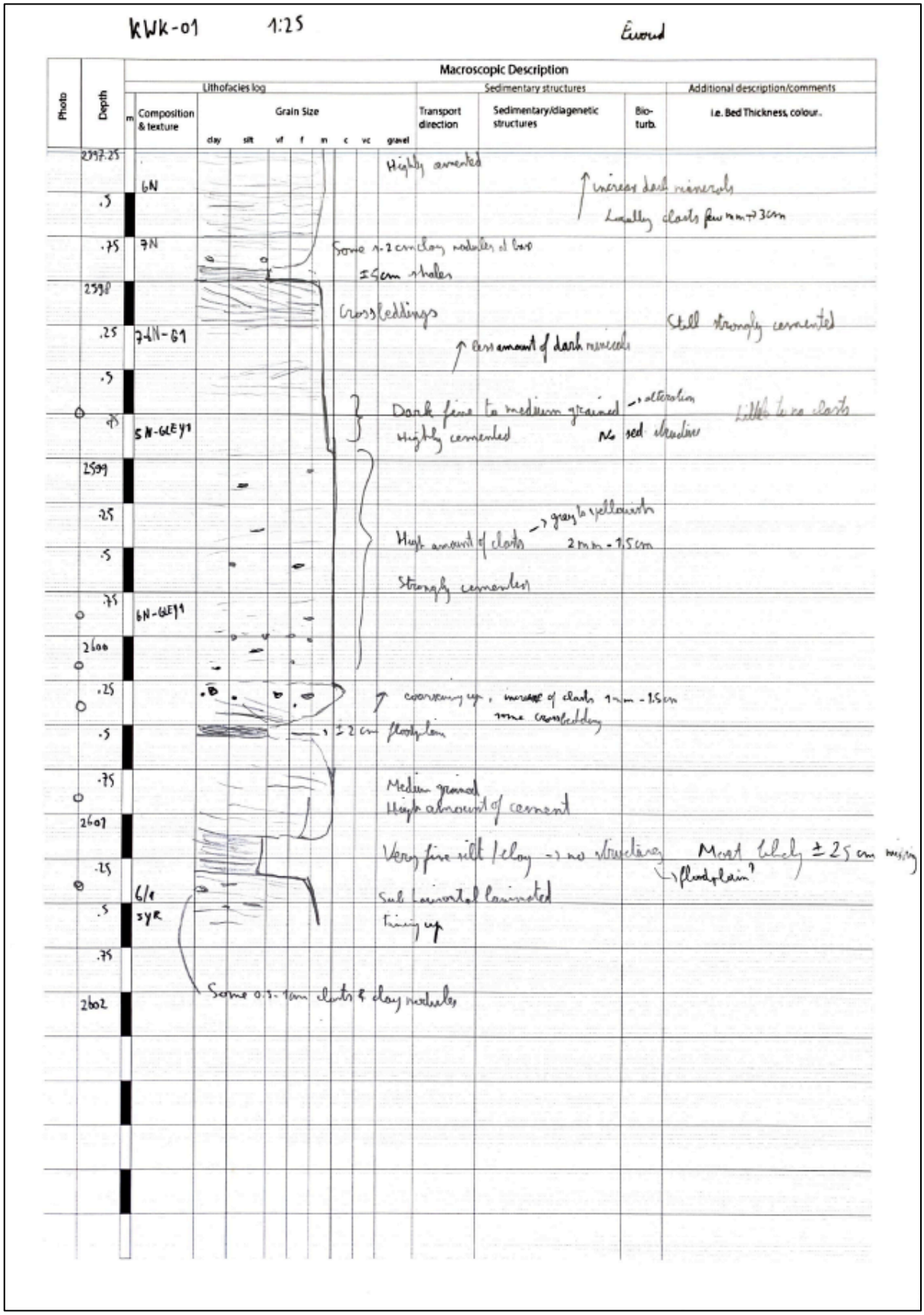

Core description #1 of KWK-01 (2601.6 – 2597.25 m).

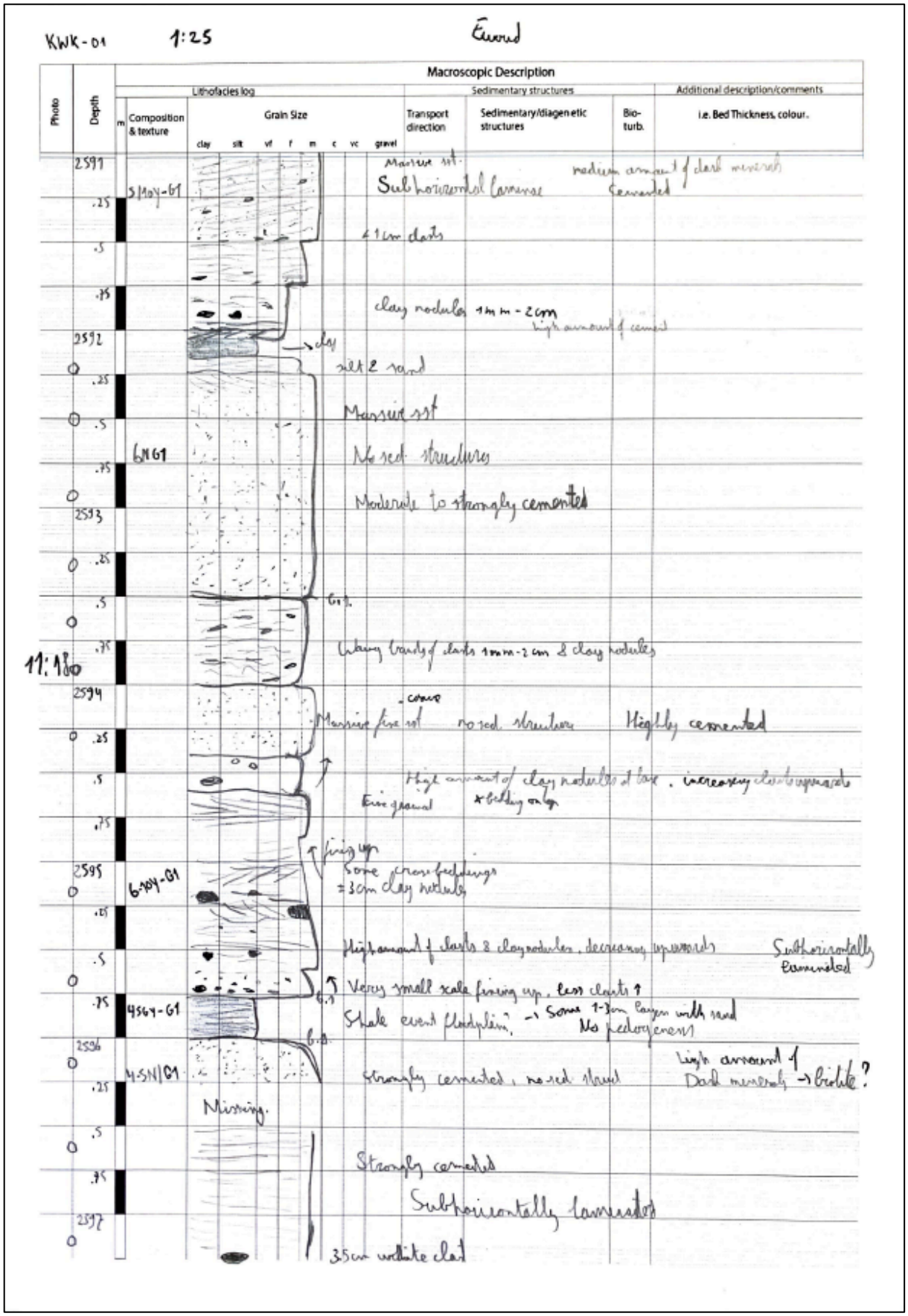

Core description #2 of KWK-01 (2597.25 - 2591 m).

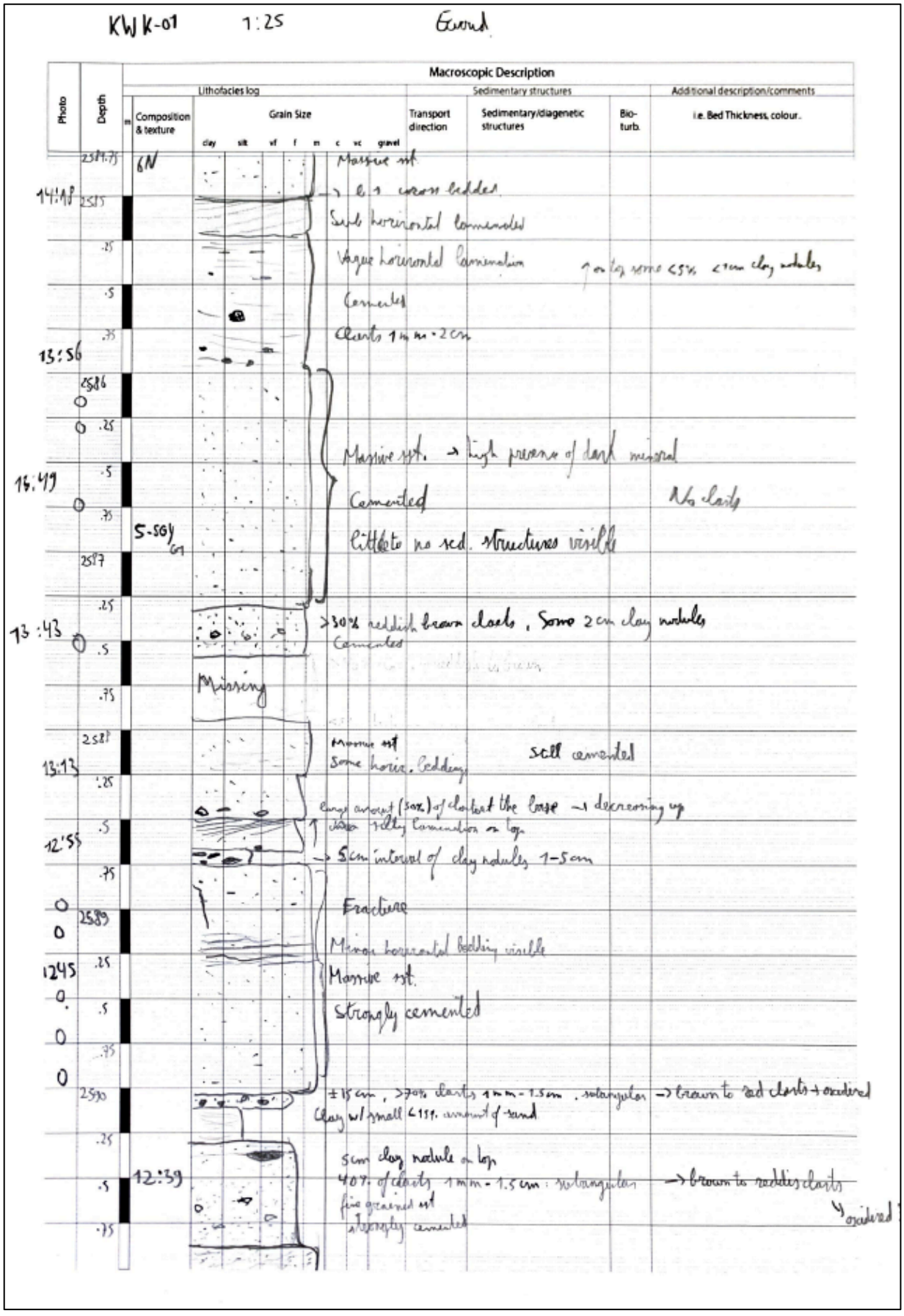

Core description #3 of KWK-01 (2591 – 2584.75 m).

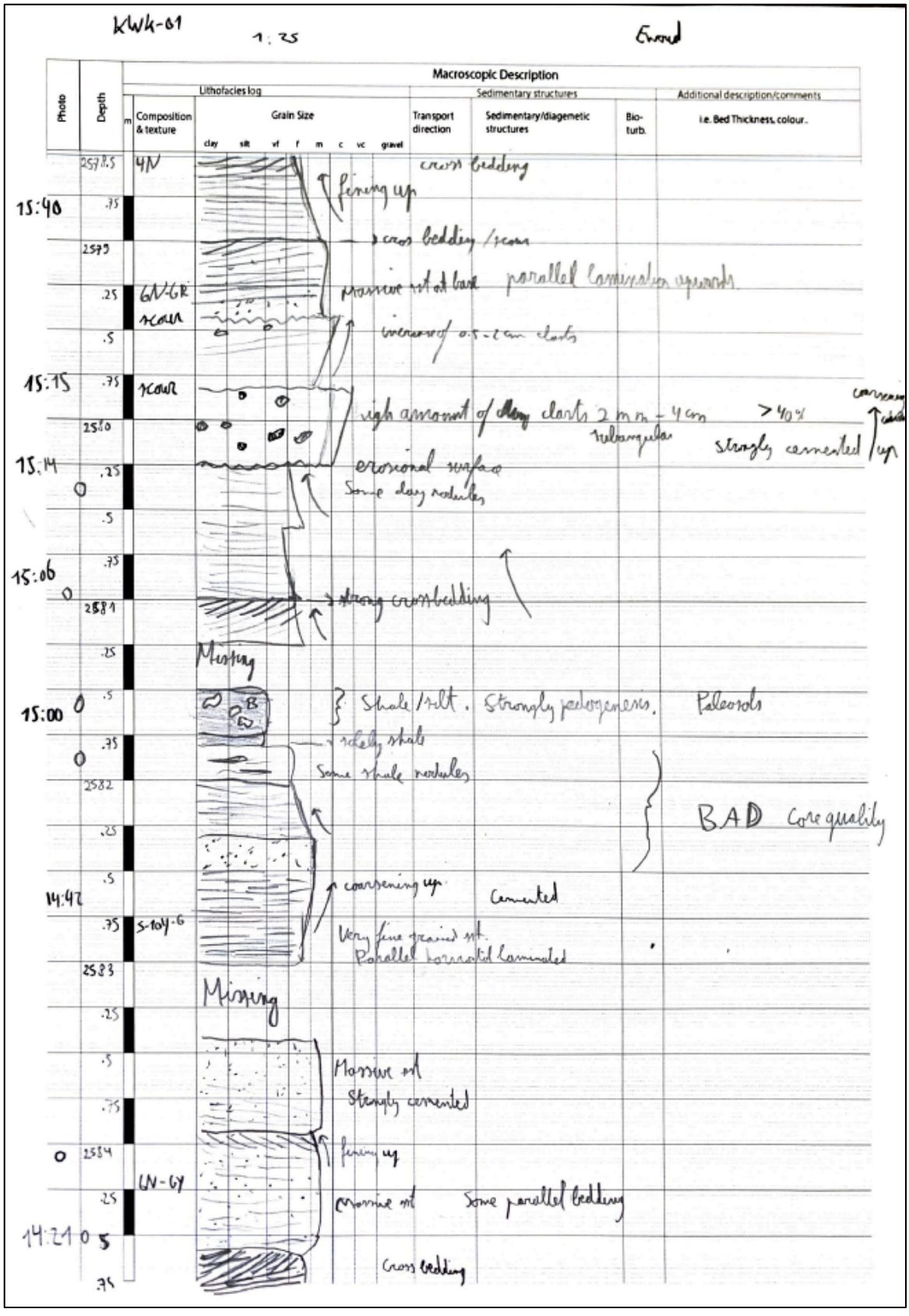

Core description #4 of KWK-01 (2584.75 – 2578.5 m).

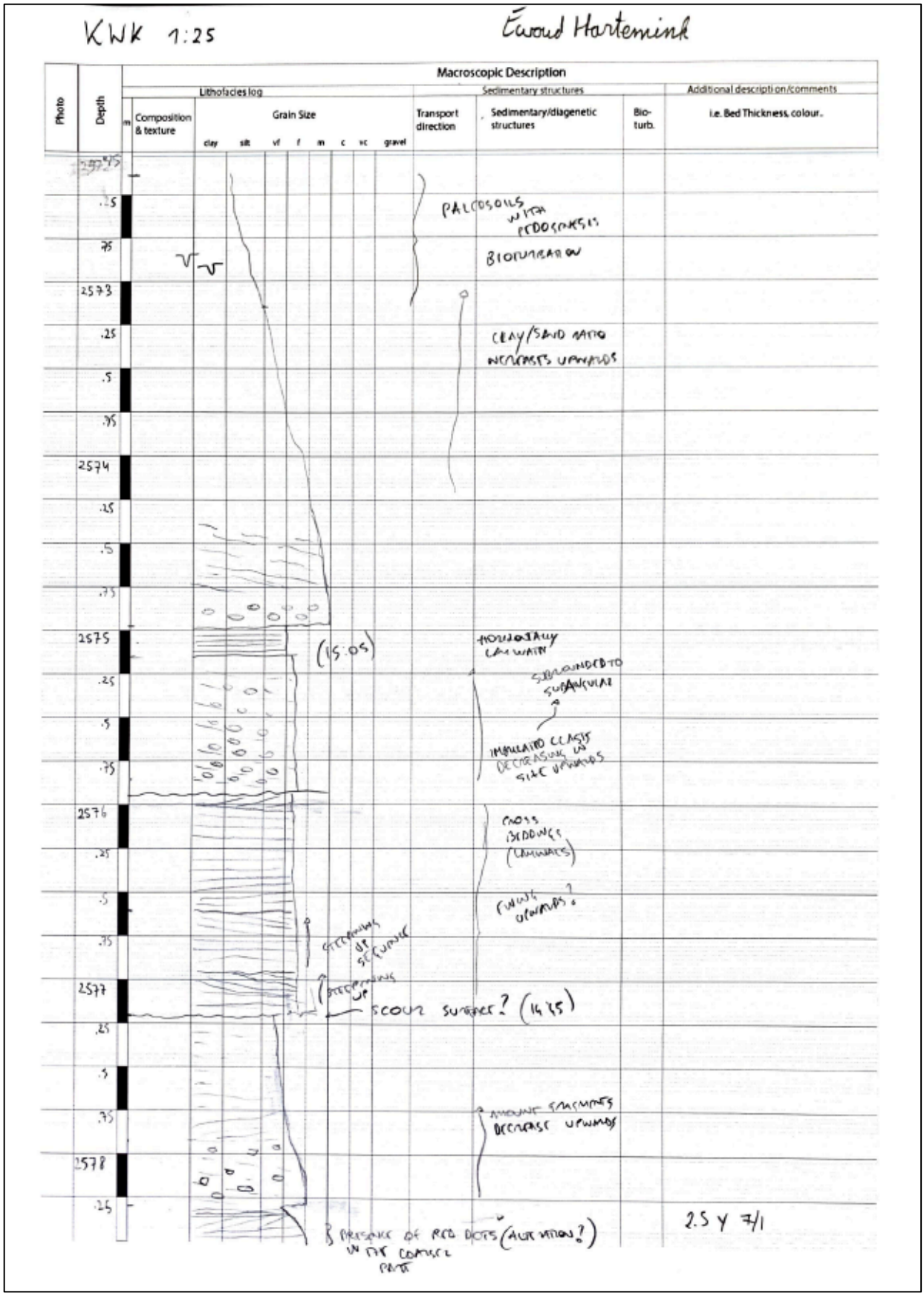

Core description #5 of KWK-01 (2578.5 - 2572 m).

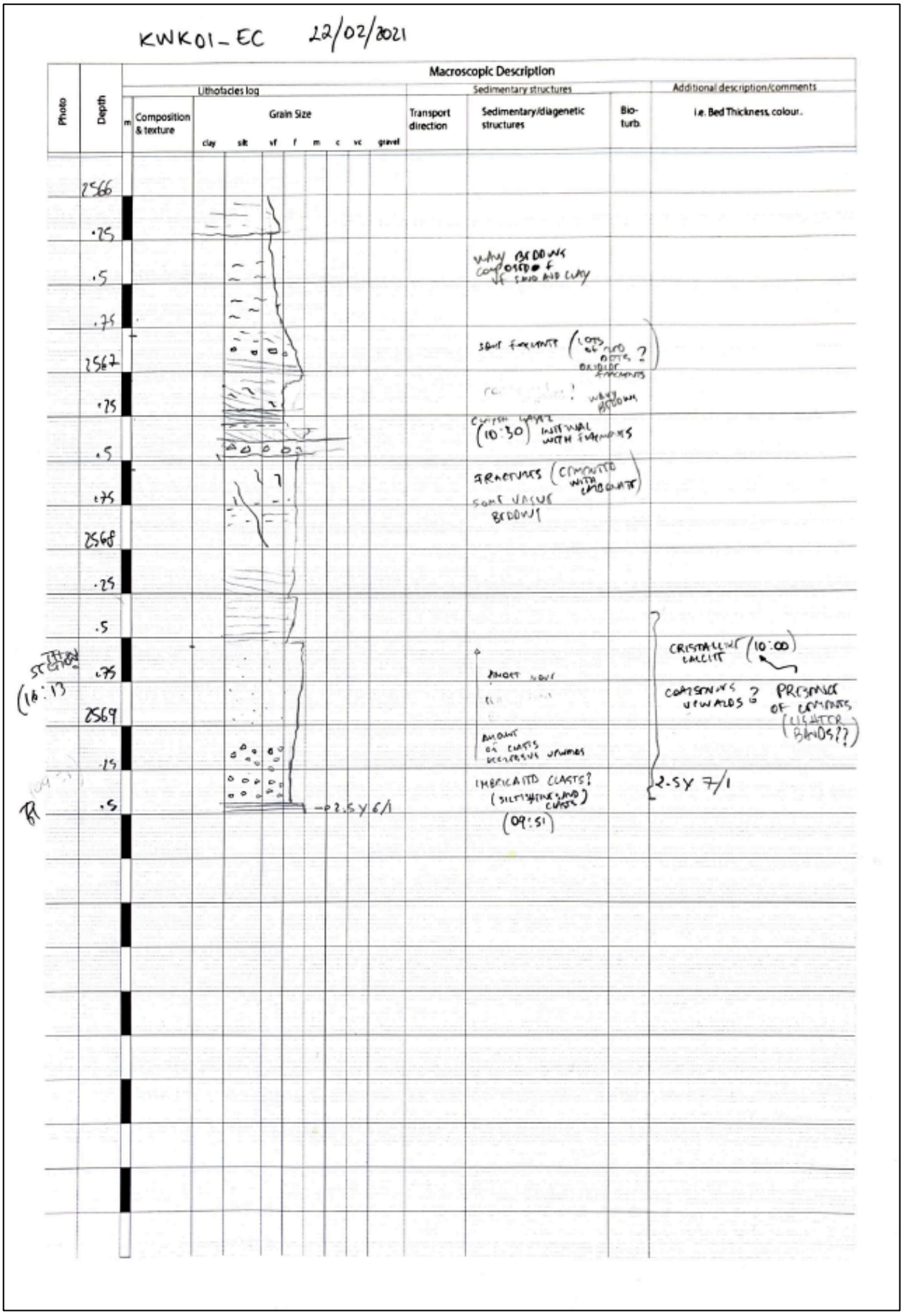

Core description #6 of KWK-01 (2569.5 - 2566 m).

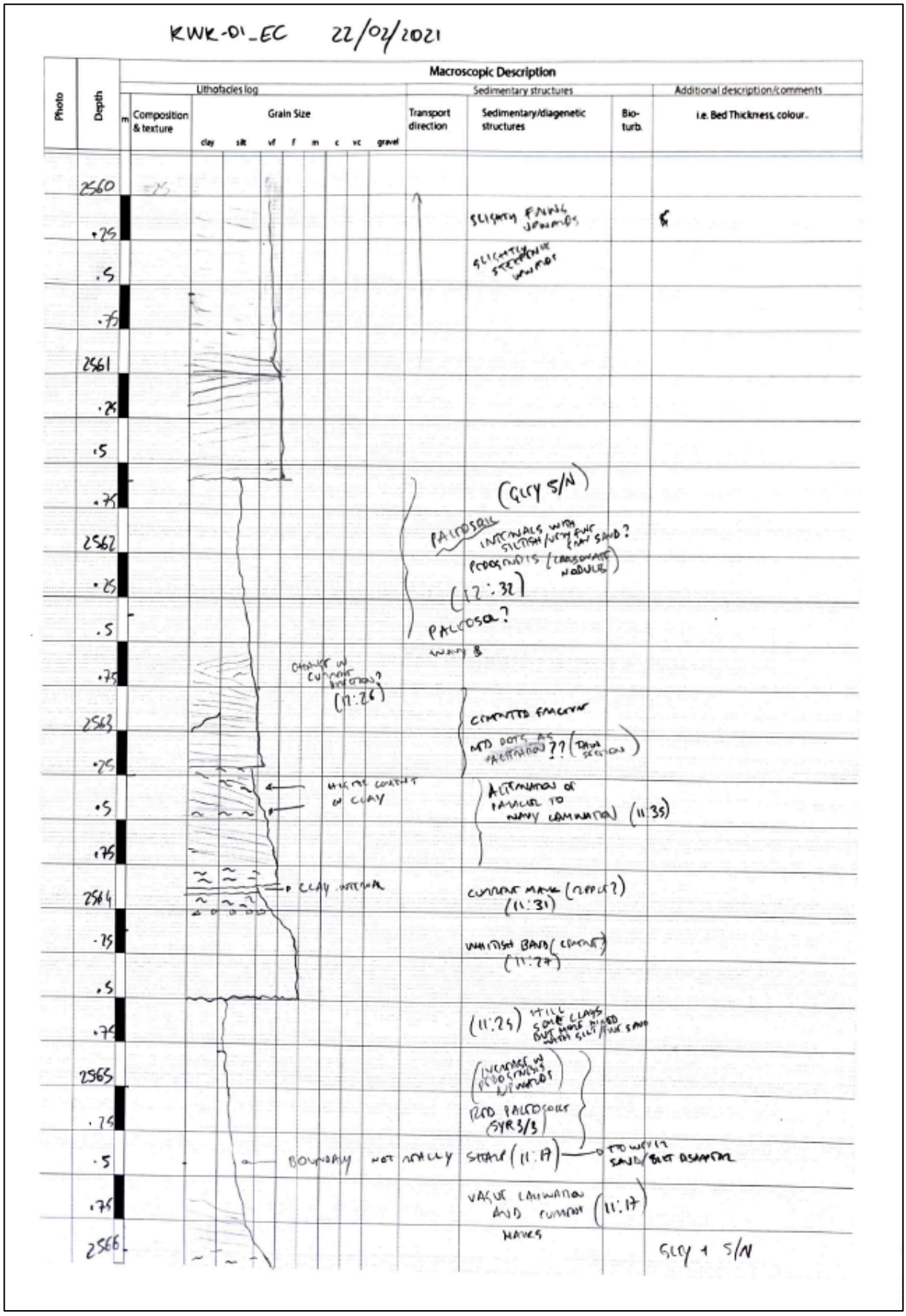

Core description #7 of KWK-01 (2566 – 2560 m).

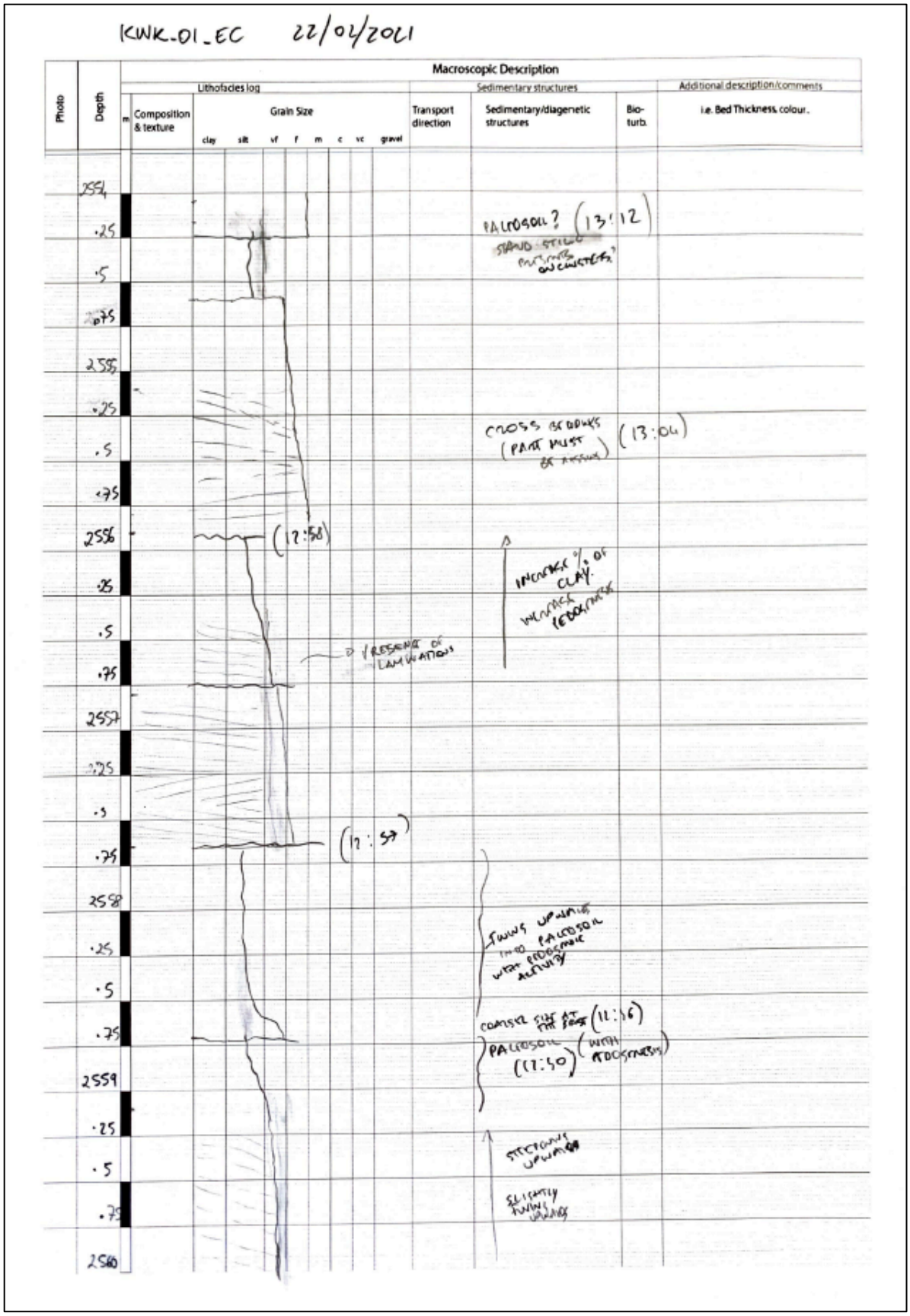

Core description #8 of KWK-01 (2560 – 2554 m).

Core Description WWN-01-S2 (Logged at 1:50 Scale)

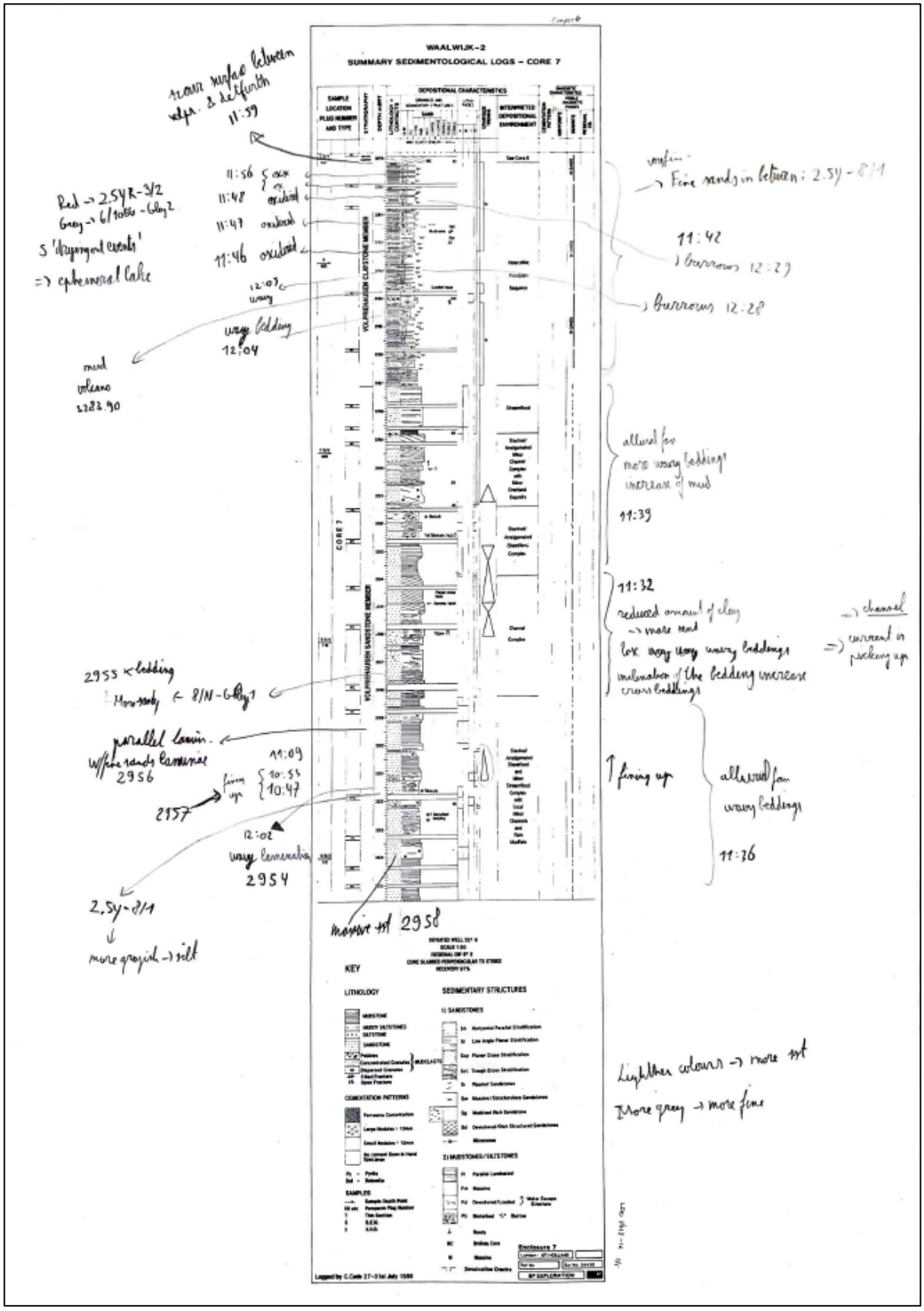

Core description #1 of WWN-01-S2 (3305.5 - 3279 m).

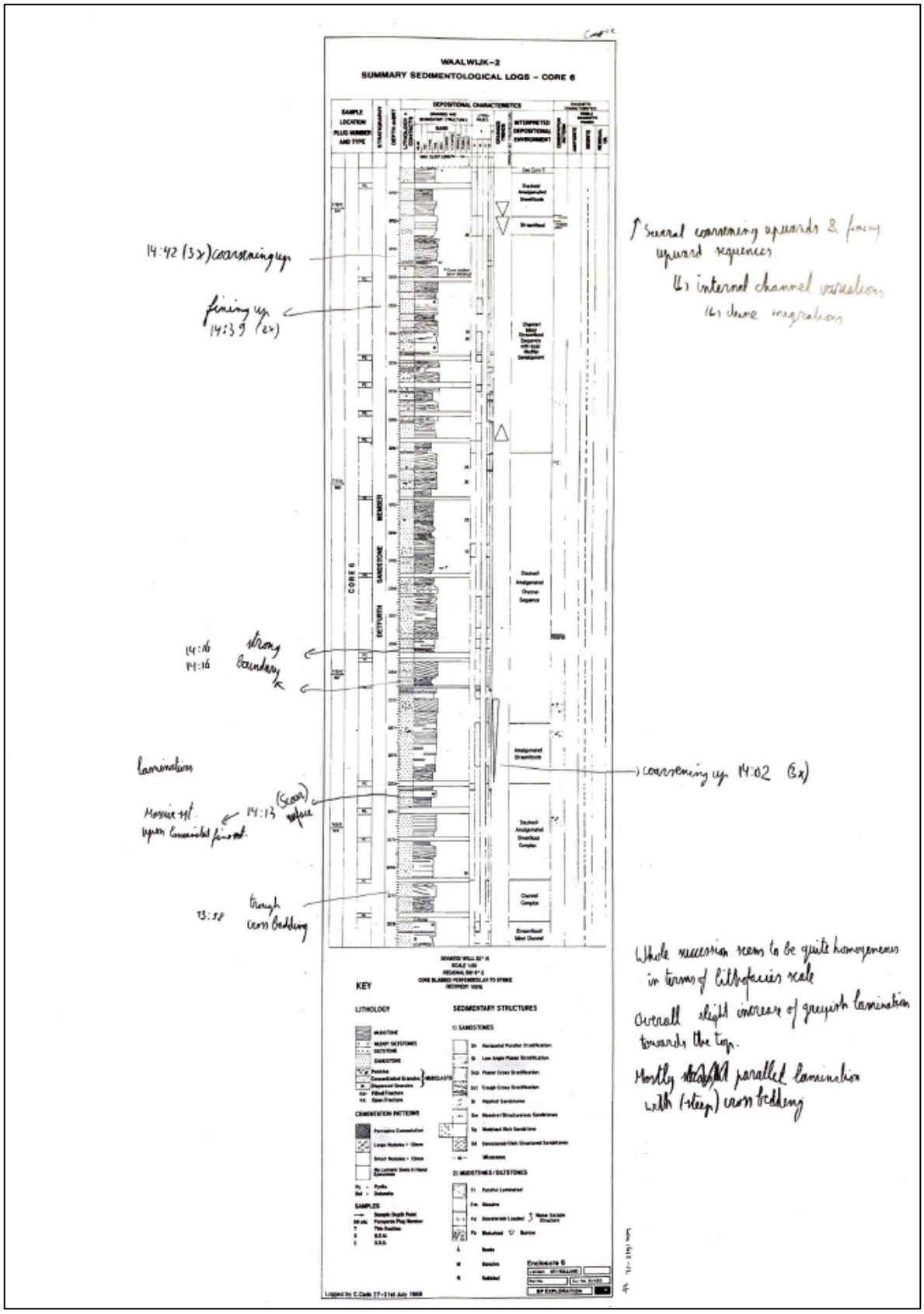

Core description #3 of WWN-01-S2 (3279 – 3251.1 m).

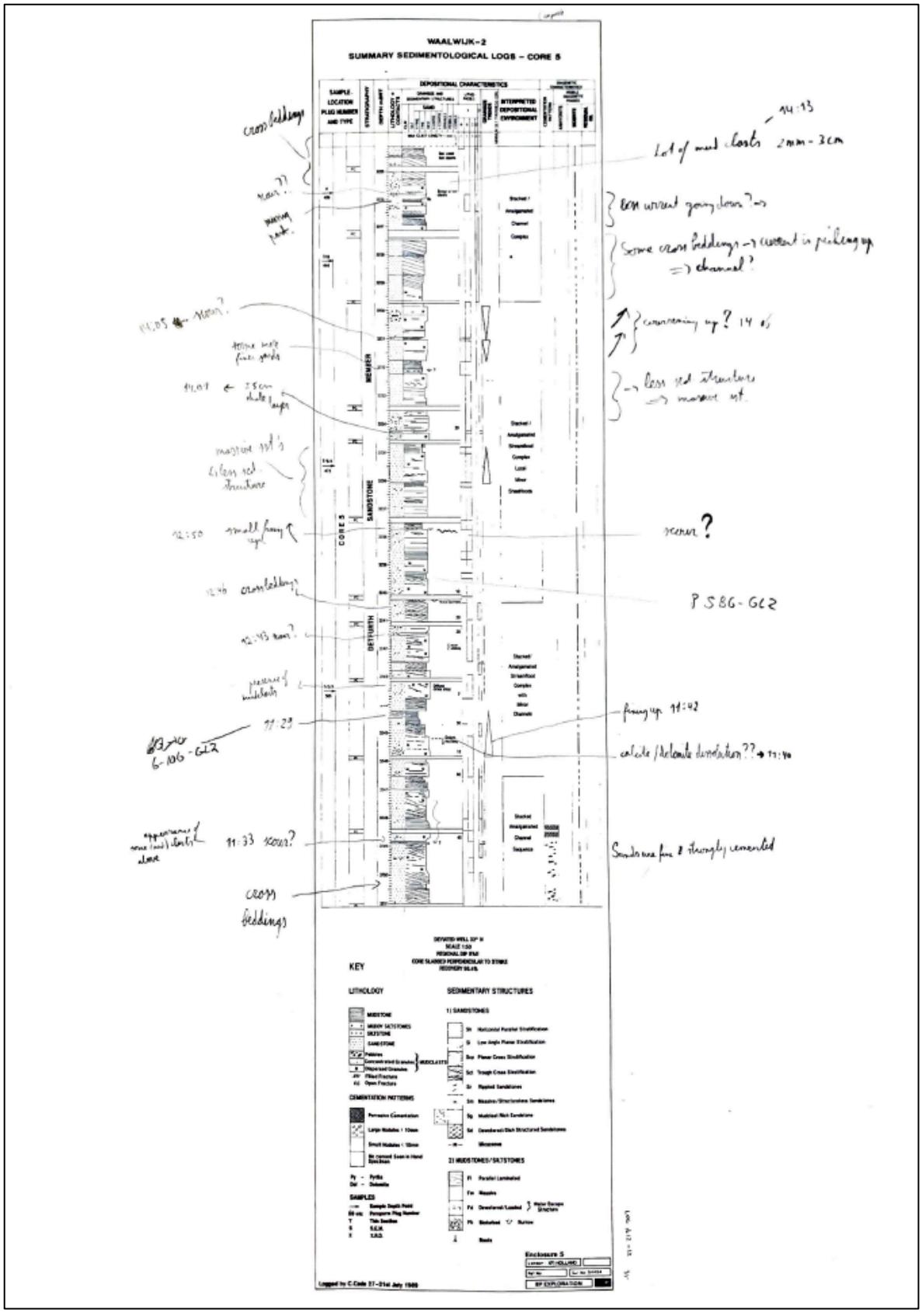

Core description #4 of WWN-01-S2 (3251.1 – 3224.1 m).

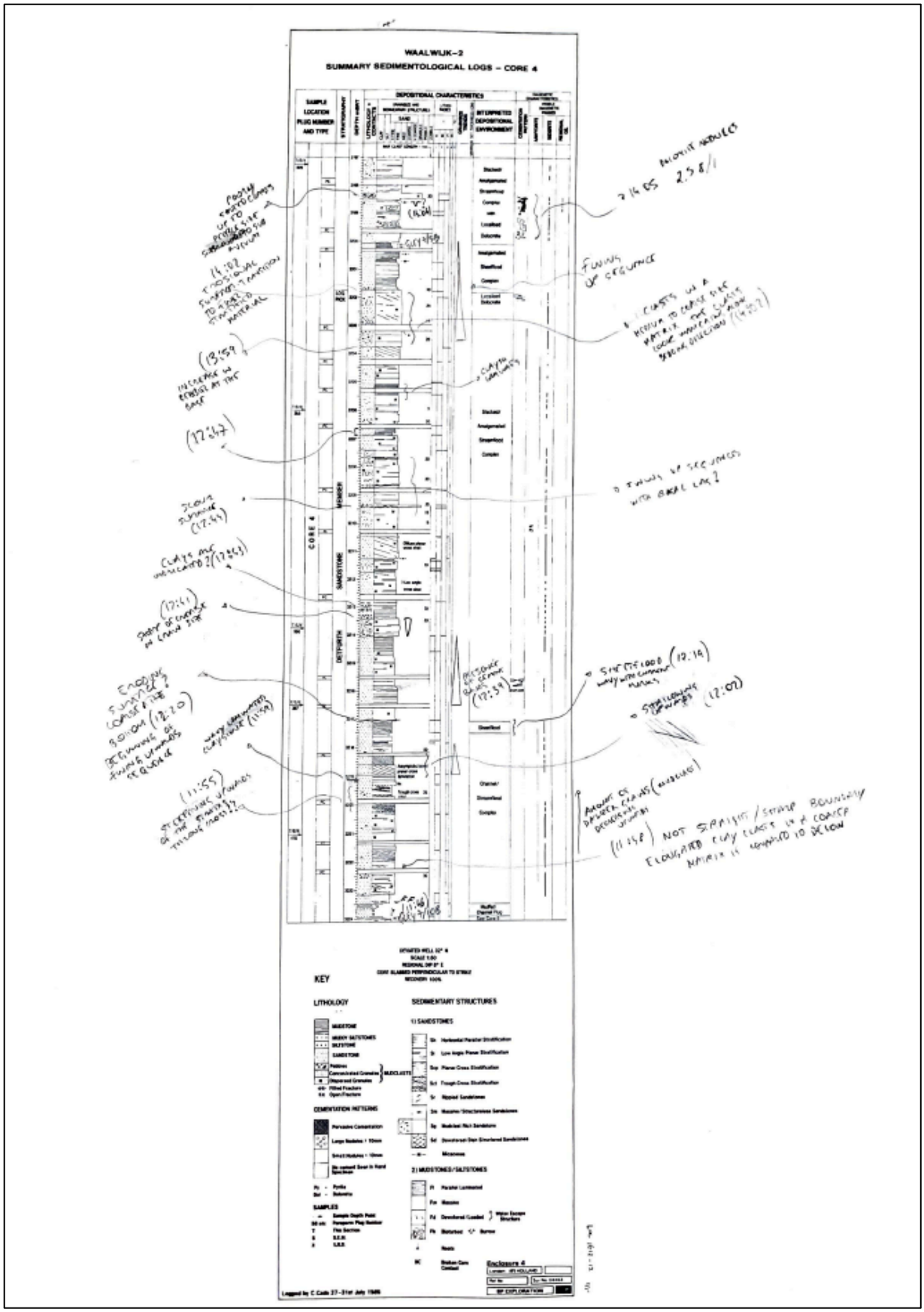

Core description #5 of WWN-01-S2 (3224.1 – 3197 m).

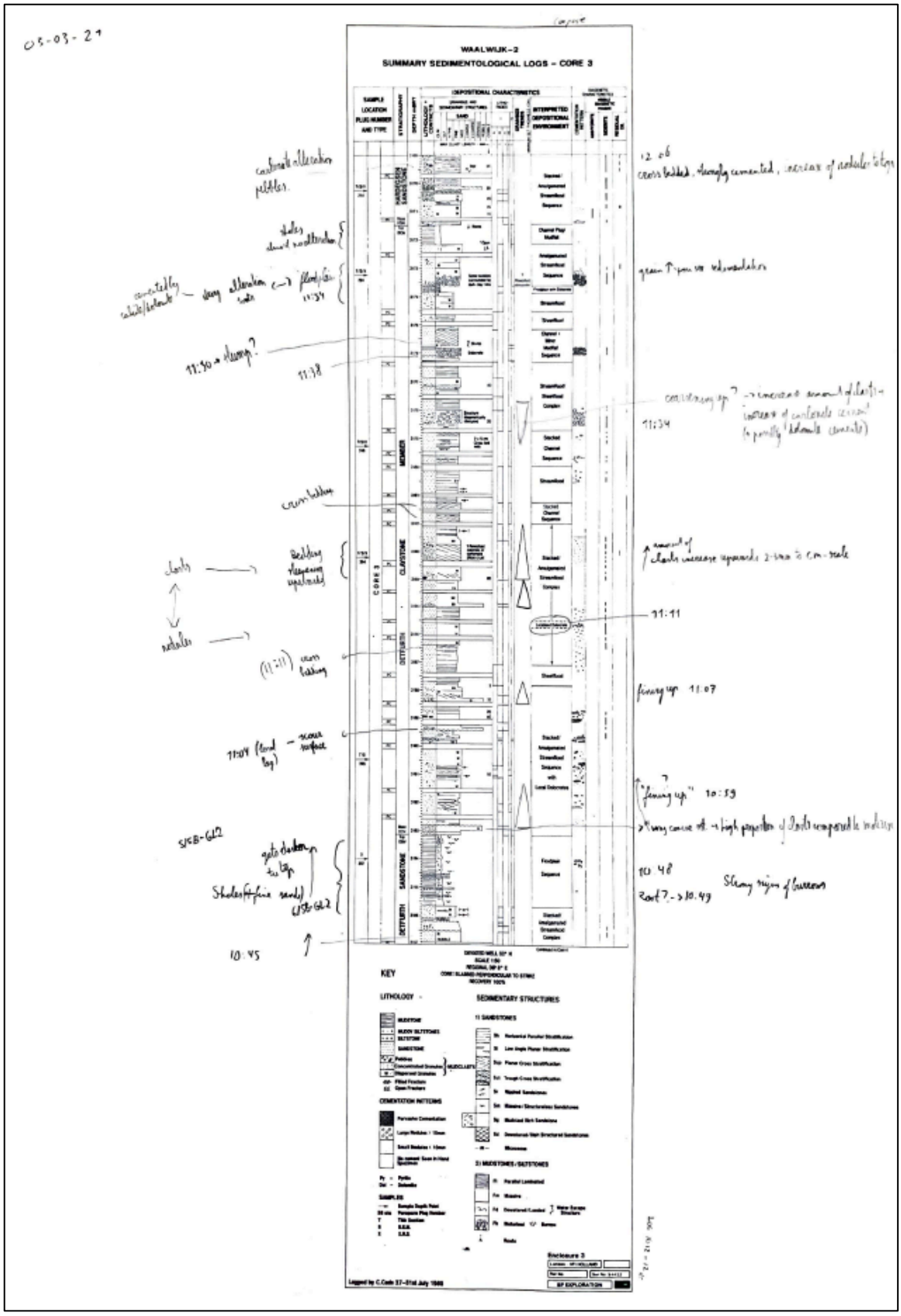

Core description #6 of WWN-01-S2 (3197 – 3169 m).

Core Description SPC-01 (Logged at 1:10 Scale)

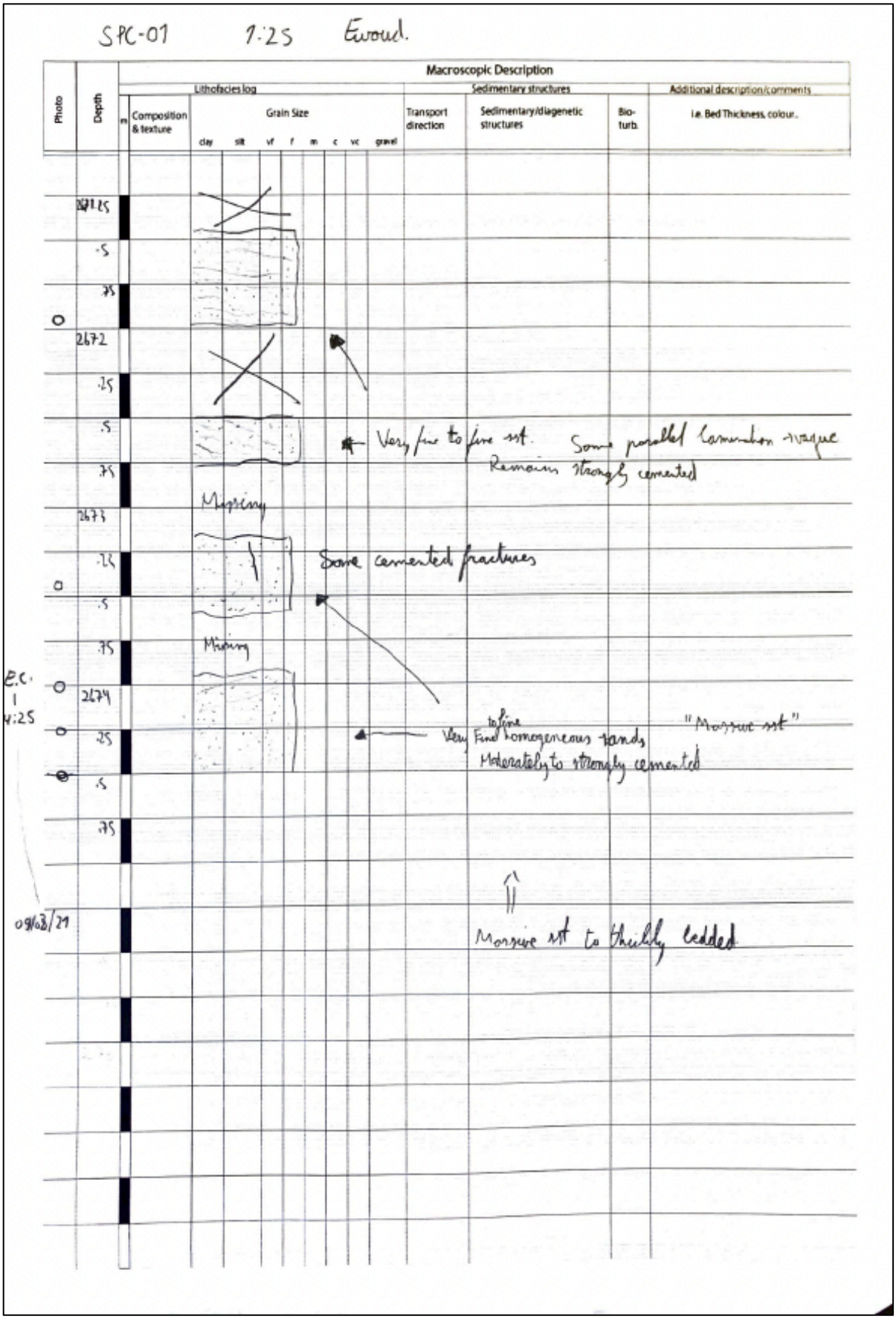

Core description #1 of SPC-01 (2671 – 2674.5 m)

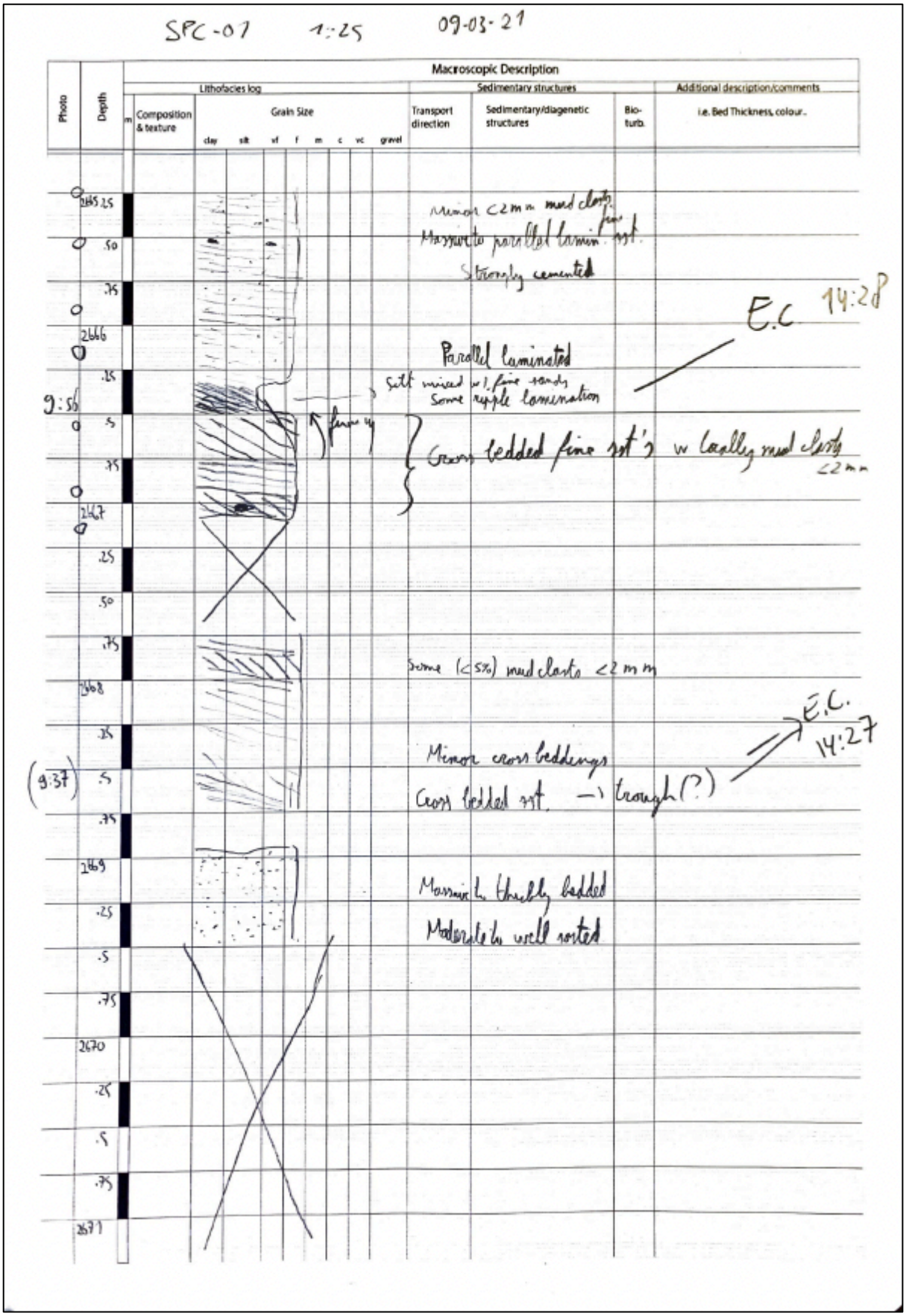

Core description #2 of SPC-01 (2674.5 – 2665 m)

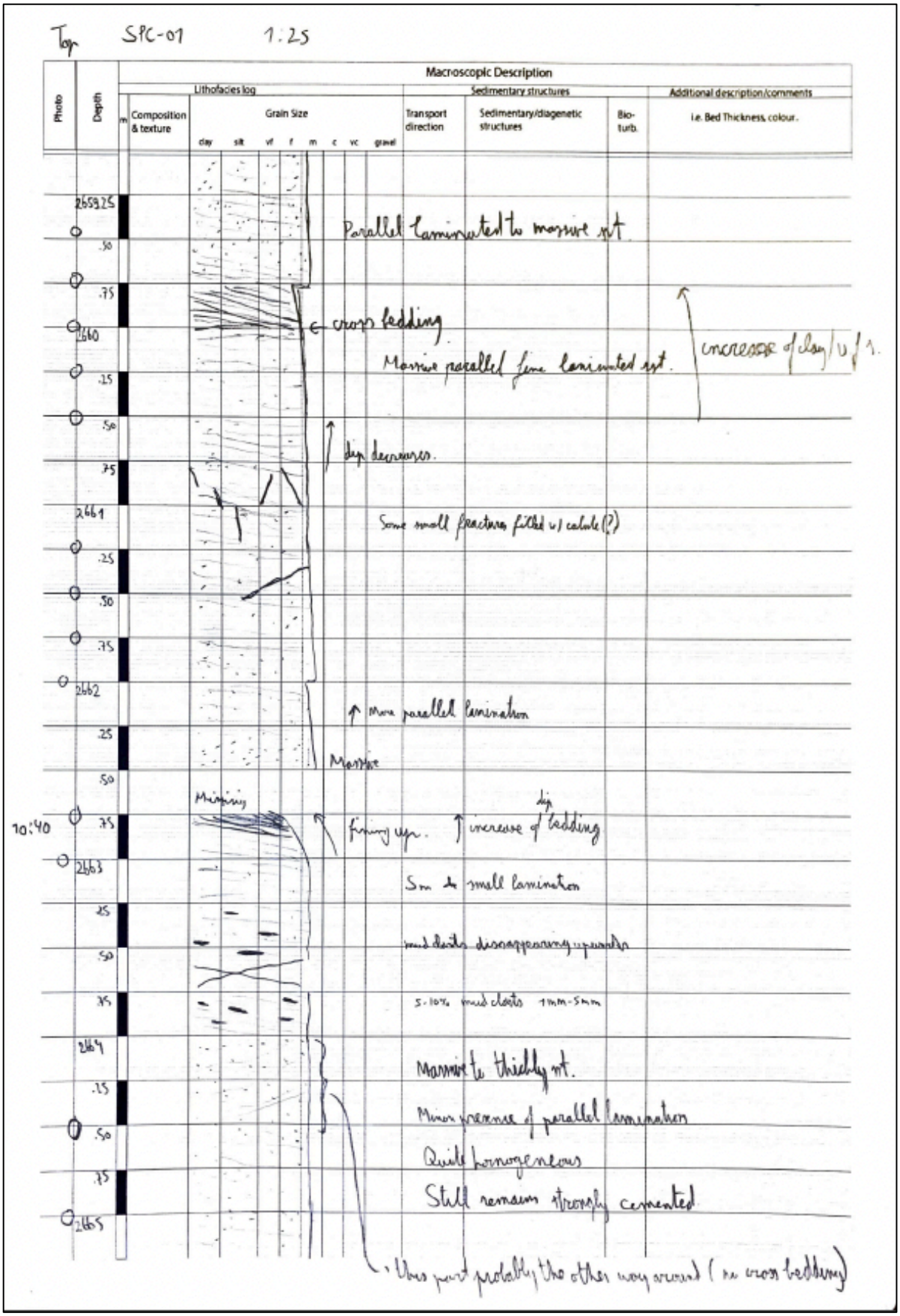

Core description #3 of SPC-01 (2665 – 2659 m)

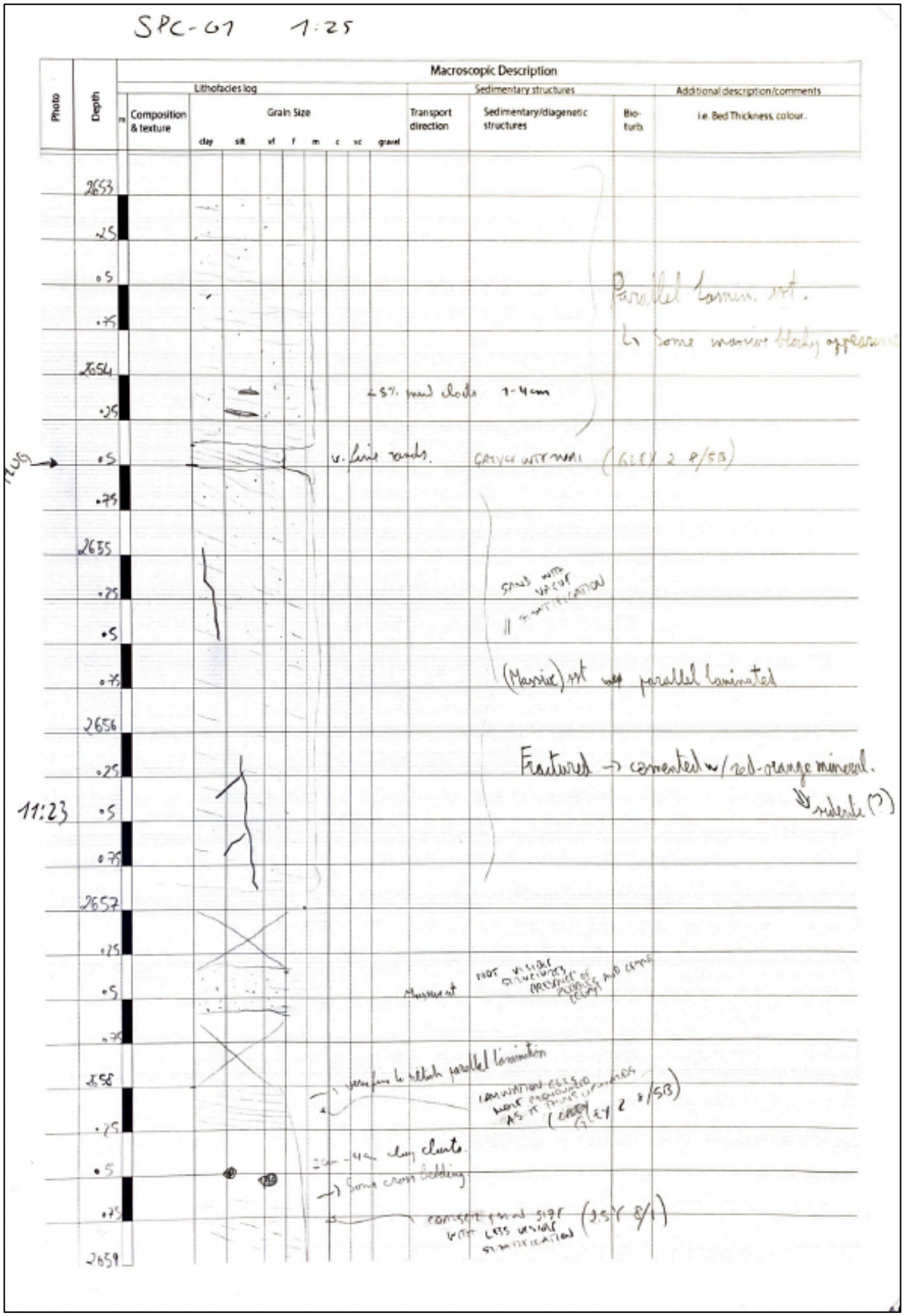

Core description #4 of SPC-01 (2659 – 2653 m)

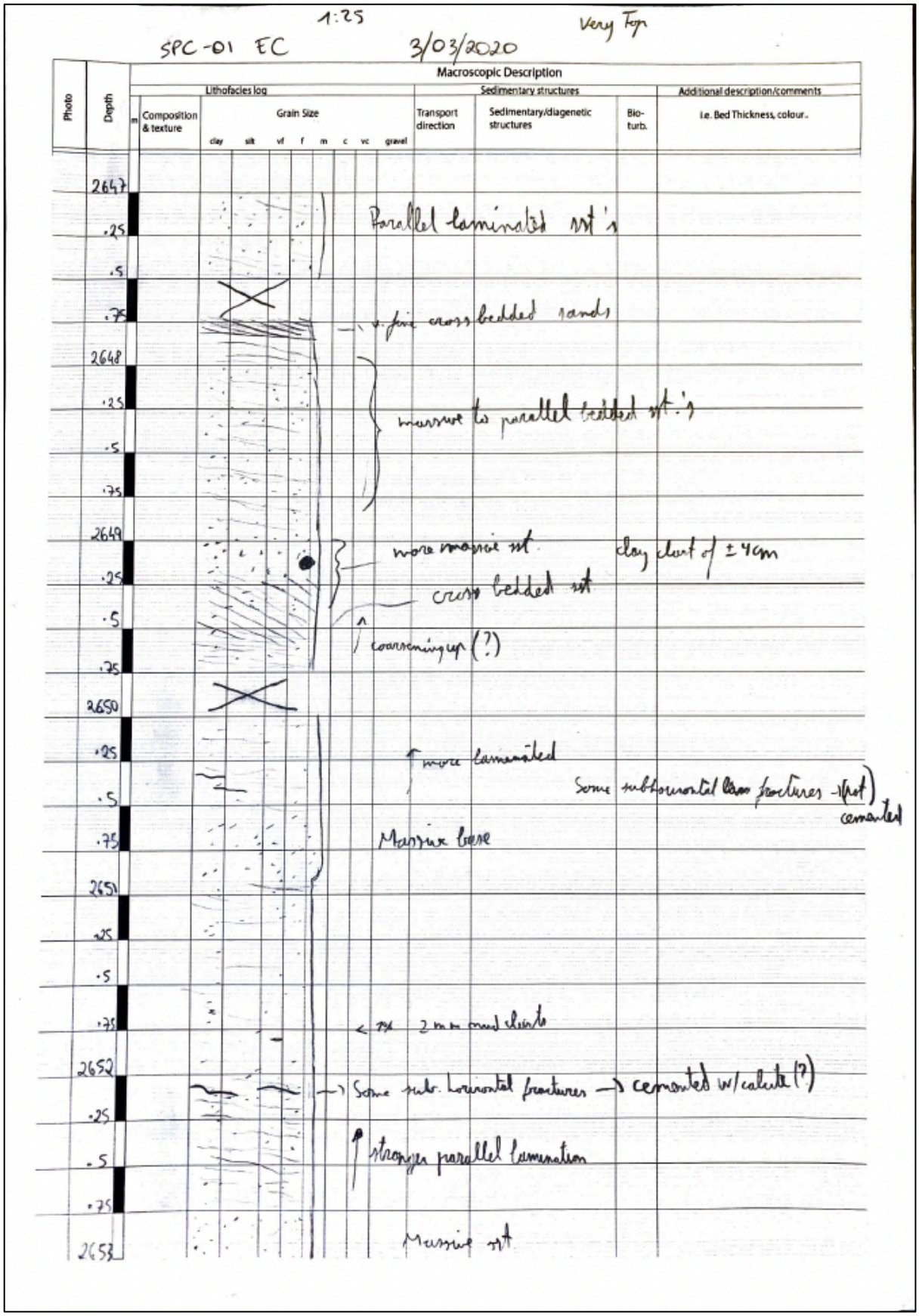

Core description #5 of SPC-01 (2653 – 2647 m)

B. Petrophysical Data

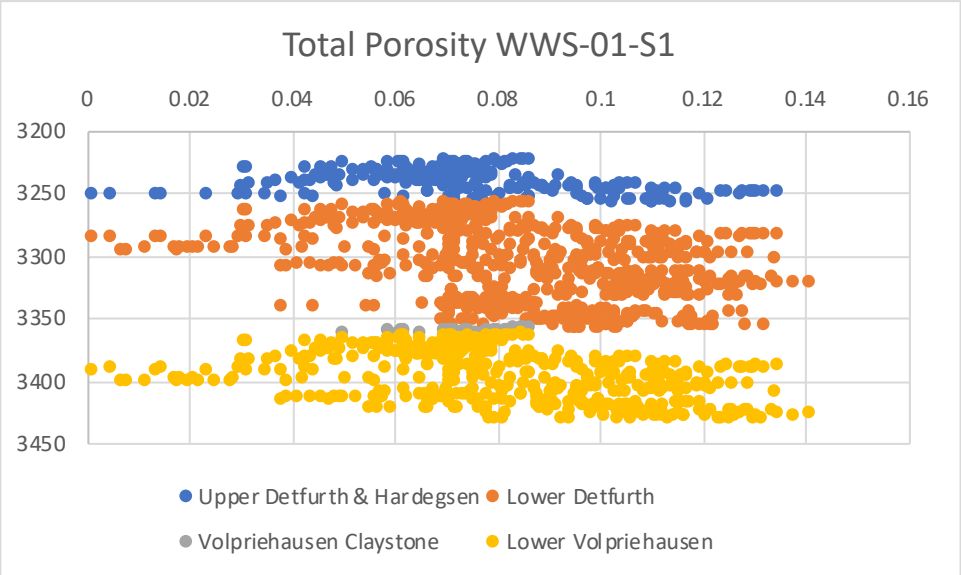

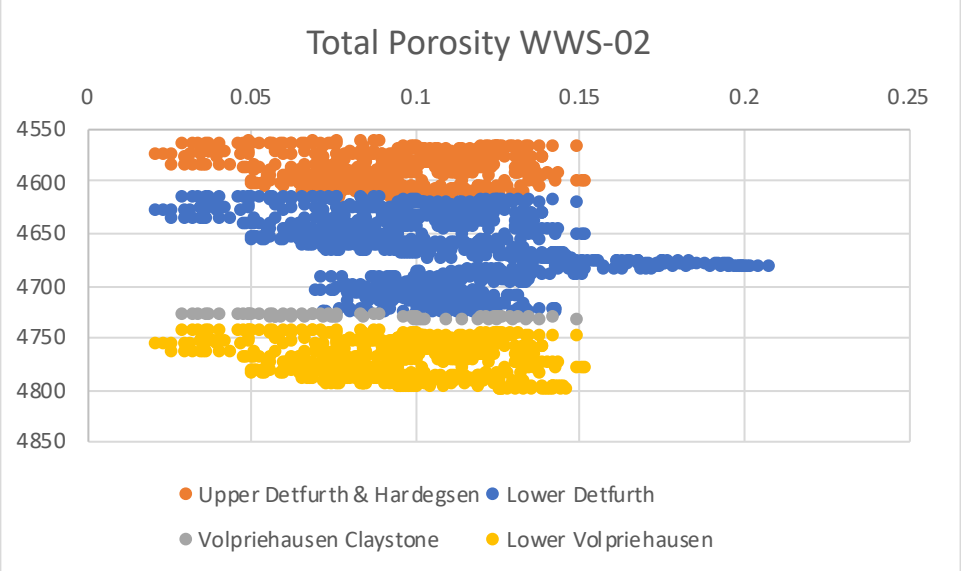

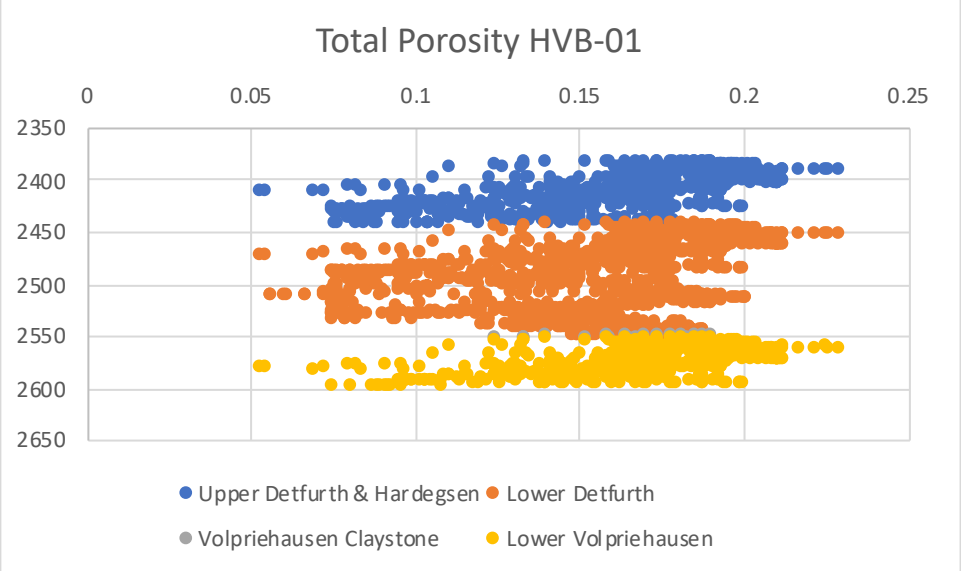

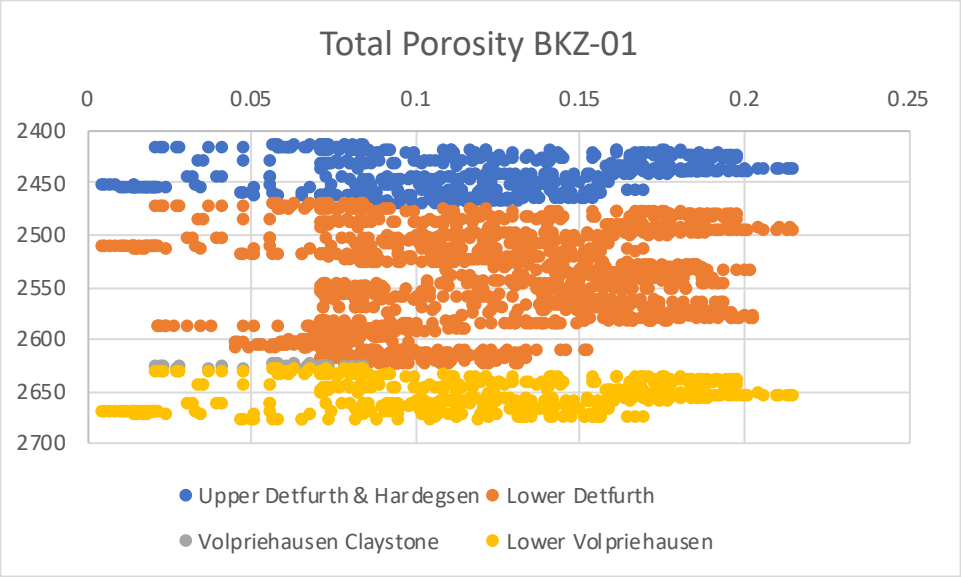

Total porosity plots of the four uncored wells.

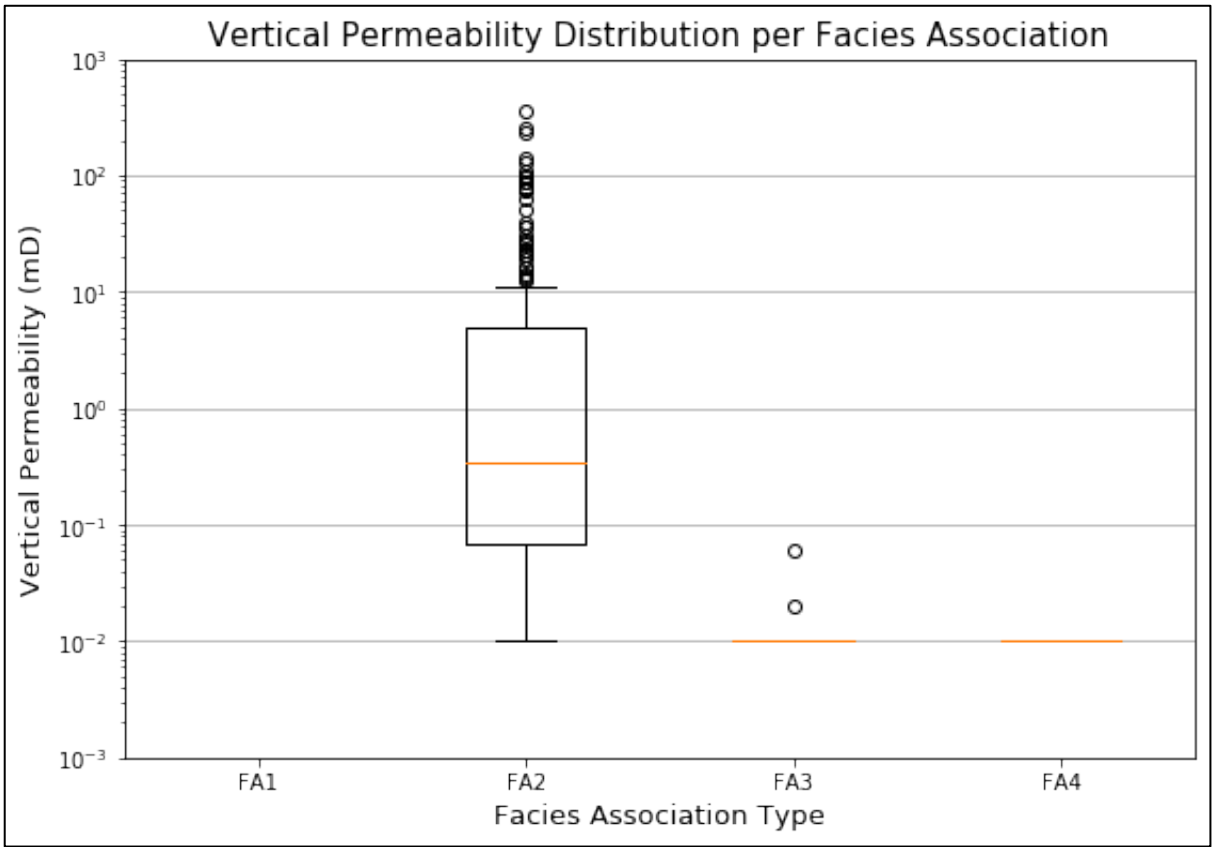

Vertical permeability boxplot of the four different facies associations.

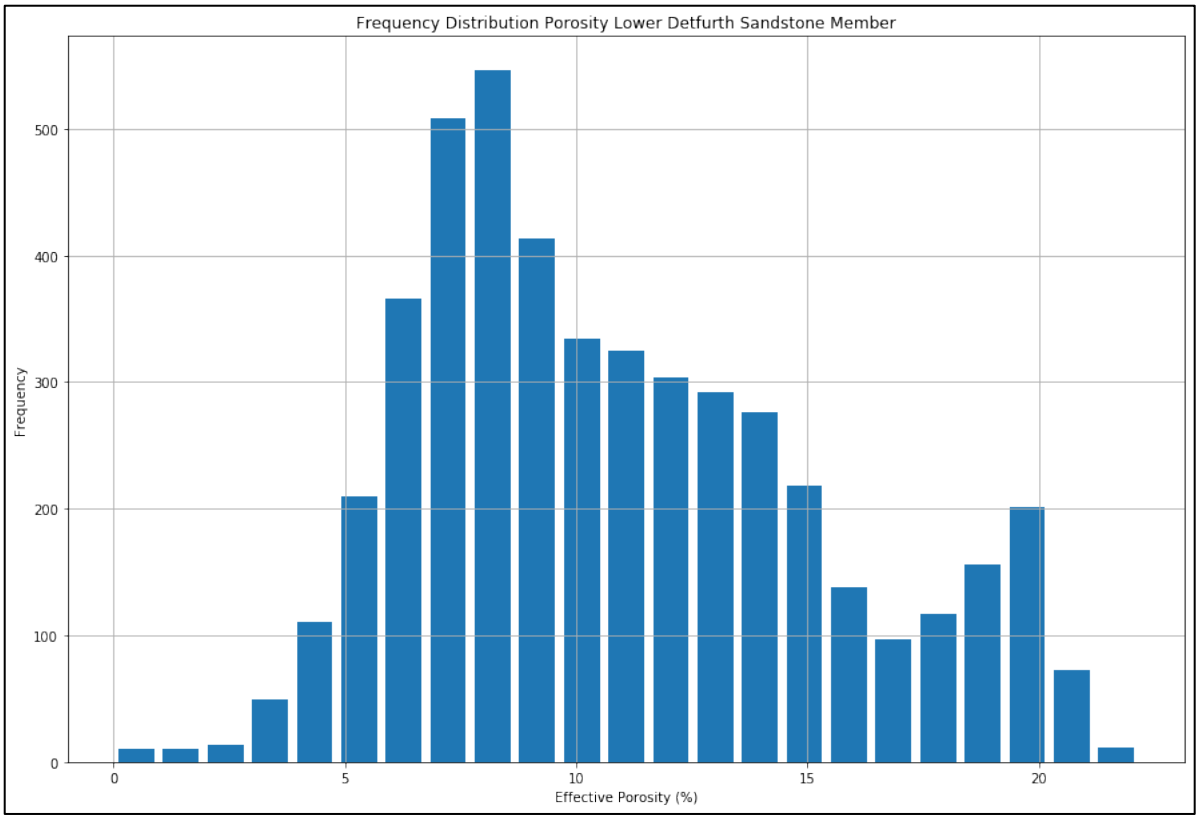

Porosity histogram of the Lower Detfurth Member

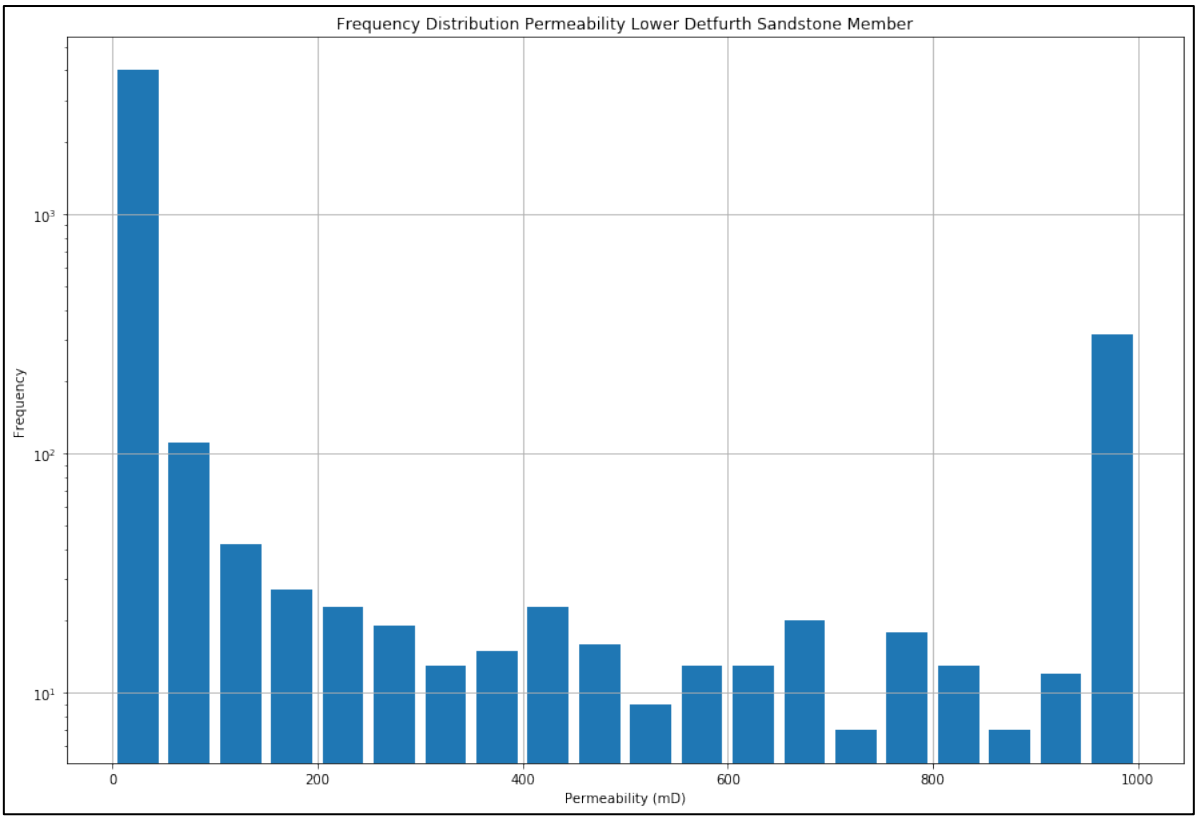

Permeability histogram of the Lower Detfurth Member

C. Full Stratigraphic Model

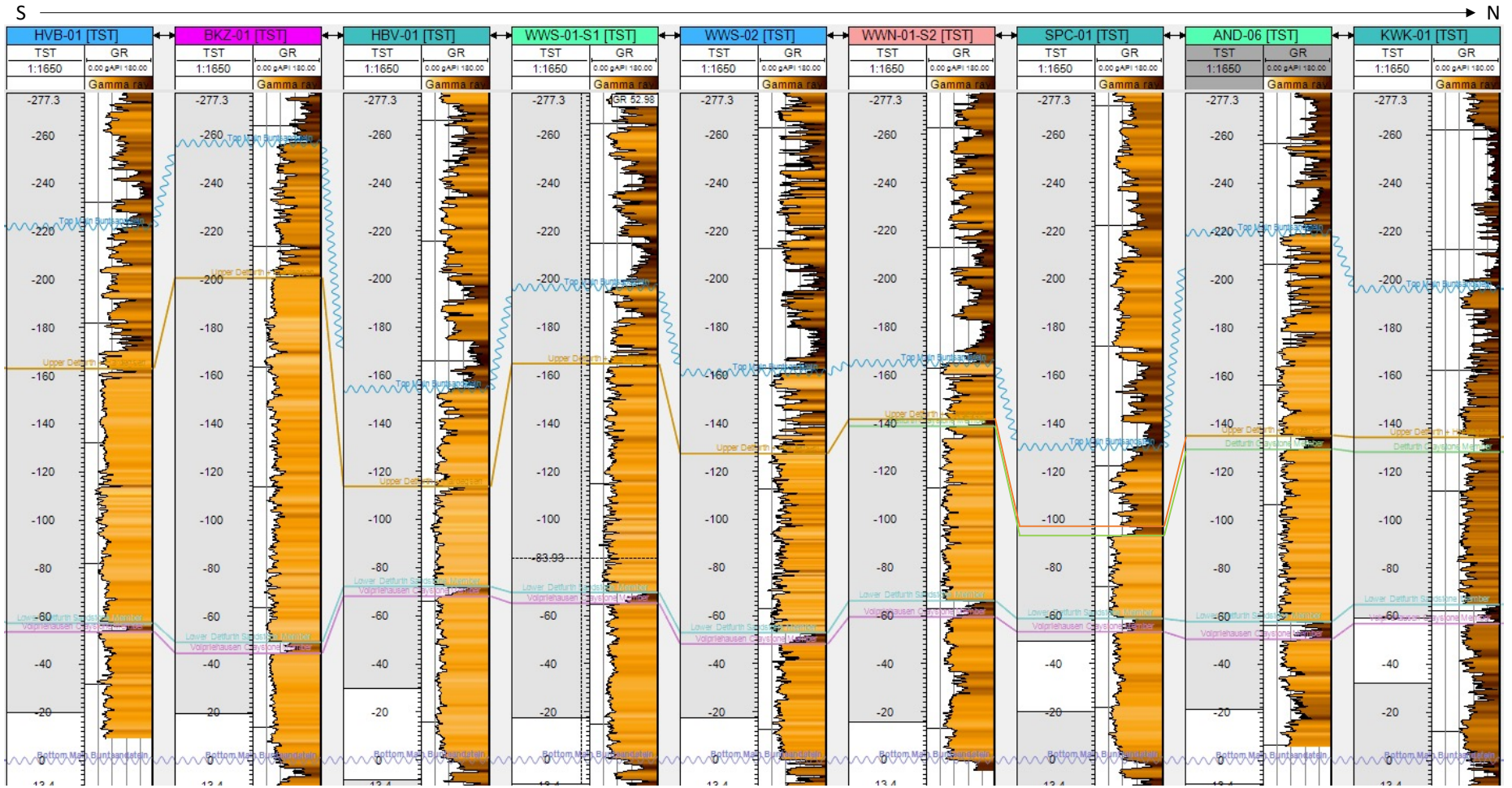

Full well correlation panel including wells (from South to North): HVB-01, BKZ-01, HBV-01, WWS-01-S1, WWS-02, WWN-01-S2, SPC-01, AND-06 and KWK-01. For the locations of the wells please refer back to the Materials chapter.

C. Full Facies Architecture Model

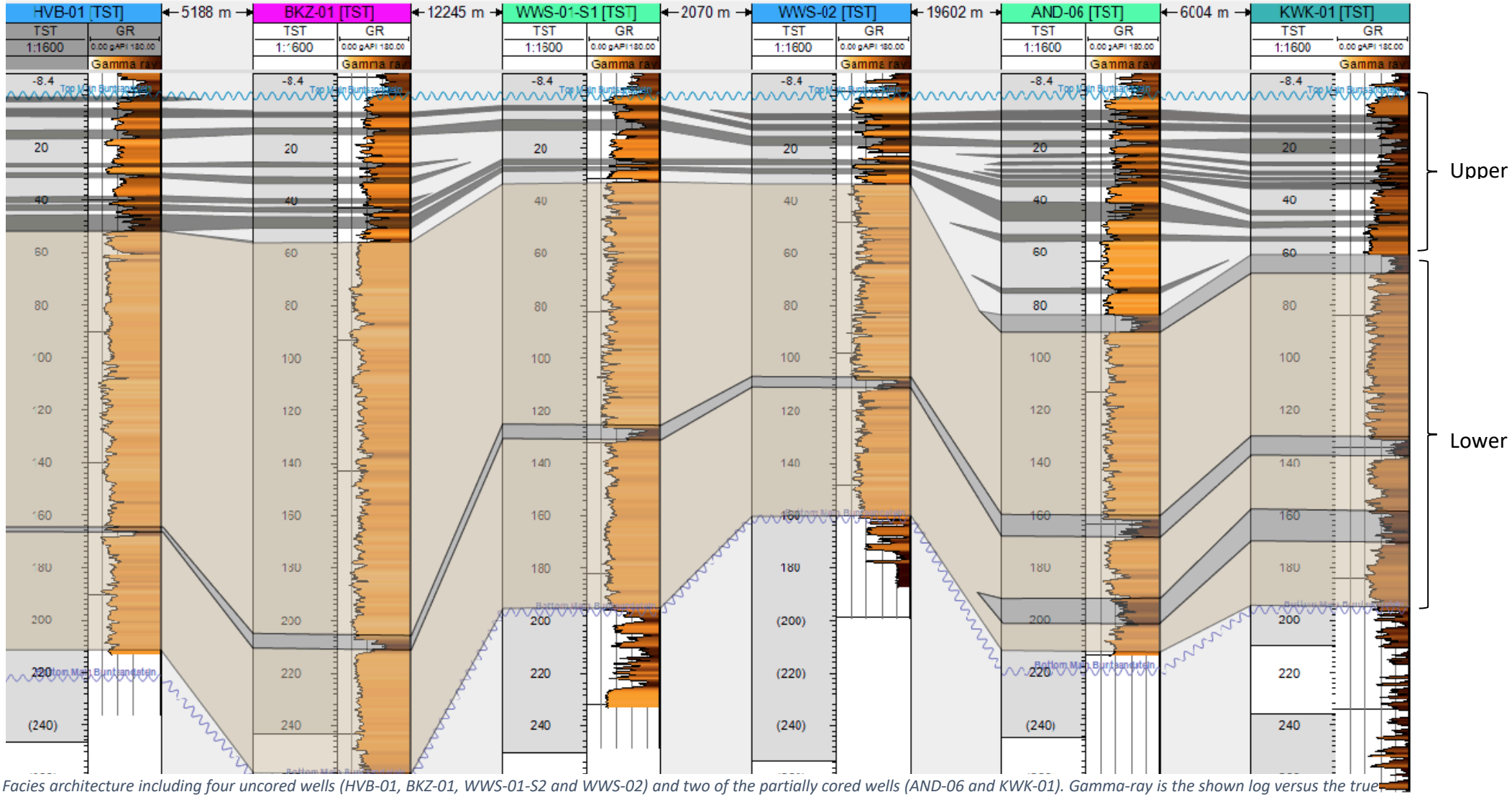

Facies architecture including four uncored wells (HVB-01, BKZ-01, WWS-01-S2 and WWS-02) and two of the partially cored wells (AND-06 and KWK-01). Gamma-ray is the shown log versus the true stratigraphic thickness. Thickness changes can be attributed to local erosion caused by the Hardegsen unconformity and/or difference in sediment deposition due to local differential subsidence. Facies correlation is conducted with respect to the gamma-ray logs. The overall architecture shows alternations of stacked amalgamated fluvial fan facies with playa-lake mudstones in the lower section (Volpriehausen and Lower Detfurth Formations). Main floodplain shale intervals are dominating in the Upper Detfurth and Hardegsen Formations (i.e., upper section), which punctuate the braided fluvial channel facies.

D. Thickness Map RBM

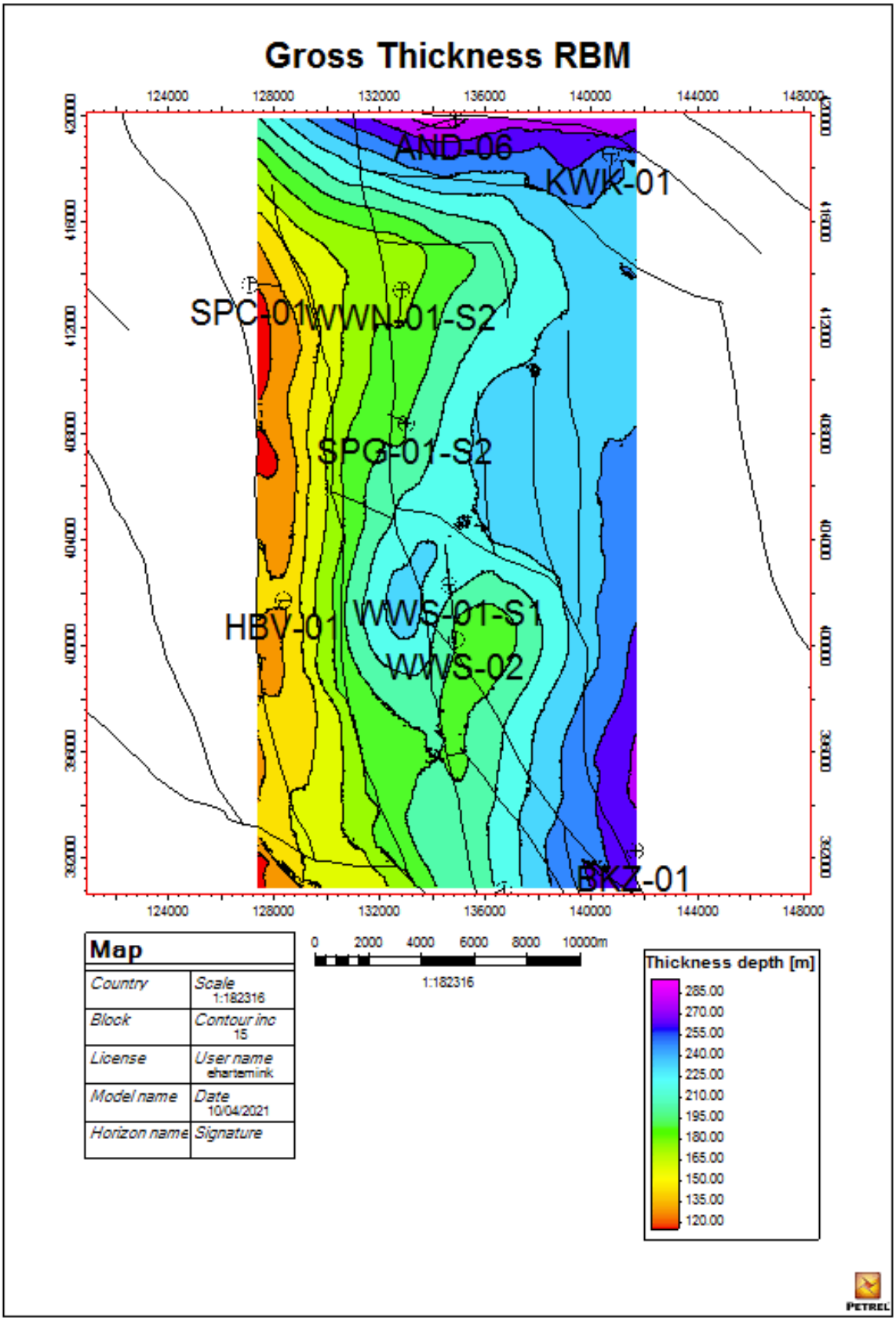

Thickness of the RBM created from the well log correlations in Petrel.. The black lines indicate the faults cuttings the Triassic Main Buntsandstein.